



**TECHNISCHE
UNIVERSITÄT
WIEN**
Vienna | Austria

Unterschrift BetreuerIn



Masterarbeit

Characterization of Natural Clinoptilolite Material for Remediation of Sr-90 and Cs-137 in Seawater

Ausgeführt am

Atominstitut

der Technischen Universität Wien

unter der Anleitung von

Univ.Ass. Dr.rer.nat. Jan Matthew WELCH

und

Ao.Univ.Prof. Dipl.-Ing. Dr.techn. Christina STRELI

durch

Viktoria GRILL, BSc

Matrikelnummer: 01225160

Datum

Unterschrift StudentIn

Abstract

The zeolite clinoptilolite may be used to remove caesium and strontium radioisotopes from aqueous nuclear wastes. In previous work the adsorption capacity of four different zeolite products from the Austrian company *LITHOS Industrial Minerals GmbH* was investigated. To better understand and compare the information gathered, detailed knowledge of the composition and structure of the zeolites used is essential. This characterisation was achieved by applying several different quantitative and qualitative analytical methods.

Differential Scanning Calorimetry (DSC) and Thermogravimetric Analysis (TGA) were used to determine the water content of the samples. This was needed for the precise determination of elementary compositions by Neutron Activation Analysis (NAA) and Total Reflection X-Ray Fluorescence Analysis (TXRF). Infrared Spectrometry gave preliminary structural knowledge and Powder X-Ray Diffraction (PXRD) was used to investigate phase compositions. Furthermore, all the data collected were analysed together to clarify the zeolite type and elemental composition. The results were compared to elemental composition of clinoptilolites in the literature.

Finally, the knowledge of the elemental composition was used to set up an experiment to determine the maximal capacity of the materials for caesium and strontium using the radiotracers ^{134}Cs and ^{85}Sr . For strontium the uptake limit was reached which lies for sample A and B at around 13.4 mg Sr per 500 mg zeolite powder. For caesium sample B has a bit higher capacity with 82.1 mg Cs per 500 mg zeolite than sample A. The milled version of sample C has an even larger capacity. It was shown that the grain size is important for the ion adsorption ([He and Walling, 1996](#)). The external sample D has the lowest capacity for Sr and Cs as expected from previous studies.

Kurzfassung

Der Zeolith Klinoptilolith wird vor allem zur Reinigung von verstrahlten Flüssigkeiten verwendet. So filtert er vor allem radioaktives Cäsium und Strontium aus Abwasser bzw. Kühlwasser von Kernkraftwerken. In vorangegangenen Arbeiten wurde die Adsorptionskapazität für vier verschiedene Zeolithe von dem österreichischen Unternehmen *LITHOS Industrial Minerals GmbH* ermittelt. Für ein besseres Auswerten der ermittelten Daten ist ein detailliertes Wissen über die einzelnen Komponenten und die Struktur der verwendeten Zeolithe notwendig. Diese Charakterisierung wurde durch verschiedene Methoden erlangt.

Mit Dynamische Differenzkalorimetrie (DSC) und Thermogravimetrische Analyse (TGA) wurde der Wassergehalt der Proben ermittelt. Diese Ergebnisse wurden für die Neutronenaktivierungsanalyse (NAA) und die Totalreflexions-Röntgenfluoreszenzanalyse (TXRF) benötigt, um eine genaue Bestimmung der Elementarkomponenten vorzunehmen. Infrarot (IR) Spektrometrie gab erste Einblicke in die Zeolithstruktur und bestätigte schnell den Zeolithetyp Klinoptilolith. Durch Pulverröntgendiffraktometrie (PXRD) wurden die Phasenzusammensetzungen und die Kristallstruktur untersucht. Die Ergebnisse der einzelnen Methoden wurden miteinander verglichen und ein Gesamtbild der Proben wurde erstellt. Die Resultate wurden mit Daten von Elementarkomponenten aus der Literatur verglichen.

Abschließend wurden durch die gewonnenen Erkenntnisse ein verbessertes Experiment für die Bestimmung der Kapazität für Cäsium und Strontium aufgebaut. Es wurden die Radioisotope ^{134}Cs und ^{85}Sr verwendet. Die maximale Sr Kapazität wurde erreicht, welche für Probe A und B ungefähr bei 13.4 mg Sr pro 500 mg Zeolithepulver liegt. Probe B hat eine höhere Cäsium Kapazität als Probe A, nämlich ungefähr 82.1 mg Cs pro 500 mg Zeolithepulver. Die gemahlene Form von Probe C hat noch eine bessere Kapazität für Cäsium. Die Teilchengröße des Pulvers ist ausschlaggebend für die Adsorption ([He and Walling, 1996](#)). Wie erwartet hat die externe Probe D die geringste Kapazität für Cäsium und Strontium.

Acknowledgements

I would like to thank all the people who helped me to accomplish this thesis. Thanks goes to my supervisor Christina Strelí, who made it possible to study the natural zeolite to this extend. I would like to thank my supervisor Jan M. Welch, who always had time for me and was explaining the chemical parts of this work with great patient to me. I am thankful to Johannes H. Sterba, who enabled the participation at the SAAGAS 27 conference where this work was also presented. There Georg Steinhauser gave the input how to determine silicon with Neutron Activation Analysis and without him the NAA and TXRF data would not be so comparable.

Also, I would like to thank Christian Knoll, who gave me a detailed explanation of the two methods Infrared Spectroscopy and Simultaneous Thermal Analysis. Werner Artner and Danny Müller helped me by the PXRD experiment and Klaudia Hradil did the analysis. Big thanks to Thomas Bretschneider, who did the TXRF performance and analysis. Michaela Foster helped me a lot to find all the needed containers in the labour and thanks to her I had not to search all the drawers and cupboards in the labour. She also did the determination of the uncertainties of the used pipettes which allowed me to use her results.

I would also like to acknowledge the great support of my family and partner. They provided financial support, food and time to talk. Without them I would not have been able to finish my studies with so many nice memories.

Contents

Abstract	i
Kurzfassung	iii
Acknowledgements	v
1 Introduction	1
2 Theory	3
2.1 Zeolites	3
2.1.1 Clinoptilolite	4
2.2 Analysis Methods	7
2.2.1 Infrared (IR) Spectroscopy	7
2.2.2 Simultaneous Thermal Analysis (STA)	9
2.2.3 Powder X-Ray Diffraction (PXRD)	9
2.2.4 Neutron Activation Analysis (NAA)	11
2.2.5 Total External Reflection X-Ray Fluorescence Analysis (TXRF)	15
2.2.6 Capacity Analysis with Radiotracers Dilution Experiment	16
3 Characterisation of the Sample Materials	19
3.1 IR Spectroscopy and Results	19
3.2 STA Experiment and Results	21
3.3 NAA Experiment	24
3.3.1 NAA Results	26
3.4 TXRF Experiment	33
3.4.1 TXRF Results	34
3.5 PXRD Experiment and Results	40
4 Determination of the Capacity for Sr and Cs	45
4.1 Concept	46
4.2 Parent (Tracer) Solution	49
4.3 Stock (Analyte) Solution	49
4.4 Experiment Setup	51
4.5 Experiment Analysis	52

4.5.1	Analysis of the Sr Capacity Experiments and Results	55
4.5.2	Analysis of the Cs Capacity Experiments and Results	60
4.6	Capacity for Stock Solution Containing Sr and Cs	67
4.7	Analysis of the Absorbed Sr or Cs Particles	68
5	Conclusion and Outlook	71
	Appendices	73
A	NAA	75
B	TXRF	87
C	PXRD	91
D	Composition of Clinoptilolite in Different Publications	109
E	Calculations for the Capacity Determination Experiments	121
F	Experimental Procedure for Capacity Determination	125
G	Spectra of the Capacity Experiments	133
H	Coal Fly Ash (CFA) Standard Data Sheet	145
I	Uncertainty of the Pipette 5000	151
	Bibliography	161
	List of Figures	165
	List of Tables	167

1. Introduction

Natural zeolites were discovered more than 260 years ago ([Čejka et al., 2007](#)). They find application in areas like drying and purification of gases, oxygen enrichment, filtration of water, extraction of metals from industrial wastes and they are even used in animal husbandry and agriculture. The structure of zeolites is defined by tetrahedral alumina AlO_4 and silica SiO_4 units sharing oxygen atoms and the resulting microporous character allows them to adsorb water molecules and ions. Their sorption characteristics depend upon these microporous channels and the size of their openings. The ion exchange selectivity of a zeolitic material is based on cation accessible sites on their internal and external surfaces. More than 40 natural and around 150 synthetic zeolites are known ([Clifton, 1987](#)).

The natural zeolite clinoptilolite is part of the heulandite-clinoptilolite group which is most commonly found in deposits all over the world ([Tsitsishvili et al., 1992](#)). Normally, it is mined as clinoptilolite tuffs, which have very homogeneous ores under a negligible cover of soil ([Tsitsishvili et al., 1992](#)). The abundant reserves and ease of extraction make clinoptilolite very important for industrial use, especially because of its low cost. One such more specialised application is the removal of caesium and strontium radioisotopes from aqueous nuclear wastes. The purification normally proceeds as adsorptive decontamination. Considering the high ion exchange selectivity for ^{137}Cs and ^{90}Sr of clinoptilolite, it can be used for full decontamination of low level aqueous radioactive waste.

The Austrian company *LITHOS Industrial Minerals GmbH* sought more detailed information regarding the adsorption capacity of their zeolite products:

- LithoFill 100 “T” → A
- LithoFill 100 → B
- LithoGran 2 → C
- “Extern I” → D

Two previous projects independently gathered some preliminary information on ^{137}Cs ([Walenko, 2013](#)) and ^{90}Sr ([Sperrer, 2013](#)) uptake by these materials, and an effort was made to summarise and compare these results ([Sterba et al., 2018](#)). However, the measurement conditions of the two previous studies were quite different and so one aim of the current effort is to gather comparable results for caesium and strontium uptake. To obtain a better understanding of the data, detailed knowledge about the compositions and structures of the used zeolites is

necessary. This was achieved by the combined application of several different analytical methods.

Simultaneous Thermal Analysis (STA), which combines Thermogravimetric Analysis (TGA) with Differential Scanning Calorimetry (DSC), was used to determine the water content and thermal stability of the samples. This was needed for the precise determination of elementary compositions by Neutron Activation Analysis (NAA) and Total Reflection X-Ray Fluorescence (TXRF). Infrared (IR) Spectrometry gave initial information about the zeolites' structure. Initially, Powder X-Ray Diffraction (PXRD) was used to investigate phase compositions. Furthermore, PXRD allows verification of the crystalline structure and the positions of adsorbed caesium and strontium.

Finally, the capacity of the material for caesium and strontium was reassessed using the radio-tracers ^{134}Cs and ^{85}Sr in the context of the above described data. The capacity determination was done under comparable experimental conditions for both nuclides to allow ready comparison of the results.

2. Theory

For more detailed information on the properties of zeolites, chapters 1 and 3 of "[Natural Zeolites](#)" by [Tsitsishvili et al. \(1992\)](#) or section 1.5 of "[Ion Exchangers](#)" by [Dorfner \(1973\)](#) are recommended. The following section 2.1 *Zeolites* and subsequent section 2.1.1 *Clinoptilolite* provide only a short overview.

2.1 Zeolites

Zeolites are an aluminosilicate, which becomes obvious after a glance at the general chemical formula (Eq. 2.1.1):



Ratios of $\frac{y}{x} = 1$ to 6 and $\frac{p}{x} = 1$ to 4 depending on the specific zeolite type are known. M corresponds to the cation-forming elements Na, K, Li and/or Ca, Mg, Ba, Sr with n representing cation charge.

Often its oxide formula (Eq. 2.1.2) is used to represent a zeolite and thus most data on the chemical composition of zeolites are given in terms of occurrence of the oxides and not of the specific element (see Appendix D).



Zeolitic materials are composed of tetrahedral alumina AlO_4 and silica SiO_4 units centred around Al or Si atom with four oxygen atoms at the corners of the tetrahedron. These oxygen centres are shared between neighbouring TO_4 tetrahedra forming the primary structure of the zeolite. Secondary substructures in zeolites "which contain up to 16 T-atoms" ([Baerlocher et al., 2007](#)) and form different types of rings may also be observed. The composite of these structural units is called the framework of the zeolite. It indicates the structure type of a zeolite and is the most consistent component of zeolitic materials. Its matrix contains voids of different sizes, in which different ions (depending on their size and charge) and water molecules can be trapped. These voids are responsible, inter alia, for ion-exchange. The monovalent and divalent cations in these channels compensate the negative charge of the framework, which is caused by the charge of Al^{3+} . Under ordinary conditions, the remaining free volume is filled by water molecules. The dimensions of the channels in a zeolite framework change with dehydration. Three types of channels are distinguished depending on their dimensions and a cation

or molecule can move in any free site (3-dimensional), on the plane (2-dimensional) or only in one direction (1-dimensional). Many voids and channels are too small to be accessible and play no role in sorption or catalysis. The "[Atlas of Zeolite Framework Types](#)" by [Baerlocher et al. \(2007\)](#) gives detailed information for the 176 known zeolite framework types. The "[Database of Zeolite Structures](#)" by [Baerlocher and McCusker](#) is publicly accessible and was last updated in November 2016. To learn more about the catalytic properties of zeolites the book "[Zeolites and Catalysis - Synthesis, Reactions and Applications](#)" by [Čejka et al. \(2010\)](#) is recommended. The water molecules and cations in the channels and voids sit mostly at specific sites in the lattice which are suitable for their size. Normally, a cation is in the centre of an irregular polyhedron with water molecules and oxygen atoms from the framework at the corners. The distances between the cation and the oxygen atom or water molecule depend primarily on the specific size of the cation. Magnesium (Mg) ions for example are surrounded by water molecules. For specific data about the distances and coordination of the cations for different zeolites, Table 1.6 in "[Natural Zeolites](#)" by [Tsitsishvili et al. \(1992\)](#) can be studied.

"Natural zeolites were the first ion exchangers" ([Perry et al., 1999](#)) but also have molecular sieving characteristics. Ion exchange and adsorption occur simultaneously and are not entirely separable. Both depend on the size of the voids and channels. Cations can only diffuse into apertures that are bigger than the ion size. Cations occupy specific sites in the framework after ion exchange again, mainly defined by their size. The exchanged cations contribute to compensation for the negatively charged framework. After a specific period of time, ion exchange equilibrium is reached. A higher temperature improves ion exchange characteristics by increasing reaction rates and allowing equilibrium to be reached faster. The isotherms for ion exchange processes shown in Fig. 2.1 illustrate three distinct possibilities for exchange selectivity. The ion exchange capacity for a cation type is the sum of all trapped cations in the zeolite and depends on the Si/Al ratio. For example, "silica-rich frameworks prefer large monovalent cations" ([Čejka et al., 2007](#)) like caesium. If required, section 3.6 "Ion Exchange Properties" of the book "[Natural Zeolites](#)" by [Tsitsishvili et al. \(1992\)](#) provides detailed information about ion exchange variables like the diffusion coefficient or the dynamic and equilibrium exchange capacity.

2.1.1 Clinoptilolite

The heulandite-clinoptilolite group are rock-forming minerals and "are the most widely distributed zeolites in Nature" ([Tsitsishvili et al., 1992](#)). The following section provides detailed background information on clinoptilolite. Its chemical formula (Eq. 2.1.3) is:



The Si/Al ratio lies between 4.0 and 5.5. For heulandite the ratio ranges from 2.75 to 4.0. A rule of thumb is that minerals of the group with a low-silica content contain mainly Ca as counter cations and often additionally Ba and Sr. High-silica members have a greater K, Na and Mg content. Fig. 2.2 shows the distribution of heulandite and clinoptilolite chemical compositions

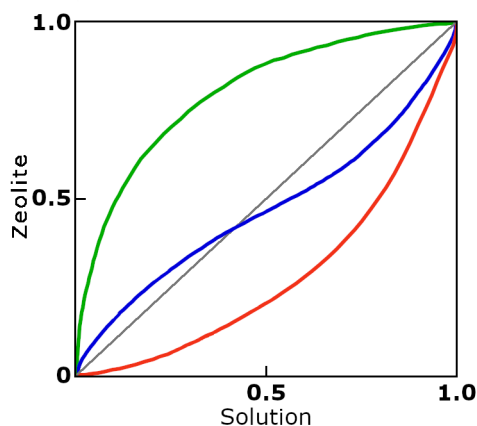


Figure 2.1: Ion exchange isotherms for three different cases plotted as the mole fraction in solution against the mole fraction in the zeolite, always for the same cation. Green: Zeolite prefers the entering cation, cation of solution replaces a cation of the zeolite; Red: Opposite of green line, zeolite is non selective for entering cation, cation of solution stays in solution; Blue: Selectivity for the entering cation varies during exchange; Grey: straight isotherm. Adapted from [Dorfner \(1973\)](#).

found in nature. For clinoptilolite the silicon content is larger leading to a Si/Al ratio greater than 4.5.

The channel system in minerals of the heulandite-clinoptilolite group is two-dimensional. It is composed of 8- and 10-membered channels in the crystallographic [001] direction, and 8-tetrahedral channels oriented in the [100] direction (Fig. 2.3). The clinoptilolite unit cell is larger than that of heulandite ([Mumpton, 1960](#)). Calcium (Ca) and sodium (Na) ions sit at the M1 and M2 sites, potassium (K) ions occupy the site M3 and magnesium (Mg) ions the site M4 (Fig. 2.4).

Clinoptilolite is used for decontamination of low and intermediate-level aqueous radioactive waste because of its ion exchange selectivity for the isotopes ^{137}Cs and ^{90}Sr . The capacity of different clinoptilolite tuffs has been evaluated by many researchers including Lloyd Leroy Ames ([Ames JR., 1963](#)) or Tsuneo Tamura ([Tamura and Struxness, 1963](#)). The clinoptilolite content of the tuff applied is critical for the selectivity for caesium and strontium. Monovalent caesium cations (Cs^+) may exchange with Na^+ , K^+ and even with water molecules, whereas divalent strontium cations (Sr^{2+}) can exchange with two Na^+ . The isotherms for Sr and Cs are plotted in chapter 27 "Natural Zeolites and Environment" of the book "[Introduction to Zeolite Science and Practice](#)" by [Čejka et al. \(2007\)](#). Ion exchange for Sr is represented by the blue curve in Fig. 2.1, indicating that the selectivity for the cation absorbed varies over the course of the ion exchange process. The ion exchange for Cs is illustrated by the green curve in Fig. 2.1 showing that clinoptilolite is clearly more selective for caesium than strontium. [Murakami et al.](#) also reproduced the isotherms for Cs and Sr exchange in clinoptilolite in [2009](#). During ion exchange, the cation sites are first occupied depending on the size of the exchange cation and if no more free sites exist, the cation may exchange with a water molecule. Table 1.9 in the book "[Natural Zeolites](#)" by [Tsitsishvili et al. \(1992\)](#) shows that Sr (divalent like Ba) prefers the M3

site and Cs mainly exchanges with water molecules. Water molecules are at seven defined sites which can depend on the presence or absence of a specific cation in the channel. This may be confirmed by detailed X-Ray Diffraction measurements which have not been reported.

Chemical compositions of different clinoptilolites from all over the world are reported in Appendix D *Composition of Clinoptilolite in Different Publications*. The article "[Clinoptilolite Redefined](#)" by [Mumpton \(1960\)](#) summarises findings about clinoptilolites.

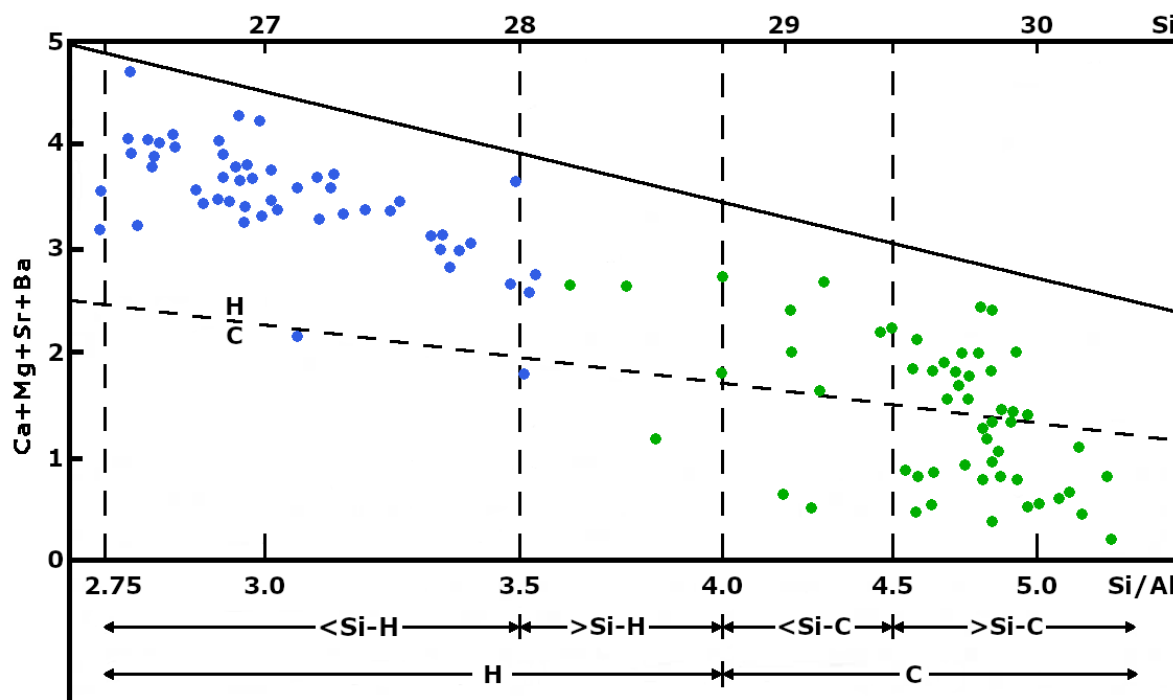


Figure 2.2: Chemical compositions of heulandites (H, blue) and clinoptilolites (C, green). Adapted from [Tsitsishvili et al. \(1992\)](#).

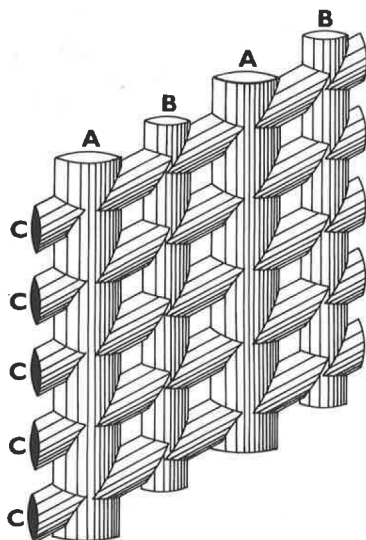


Figure 2.3: A and B are the 10- and 8-membered channels which are parallel to $[001]$ and C are the 8-tetrahedral channels which are along $[100]$. Reproduced from [Tsitsishvili et al. \(1992\)](#).

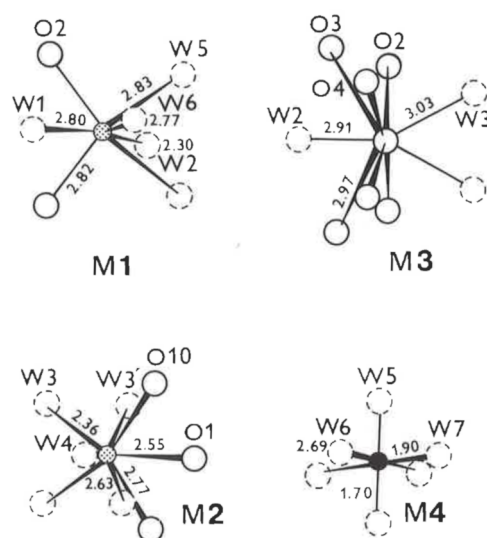


Figure 2.4: Coordinate environment for Ca and Na (M1 and M2), K (M3) and Mg (M4) ions. Reproduced from [Tsitsishvili et al. \(1992\)](#).

2.2 Analysis Methods

As discussed in the previous section *2.1.1 Clinoptilolite*, each zeolite group has special element modules which form the framework. Before setting up the capacity experiment, it is necessary to know as much as possible about the zeolite samples. The different methods used are explained but briefly in the following section, because a lot of literature exists for detailed explanation. Also the underlying principle of the capacity experiments with strontium and caesium radiotracers is explained at the end of this section.

2.2.1 Infrared (IR) Spectroscopy

Very small sample sizes of less than 10 mg are used for the measurements and the possibility of a non-homogeneous sample has to be considered. The IR spectra are representative for minerals, which contain only one zeolite type ([Tsitsishvili et al., 1992](#)). If a mixture is present, the bands of the same frequency can overlap and it is not possible to separate them. The spectra do not give information about the zeolite content of the sample ([Tsitsishvili et al., 1992](#)). The data just gives a first clue, which zeolite type can be expected.

The IR spectroscopy only considers vibrational behaviour, which is caused by a changing dipole moment ([Čejka et al., 2007](#)). IR spectra can be measured in the transmittance or the absorbance mode against the frequency on the horizontal axis. For this work, the transmittance (%T) mode was used, which means the peaks of interest face downwards. This mode is the older one, because the absorbance mode needs additional electronics like microprocessors to convert the signal ([Siddall, 2014](#)). The frequency or also called the wave number has the unit cm^{-1} .

General wave numbers and their meaning for zeolite samples are shown in Tab. 2.1. The ranges in the literature can vary a bit. [Čejka et al.](#) published different ranges for the structure insensitive asymmetrical ($950\text{-}1250\text{ cm}^{-1}$) and symmetrical ($650\text{-}720\text{ cm}^{-1}$) stretch. Characteristic

absorption bands for clinoptilolite are shown in Tab. 2.2. The bands which are caused by the vibrated Si-O(Al) and Al-O(Si) bonds are extreme in the range 1040-1100 cm^{-1} (Tsitsishvili et al., 1992).

For a more detailed understanding it is recommended to study the section 3.3 "Spectroscopic Investigations" in the book "Natural Zeolites" by Tsitsishvili et al. (1992) and the chapter 13 "Infrared and raman spectroscopy for characterizing zeolites" in the book "Introduction to Zeolite Science and Practice" by Čejka et al. (2007). The meaning of the different vibrations can be looked up at there.

Structure insensitive vibrations	Wavenumber in cm^{-1}
Asymmetric stretching vibrations	1200-1000
Symmetric stretching vibrations	850-700
Bending vibrations	600-400
Structure sensitive vibrations	
Asymmetric stretching vibrations	1050-1150
Symmetric stretching vibrations	750-820
Double ring vibrations	500-650
Pore opening vibrations	300-420

Table 2.1: Structure sensitivity and insensitive lattice vibrations of zeolites. Adapted from Auerbach et al. (2003).

Correspond to	cm^{-1}		
vibrations of Si-O(Al) and Al-O(Si) bonds	550-650	650-720	750-820
	850-900	1000-1100	1150-1250
vibrations of Si-O(Al) bond due to internal deformations	650-720	780-820	900-1250
symmetric vibrations of the Si-O bond	750-820		
oscillations of chains of aluminosilicate oxygen tetrahedra	550-650		
concentration of OH groups	3100-3700		
hydroxonium ion H_3O^+	1600-1700		

Table 2.2: Typical frequency ranges for clinoptilolite. Adapted from Tsitsishvili et al. (1992).

2.2.2 Simultaneous Thermal Analysis (STA)

"At room temperature under conditions of normal humidity, the three components of the zeolite structure (framework, cations and water) are in equilibrium." (Tsitsishvili et al., 1992) Heating or evacuation requires new equilibrium conditions, and they are reached mainly by releasing water molecules (Tsitsishvili et al., 1992). The specific temperature for the release and the rate of water loss is related to the water vapour pressure (Tsitsishvili et al., 1992).

The dehydration process can be studied by Simultaneous Thermal Analysis (STA), which combines Thermogravimetric Analysis (TGA) and Differential Scanning Calorimetry (DSC) in the same instrument. TGA measures the mass change versus temperature or time, and DSC the heat flow change versus the temperature or time. The mass loss of the zeolite samples relates to the water loss due to heating. The three different curves which are provided by the STA are shown in Fig. 2.5. The green curve is referring to the TGA, the blue curve to DSC, and the red curve is the temperature over time. For the later analysis just the TGA curve is of interest. Fig. 2.5 presents the data of sample A. For this measurement 8.4 mg of the sample were measured in a temperature range of 20 to 450°C. The temperature was raised by 10 K per minute and lowered by 20 K per minute.

"Clinoptilolite is stable to 750-800°C" (Tsitsishvili et al., 1992), which temperatures will not be reached during the experiments. The structure of the crystals would crack over that temperature limit. Dehydration causes shrinking of the unit cell of clinoptilolite. Clinoptilolite regains its original structure again during the cooling process if it was not completely destroyed before. "Zeolitic water" (Tsitsishvili et al., 1992) can be released from the zeolite structure without destroying the original structure. Na and Ca ions can change their site during the heating process, which destroys the original symmetry of the structure. Si-O-Si bonds are normally more stable against heat than Al-O-Si bonds. So the Si/Al ratio affects the thermal stability of zeolites. The last paragraph was summarized from the book "Natural Zeolites" by Tsitsishvili et al. (1992). For a detailed understanding of thermal analysis it is recommended to study the book "Handbook of Thermal Analysis and Calorimetry: Principles and Practice" by Brown (1998).

2.2.3 Powder X-Ray Diffraction (PXRD)

The X-Ray Diffraction (XRD) reveals information about the crystal structure, the average spacing between layers of atoms, the phases of the system, the size, shape and internal stress of the crystalline regions and the orientation. In detail, a diffractogram helps to distinguish between crystalline and amorphous materials. Furthermore, it determines the texture of polygrained materials and the electron distribution within the atom and the unit cell. XRD is based on elastic scattering of X-rays in matter. The distribution of the scattering is depending on an angle. Due to that fact a diffractogram is the position of the detected signal in 2θ vs. the intensity in counts.

For the Powder X-Ray Diffraction (PXRD) no single crystal and no rotation of the sample is needed. This simplifies the preparation of the samples. The monochromatic X-ray beam inci-

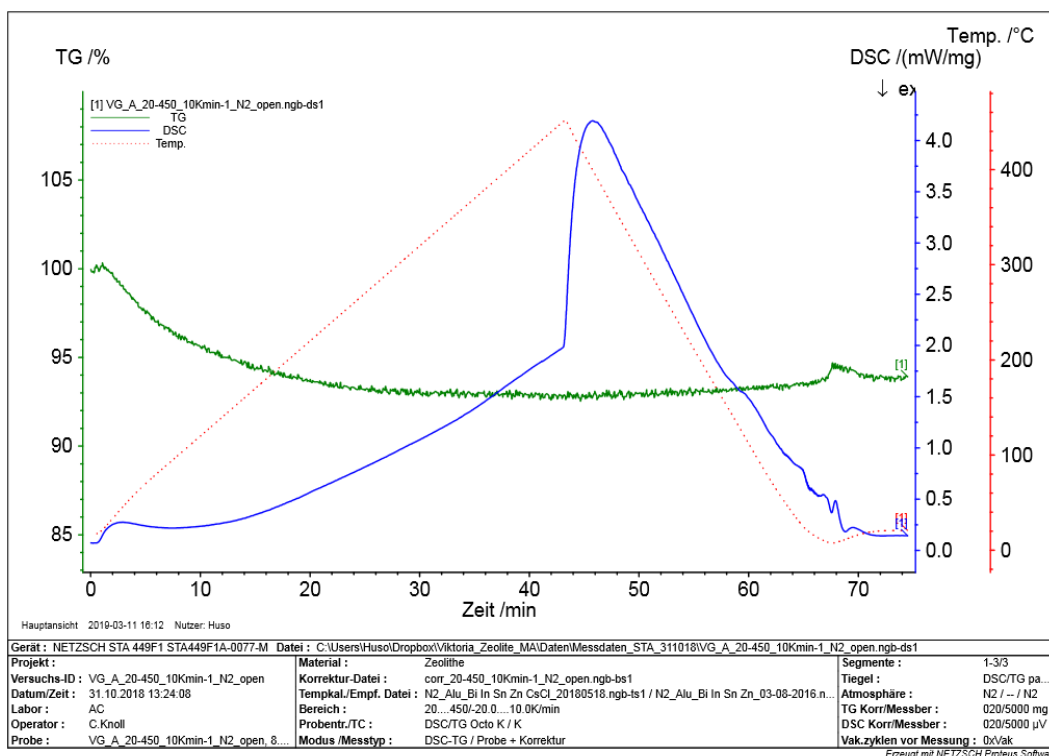


Figure 2.5: Output of a STA measurement for sample A.

dents on the powdered sample. In the powder some crystals will always exist in a set of crystal planes, which are at the right orientation to satisfy the Bragg's law (Eq. 2.2.1). The path differences of two waves $2d \sin \theta$ depend on the interplanar distance d and the scattering angle θ . n is a positive integer and λ is the wave length of the incident waves. Bragg's law is fulfilled for all θ which lead to constructive interference. This means the path length $2d \sin \theta$ is proportional to an integral multiple of the wavelength. Each detected spot is caused by a separate crystal. It appears that a continuous diffraction line is detected, because so many crystals contribute in the signal. The variable symbols can be looked up in Tab. 2.3.

$$2d \sin \theta = n\lambda \quad (2.2.1)$$

To analyse the PXRD diffractogram the detected peaks have to be compared to a database which contains different peak lists of minerals. "The measured diffraction peak positions and intensities are like a fingerprint of a particular crystalline phase." (Malvern Panalytical, 2019) An algorithm in the evaluation program searches the database for matches. In a zeolite it is common to have different phases. The major phase is the main component of the mineral. A variable number of minor phases can exist next to it. Fig. 2.6 shows the diffractogram for sample A. The blue reflexes are the found major phase and indicate the position and intensity of the peaks for this reference.

For a detailed understanding of XRD and in particular PXRD it is recommended to study the book "Powder Diffraction: Theory and Practice" by Dinnebier and Billinge (2008).

Symbol	Name	Unit
d	interplanar distance	nm
λ	wave length of the incident waves	nm
n	positive integer	/
θ	scattering angle	°

Table 2.3: Parameters and their units for PXRD.

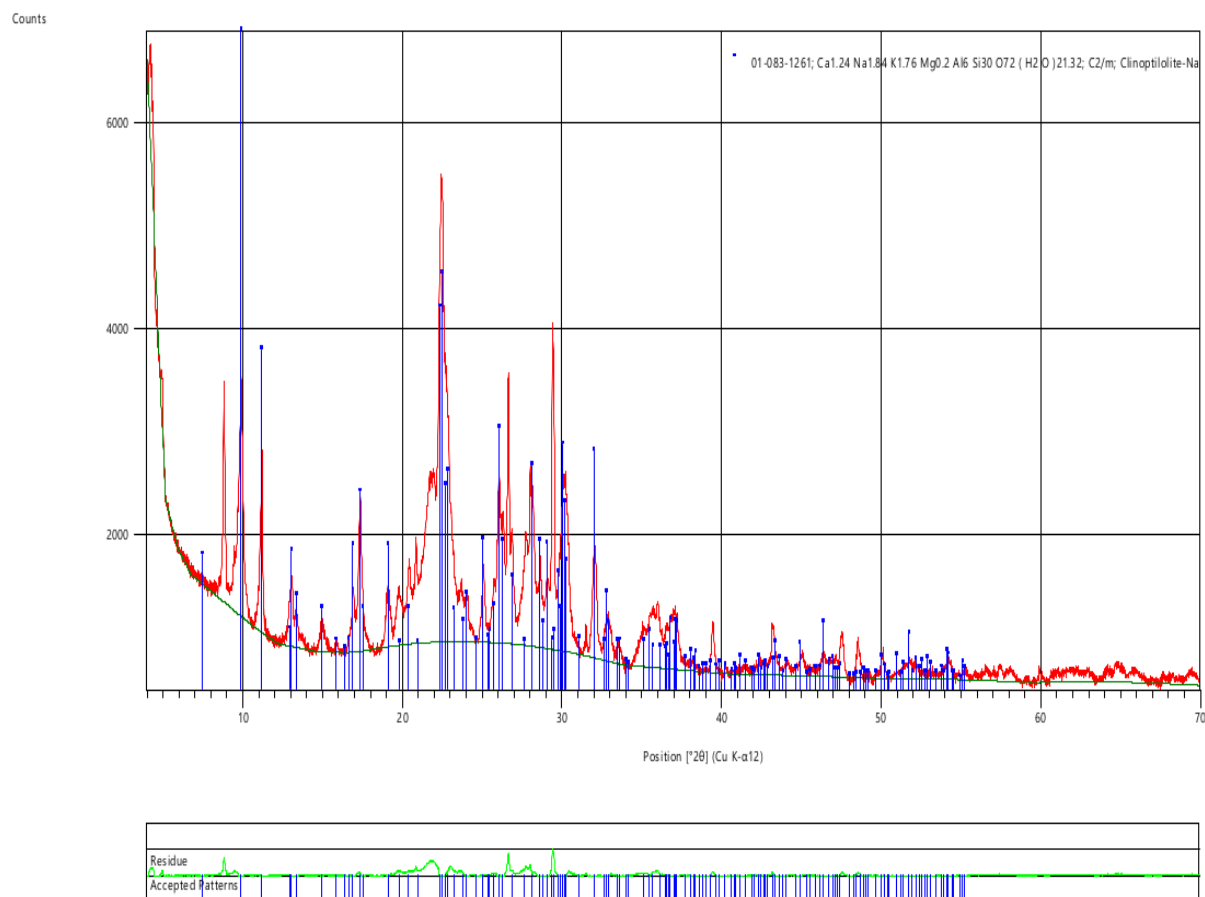


Figure 2.6: Diffractogram of sample A using one major phase.

2.2.4 Neutron Activation Analysis (NAA)

Neutron Activation Analysis (NAA) determines the elemental concentrations of materials. It is necessary to have access to a research reactor because the samples get activated by neutron absorption and the radioactivity is measured by γ -spectroscopy.

In detail, the nuclear reactions inside the reactor activate the nuclides of the samples. The number of the produced radionuclides N_A per time t depends on the existing target atoms N , the neutron flux density Φ and the cross section of the nuclear reaction σ . The Equation 2.2.2 clarifies the strong dependence on the cross section. The higher σ is, the bigger is the possibility for activation of the nuclide. The activated atoms are radioactive and decay after the radioactive decay law (Eq. 2.2.3). λ is the decay constant and is inversely proportional to the half-life time

$T_{1/2}$ (Eq. 2.2.4).

$$\frac{dN_A}{dt} = \sigma\Phi N \quad (2.2.2)$$

$$\frac{dN_A}{dt} = -\lambda N_A \quad (2.2.3)$$

$$T_{1/2} = \frac{\ln 2}{\lambda} \quad (2.2.4)$$

The equation of the sum of the two differential Equations 2.2.2 and 2.2.4 with the initial condition $N_A(t = 0) = 0$ is the equation for the activity A (Eq. 2.2.5). t in the following equations is the irradiation time of the atoms. The specific activity A_S (Eq. 2.2.6) is a modification of Equation 2.2.5 with the Avogadro constant N_{Av} , the atomic mass of the element M and the relative abundance of the nuclide H . It is more convenient to calculate with a cross section in the unit barn and to add the value of N_{Av} which leads to Equation 2.2.7. The names for the physical quantities and their units for the Equations 2.2.2 to 2.2.7 are described in Table 2.4.

$$A(t) = \sigma\Phi N \left[1 - \exp\left(-\frac{\ln 2}{T_{1/2}} t\right) \right] \quad (2.2.5)$$

$$A_S(t) = \sigma\Phi \frac{N_{Av}}{M} H \left[1 - \left(\frac{1}{2}\right)^{\frac{t}{T_{1/2}}} \right] \quad (2.2.6)$$

$$A_S(t) = 0.602\sigma[b]\Phi \frac{H}{M} \left[1 - \left(\frac{1}{2}\right)^{\frac{t}{T_{1/2}}} \right] \quad (2.2.7)$$

After the activation the sample is measured in a γ -spectrometer. γ -ray emission is a "by-product of alpha or beta decay" (Gilmore, 2008), and is emitted due to radioactive decay. It is necessary to wait until the dose rate of the sample is in a range safe (about 50-80 $\mu\text{Sv/h}$) to transport the experiment to the spectrometer. "The intensity I of the γ -rays [(Eq. 2.2.8)] produced by the nuclear reaction is proportional to the rate of the nuclear reaction" (Kratz and Lieser, 2013). One radionuclide can have different γ -rays, which differ in their energy and intensity. As a rule of thumb, the intensity can be understood as the probability to detect the γ -peak with the specific energy. If the concentration of the element is high, the probability to detect also γ -peaks with low intensity will be more likely.

$$I \propto \frac{dN}{dt} = \sigma\Phi N_A \quad (2.2.8)$$

A real γ -spectrum contains different physical effects. The following paragraph summaries the first and second chapter of the book "Practical Gamma-Ray Spectrometry" by Gilmore (2008). At an energy of 511.00 keV the annihilation peak can be detected. It is caused by escaping photons from the surroundings of the detector (e.g. shielding) which occur during pair production. During pair production the γ -ray interacts with the whole atom and generates an electron-positron pair which shares the energy of the γ -ray equally. The electron and positron slow down

on their way through matter. Eventually the positron meets an electron and they annihilate each other. During this process two annihilation photons of an energy of 511 keV are released. The photons will move in opposite directions and one of them can be detected, which gives rise to the annihilation peak. Mostly the positron interacts with an electron bound to an atom. That is why some energy is used to remove the electron from its bounded state and the released photons have a bit lesser energy. For example, the annihilation peak of the spectrum of sample A (Appendix Tab. A.6) can be found at 510.29 keV. The annihilation peak is broader than other peaks because of the Doppler effect. The positron and electron have both a different kinetic energy, which can cause a net momentum during the interaction process. One released photon will have a slightly lower energy than the other one and this causes a variation of the energy of the detected photons, which widens the peak. The energy summation makes still 1022.00 keV. It can happen that both released photons during pair production can leave the detector. Their information gets lost and the detected peak is 1022 keV "below the position of full energy absorption" (Gilmore, 2008). This peak is called the double escape peak and the abbreviation DE is used in the spectra to indicate it. Sometimes just one of the photons escapes the detector and this results in the single escape (SE) peak which is at the position 511 keV smaller than the full peak energy. The γ -rays mainly interact with electron bound to an atom and its binding energy changes the form of the detected peak. The peak point gets rounder and the edges become wider due to backscattering. This effect is called the Compton scattering and causes a partial absorption of the γ -rays which does not give any useful information. The Compton continuum can cause rising of the background by detecting of Compton scattered γ -rays, which are produced

Symbol	Name	Unit
A	activity	Bq
A_S	specific activity	Bq
H	relative abundance of the nuclide	/
I	intensity of the γ -rays	arbitrary unit
λ	decay constant	s^{-1}
M	atomic mass of the element	u
N	existing target atoms	particles
N_A	produced radionuclides	particles
N_{Av}	Avogadro constant	$6,022 \cdot 10^{23}$ particles
ϕ	neutron fluxdensity	$cm^{-2}s^{-1}$
σ	cross section of the nuclear reaction	cm^2
$\sigma[b]$	cross section of the nuclear reaction in barn	1 b= 10^{24} cm^2
$T_{1/2}$	half-life time	s
t	irradiation time	s

Table 2.4: Parameters and their units for NAA.

in the surrounding materials of the detector. Its upper limit is called the Compton edge. The detected γ -peaks and their intensity are shown in Tab. 2.5. SE stands for single escape peak and DE for double escape peak. The elements might have more γ -peaks but their intensity was too low to detect and so they are not included in this table. If interested, they can be looked up on the "NuDat 2 Database" from the [National Nuclear Data Center](#) (f).

The book "[Practical Gamma-Ray Spectrometry](#)" by [Gilmore \(2008\)](#) provides a detailed explanation about γ -spectroscopy. Chapter 20 of the book "[Nuclear and Radiochemistry - Fundamentals and Applications](#)" by [Kratz and Lieser \(2013\)](#) gives a short overview and also explains NAA briefly.

Element	Gamma radiation	
	Energy in keV	Intensity in %
beta annihilation	511.00	
Na-24	1368.626 5	99.9936 % 15
	2754.007 11	99.855 % 5
	2243.007 11	SE
Mg-27	1732.007 11	DE
	170.82 10	0.860 % 20
	843.76 10	71.800 % 20
Al-28	1014.52 10	28.200 % 20
	1778.987 15	100%
	1267.987 15	SE
Al-29	756.987 15	DE
	1273.361 9	91.26 %
	K-42	1524.6 3
Ca-49	3084.4 1	90.72 % 4
	2573.4 1	SE
	2062.4 1	DE
Ti-51	320.076 6	93.1 %
V-52	1434.06 1	100.0 % 14
Mn-56	846.7638 19	98.85 %
	1810.726 4	26.9 % 4
	2113.092 6	14.2 % 3
	2657.56 1	0.645 % 7

Table 2.5: Energy and intensity of the detected γ -peaks in the zeolite and Coal Fly Ash (CFA) samples. The information about the energy and intensity of the elements was extracted from the NuDat 2 Database from the [National Nuclear Data Center](#) (f).

2.2.5 Total External Reflection X-Ray Fluorescence Analysis (TXRF)

The analysis technique X-Ray Fluorescence (XRF) is used for determination of the elemental components and their ratios in a sample. An X-ray source, like an X-ray tube, is emitting the X-ray photons onto the sample where they interact in three different manners. The dominant interaction for x-ray energies under 100 keV is the photoelectric effect (= photo effect). The X-ray photon strikes an electron bounded to an atom which absorbs the whole energy and if the energy of the photon is higher than the binding energy of the electron, the electron will be ejected from its state. This effect is dominant for elements with high atomic numbers in comparison to the Auger effect which is highest for low atomic numbers. The hole in the inner shell can be filled with an electron from an outer shell which releases its characteristic energy difference as a photon. These photons are called fluorescence radiation. If this radiation ejects an electron of an outer shell, this electron is called Auger electrons (= Auger effect). The fluorescence radiation can be detected with energy or wavelength dispersive detectors. For this work an energy dispersive Si(Li) detector was used. It is built out of a Si(Li) diode, in detail out of a p-type Si single crystal and a high content of n-type Li at the rear of the diode. The crystal has to permanently be cooled by liquid Nitrogen in order to reduce the noise signal. As a result the fluorescence photons enter the detector through a Beryllium window, which does not absorb many X-rays. Each photon produces a cloud of electron-hole pairs in the detector material until all of its energy is absorbed. 3.86 eV are necessary to produce an electron-hole pair in silicon (Klockenkämper and Bohlen, 2015). The holes drift to the front and the electron to the rear of the detector because of the applied potential. At the rear the total charge is collected. The number of produced electrons n is proportional to the energy of the detected photon E_{photon} (Eq. 2.2.9).

$$n = \frac{E_{photon}}{3.86} \quad (2.2.9)$$

The first 0.1 μm of the Si layer after the Be window have a too low electrical resistivity which means no full collection of the electron-hole pairs is allowed there. Due to this effect the full energy of the fluorescence photon cannot be detected, and the fluorescence peak shows a tail on the low energy side. Elements with a small atomic number have a higher possibility to be absorbed in this dead layer of Si. To get reliable results, it is necessary to reduce the thickness of the dead layer as much as possible. They are also absorbed by the Be window and also the thickness of the window has to be reduced.

A special method of the Energy Dispersive X-Ray Fluorescence (EDXRF) is the Total Reflection X-Ray Fluorescence Analysis (TXRF). The main difference to XRF is the angle of the primary X-ray beam. It hits the sample at an angle smaller than 0.1° and not at about 40° like in a XRF experiment (Klockenkämper and Bohlen, 2015). The primary beams get totally reflected on the samplecarrier. The intensity of the fluorescence radiation depends on the excitation of the sample by the primary and the reflected beam. The distance between the detector and the sample is about 1 mm which is due to the small angle of the incident beam. Due to the small distance between the detector and the sample the solid angle is quite big. For a measurement

only a very small sample mass in the range of ng or μl is required. The background is very low, because the primary beam hardly penetrates the sample carrier (only a few nm). The whole sample is screened by the X-rays. The fluorescence signal carries different types of information depending on how far the X-rays have penetrated the sample, which depends on the incident angle.

To analyse an XRF spectrum the intensity of the fluorescence radiation is key. It is dependent on many different factors like the geometries of the whole experiment, the absorption of the fluorescence radiation, the detector efficiency, and the penetration and information depth of the X-rays. One critical variable is the thickness of the sample. For TXRF the thin film approximation is used because it is assumed that the thickness of the sample is very, very small. Due to this approximation the formula for the intensity of the fluorescence radiation I simplifies to a linear relation (Eq. 2.2.10), because self-absorption can be neglected.

$$I^i = S^i c^i m \quad (2.2.10)$$

The sensitivity S only depends on fundamental parameters and measuring conditions which are constant for a experimental setup. The mass m of a specific element i is known and its concentration c is of interest. The relative sensitivity factor S_{rel}^i (Eq. 2.2.11) is calculated or determined experimentally with a standard sample s .

$$S_{rel}^i = \frac{I^i}{I^s} \quad (2.2.11)$$

The concentration of an element in the sample c^i can be calculated with Equation 2.2.12. All the used variables are listed in Tab. 2.6.

$$c^i = \frac{I^i}{I^s} \frac{1}{S_{rel}^i} c^s \quad (2.2.12)$$

For a detailed understanding of XRF and in particular TXRF, it is recommended to study the book "[Total-Reflection X-Ray Fluorescence Analysis and Related Methods](#)" by [Klockenkämper and Bohlen \(2015\)](#).

2.2.6 Capacity Analysis with Radiotracers Dilution Experiment

Dilution experiments utilising radiotracers are a simple and effective tool for the study of ion-exchange capacity and to acquire information about the nature of ion-exchange processes. Such experiments utilise the simple proportionality between readily measurable tracer activity and analyte concentration to assess the distribution of material between two phases. Radiotracers are easy to detect via γ -spectroscopy if they decay by gamma emission. They can be produced via neutron capture in a reactor which is already explained in previous section 2.2.4 *Neutron Activation Analysis (NAA)*.

In this thesis the strontium (Sr) or caesium (Cs) capacity of the zeolite samples were of interest.

Symbol	Name
c^i	concentration of an element i
c^s	concentration of the internal standard s
E_{photon}	energy of the detected photon
I^i	intensity of the fluorescence radiation for an element i
I^s	intensity of the fluorescence radiation for the internal standard s
m	mass of an element i
n	number of produced electrons
S^i	sensitivity of an element i
S_{rel}^i	relative sensitivity factor of an element i relative to internal standard s

Table 2.6: Parameters for TXRF.

Both Sr and Cs are available as readily soluble nitrate salts. The activation of strontium nitrate $\text{Sr}(\text{NO}_3)_2$ can produce the two strontium radioisotopes ^{85}Sr and ^{89}Sr due to neutron capture. The cross sections are quite small for both processes (Tab. 2.7), but ^{89}Sr decays for 100 % via β^- and cannot be used for γ -spectroscopy. The main γ -line for ^{85}Sr with an intensity of 96 % is at 514.0048 22 keV ([National Nuclear Data Center, c](#)) and the full set of the γ -lines can be looked up in the Appendix *G Spectra of the Capacity Experiments*. The activation of caesium nitrate CsNO_3 is more efficient because the relative abundance of the nuclide ^{133}Cs is 100 %. The cross section for the production of the radioisotope ^{134}Cs is 29 b ([National Nuclear Data Center, b](#)). For ^{134}Cs two γ -lines were significant. The one at 604.721 2 keV has an intensity of 97.62% and the other at 795.864 4 keV has an intensity of 85.46% ([National Nuclear Data Center, a](#)). The full set of the γ -lines can be looked up in the Appendix *G Spectra of the Capacity Experiments*.

The activity A of the activated nitrates should be of the magnitude of 10^5 Bq to allow reasonable measure times later on. A was calculated before the activation of the nitrates to know how much nitrate can be activated safely and with a reasonable decay time before handling the active substance. The calculation is already explained in previous section 2.2.4 *Neutron Activation*

Isotope	M in u	H in %	σ in b
^{84}Sr	83.913425(4)	0.56(1)	0.8221
^{86}Sr	85.909262(2)	9.86(1)	
^{87}Sr	86.908879(2)	7.00(1)	
^{88}Sr	87.905614(2)	82.58(1)	0.008688

Table 2.7: Chemical properties of the stable strontium isotopes in $\text{Sr}(\text{NO}_3)_2$. The atomic mass of the element M ([Generalic, *Eni.*, 2019](#)), the relative abundance of the nuclide H ([Generalic, *Eni.*, 2019](#)), the cross section $\sigma_{\text{Sr}84 \rightarrow \text{Sr}85}$ ([National Nuclear Data Center, d](#)) and the cross section $\sigma_{\text{Sr}88 \rightarrow \text{Sr}89}$ ([National Nuclear Data Center, e](#)) are listed.

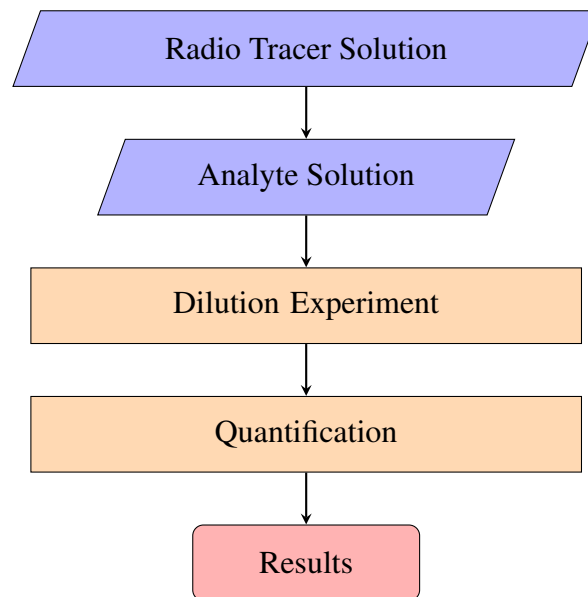


Figure 2.7: Flow chart of a general experimental set up for capacity determination.

Analysis (NAA).

The efficiency of the γ -detector "Dicker Fritz" at the Atominstitut of TU Wien is only about 1 %. To achieve about 10 000 counts per 5 minutes measure time the sample must have at least about 3.3 kBq. The activated nitrates had an activity of the magnitude of 10^5 Bq because they were used for the production of different stock solutions of different ion concentration. These stock solutions had the lowest possible activity for reasonable measurement times.

For a dilution experiment typically, a suitable tracer is prepared, tracer-containing analyte solutions are created and the solutions are then applied to the material under study followed by homogenisation. The phases are subsequently separated, the radionuclide distribution quantified and the resulting data analysed (Fig. 2.7).

The half-life time of the used radiotracers $^{85}_{38}\text{Sr}$ (about 64.849 days ([National Nuclear Data Center, c](#))) and $^{134}_{55}\text{Cs}$ (about 2.0652 years ([National Nuclear Data Center, a](#))) are relatively long which allows stress-free experiments. Mixing, homogenisation and separation may be carried out by a variety of means which is explained in detail in chapter 4 *Determination of the Capacity for Sr and Cs*. The distribution of the nuclides is easily quantified by gamma-spectroscopic measurements as described in previous section 2.2.4.

3. Characterisation of the Sample

Materials

In this chapter the experimental set-ups and their results will be discussed. The zeolites were first measured by Infrared (IR) Spectroscopy to determine whether they are really out of clinoptilolite quickly. The reaction to heat was determined with combining Differential Scanning Calorimetry (DSC) and Thermogravimetry Analysis (TGA). After these pre-trials, the actual determination of the zeolite elements was done by Neutron Activation Analysis (NAA) and Total Internal Reflection X-Ray Fluorescence (TXRF). The determined elemental composition of the samples was compared to literature results of clinoptilolite. Additionally, a Powder X-Ray Diffraction (PXRD) was done.

The company *LITHOS Industrial Minerals GmbH* provided the following information about the zeolite samples. Sample A and D have a grain size of 0-125 μm , sample B of 0-100 μm and sample C of 0.5-2 mm. Sample C was milled for the analysis IR, STA/TGA, NAA, TXRF and PXRD. Sample A, B and C should contain 90 % of clinoptilolite and sample D only less than 60 %.

3.1 IR Spectroscopy and Results

The infrared spectra were observed in a range from 450 to 4000 cm^{-1} . The measurements were done in the transmittance (%T) mode. The expected result for minerals containing clinoptilolite can be looked up at previous section 2.2.1 *Infrared (IR) Spectroscopy*. The IR spectra for the four samples are plotted in Fig. 3.1.

IR Spectroscopy allows rapid qualitative characterisation of zeolite type ([Tsitsishvili et al., 1992](#)). This method was used for quick classification of the samples and to check the information provided about the materials.

[Tsitsishvili et al.](#) described most of the observed peaks. The peak ranges are summarised in Tab. 2.2. The maximal band in the area 900-1100 cm^{-1} corresponds to the Al content of the sample ([Tsitsishvili et al., 1992](#)).

The relevance of the peak in the range of 1400-1550 cm^{-1} is not found in the book. The peak only occurs for sample A and B significantly. Normally, this peak is not found in an IR spectrum for clinoptilolite. [Elghniji et al.](#) did some research on clinoptilolite-supported TiO_2 and said the peak in the range of 1400-1550 cm^{-1} corresponds to "stretching vibrations of the Ti-O-Ti in

TiO₂" (Elghniji et al. (2018)) after a paper from Peter et al. Peter et al. (2014). Eventually, the peak is caused by tetramethylammonium (TMA) (Murakami and 7th International Zeolite Conference Tokyo, 1986) or by urea (Byler et al., 1991). Snellings et al. did IR spectra for clinoptilolite tuff, calcium aluminate hydrates and calcium silicate hydrates. The two hydrates both had a peak in the range 1400-1550 cm⁻¹, which corresponds to carbonate asymmetric stretching. Sadeghi et al. did some research on a CuO NPs/Ag-clinoptilolite zeolite and said "the absorption bands in the 1467 cm⁻¹ region is referred to C–C bonding of probable trivial impurities existing in the applied stock materials" (Sadeghi et al., 2016).

Furthermore, the peaks at around 3441 and 1632 cm⁻¹ were explained by vibrations of absorbed water molecules, which is consistent with the values in Tab. 2.2. Also in this range are the peaks which are caused by "H–O–H bending O–H bonding (hydroxyl groups) vibrations and discrete water absorption bands of the clinoptilolite" (Sadeghi et al., 2016).

The IR spectra of the samples confirmed that all four samples contain clinoptilolite. However, as mentioned above, the exact content cannot be determined by this method. To determine the exact origin of the peak in the range 1400-1550 cm⁻¹ found for sample A and B, a more detailed investigation (not carried out) would be necessary.

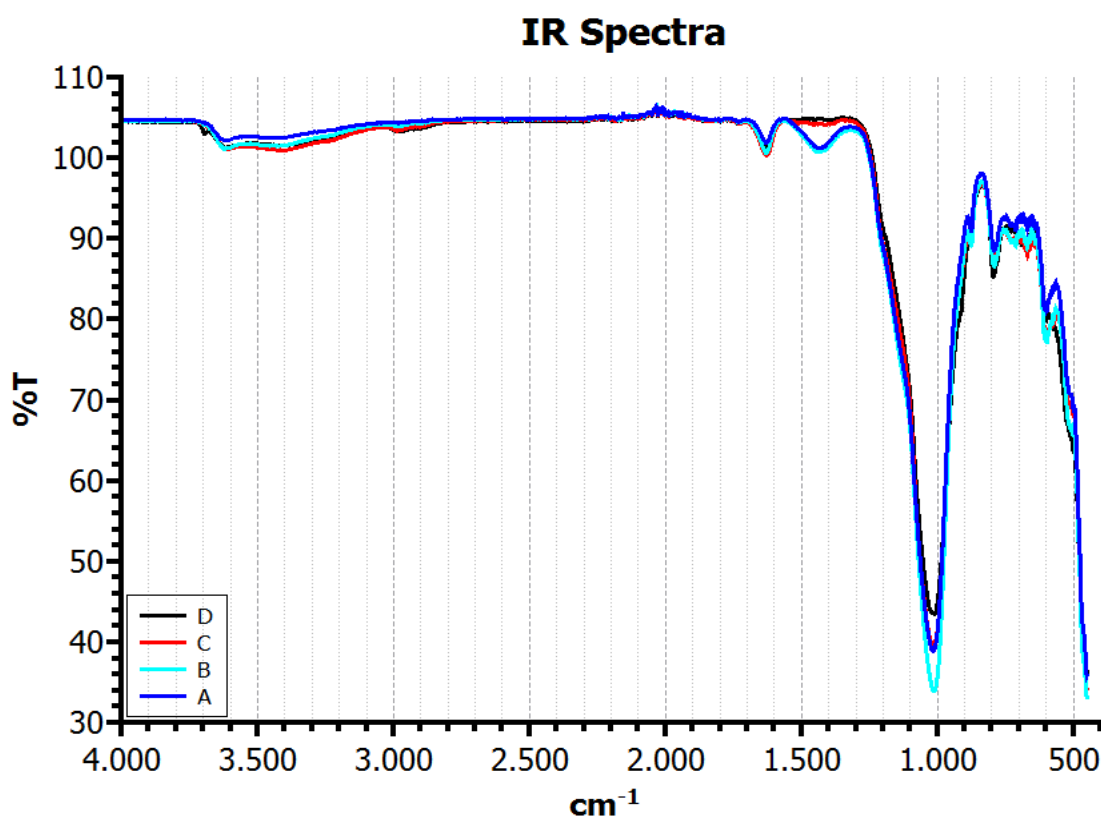


Figure 3.1: IR spectra for the four zeolite samples.

3.2 STA Experiment and Results

The stability of the zeolite samples against heat was checked with Simultaneous Thermal Analysis (STA). The samples were measured in the range 20-450°C and the temperature changed 10 K/min. It took 43 minutes to reach the end temperature of 450°C. The cooling process down to 20°C was done by 20 K/min steps. For each zeolite sample A, B, C (provided and milled form) and D the crucibles were filled up in two ways. Once just a tiny sample size was used and the other time, the whole crucible was filled up. The data names are explained in Tab. 3.1. The measurements were done with the help of Christian Knoll at the Faculty of Technical Chemistry of TU Wien.

Under heating, zeolites may lose water and the theory of thermal analysis is explained in detail in the previous section 2.2.2 *Simultaneous Thermal Analysis (STA)*. The stability of the structure of the samples under heating was assessed in preparation for subsequent elemental analytical experiments.

A crucible filled up with sample A was exposed to the labour air for about six hours until the measurement was done. Fig. 3.2 shows the results for zeolite A. It might be possible that the zeolite caught water molecules out of the air while awaiting measurement, but for an exact answer about the absorbed water amount, the sample size should have been weighted before loading it to the instrument.

All the data is illustrated in Fig. 3.3. The mass of the samples and the loss in per cent can be looked up in Tab. 3.2. [Tsitsishvili et al.](#) wrote that clinoptilolite loses about 8% of its free volume at 300°C. Considering that the samples were heated up to 450°C for this experiment, this is consistent with the collected data for the four zeolite samples A, B, C and D.

It is clear from the data that the water content of the sample materials does not change drastically over the temperature range studied, and no further consideration is necessary for the following NAA and TXRF experiments.

Sample	Data Name	Description
A	VG_A_20-450_10Kmin-1_N2_open	
	VG_A_voll_20-450_10Kmin-1_N2_open	full crucible
	VG_A_wait_voll_20-450_10Kmin-1_N2_open	exposed to air before measurement
B	VG_B_20-450_10Kmin-1_N2_open	
	VG_B_voll_20-450_10Kmin-1_N2_open	full crucible
C	VG_C_20-450_10Kmin-1_N2_open	
	VG_C_voll_20-450_10Kmin-1_N2_open	full crucible
	VG_Cm_20-450_10Kmin-1_N2_open	milled
	VG_Cm_voll_20-450_10Kmin-1_N2_open	milled, full crucible
D	VG_D_20-450_10Kmin-1_N2_open	
	VG_D_voll_20-450_10Kmin-1_N2_open	full crucible

Table 3.1: Explanation of the STA data names.

Sample	Mass in mg	Mass loss in %
VG_A	8.4	7.14
VG_A_voll	21.0	7.80
VG_A_wait_voll	22.5	7.87
VG_B	8.5	8.94
VG_B_voll	20.1	9.45
VG_C	11.6	9.66
VG_C_voll	36.8	10.08
VG_Cm	8.9	10.34
VG_Cm_voll	32.8	10.88
VG_D	8.4	8.33
VG_D_voll	27.0	8.85

Table 3.2: The mass of the measured samples and the mass loss in %.

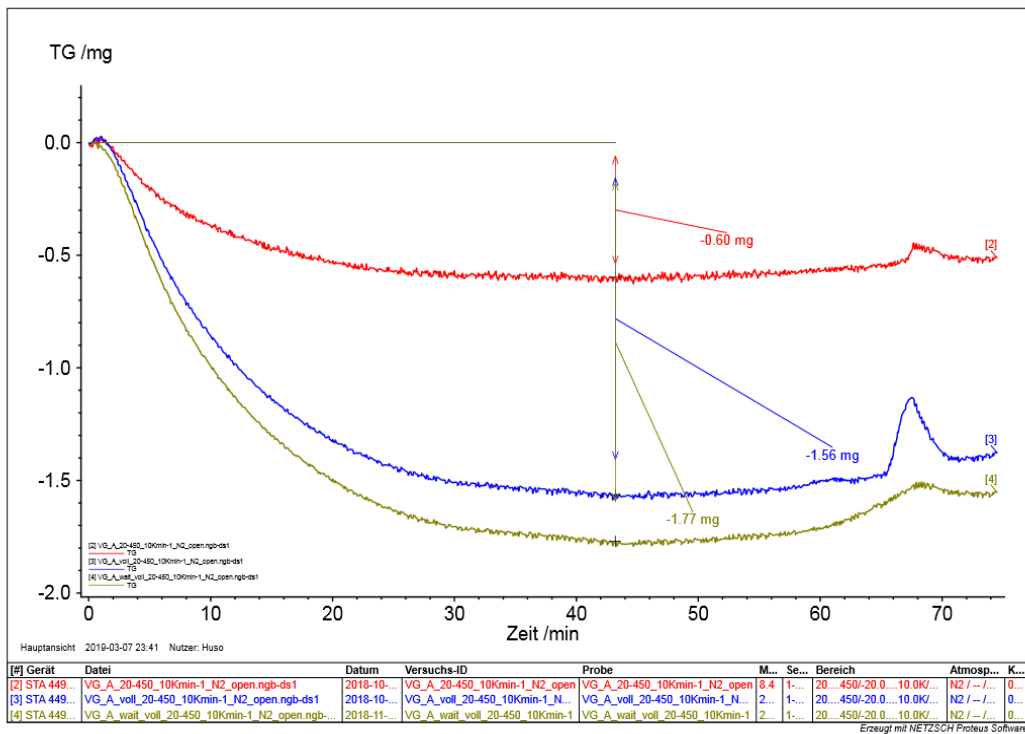


Figure 3.2: STA curves for zeolite A. Red: VG_A; Blue: VG_A_voll; Green: VG_A_wait_voll.

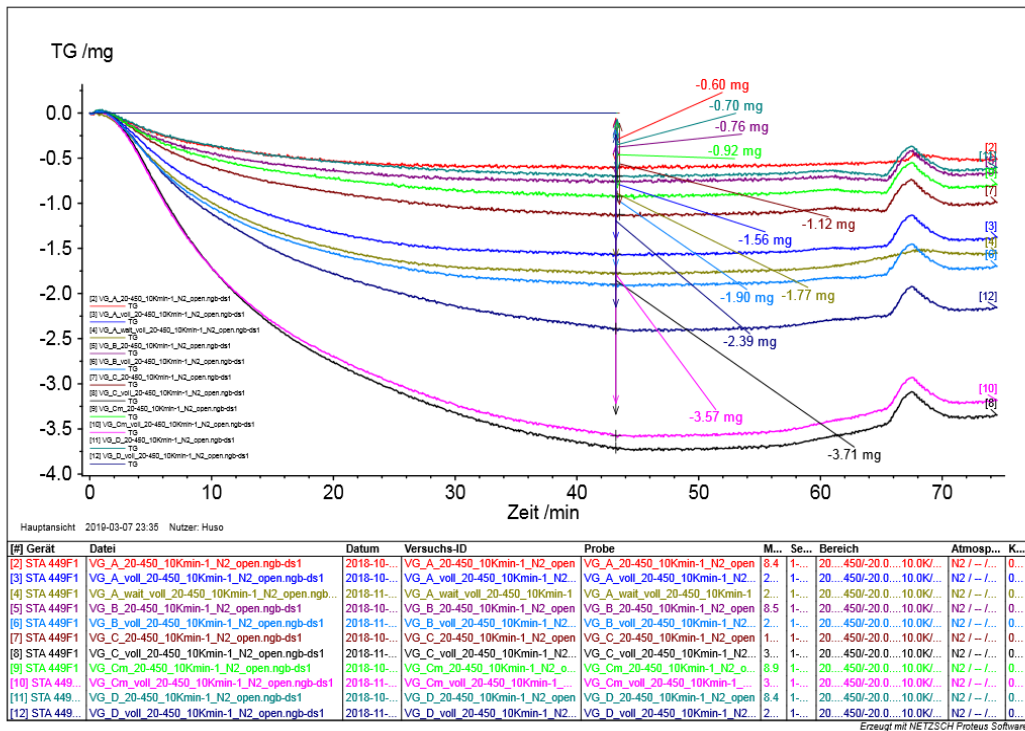


Figure 3.3: STA curves for all measurements.

3.3 NAA Experiment

For this thesis the TRIGA Mark II reactor of the Atominstitut was used, which is part of the Technical University of Vienna. The acronym TRIGA stays for Training, Research, Isotope Production, General Atomic and the reactor is of the swimming-pool type. The flux density in the used irradiation tube is $1.7 \cdot 10^{12} \text{ cm}^{-2}\text{s}^{-1}$.

The Neutron Activation Analysis (NAA) was used to quantify the principal elemental components of zeolite materials. Normally zeolites are not analysed with NAA because the access to a research reactor is limited. NAA allows precise, simultaneous determination of multiple elements. The procedure and analyses are relatively straightforward, well-known and proven. Before the measurement was started, the specific activities (Eq. 2.2.7) for different irradiation times were calculated for the ingredients after previous section 2.1.1 *Clinoptilolite*. The necessary information is provided in Appendix Tab. A.1. The specific activity for an irradiation time of 30 s, 60 s, 90 s, 120 s and 180 s can be looked up in the Appendix Tab. A.2. After this consideration, it was chosen to activate the samples for 60 s and the zeolite powders were weighted in a micro tube to perform the pilot tests (Appendix Tab. A.3). The micro tube was put in an activation tube with its lid first. To keep the micro tube in its position, a tampon with some drops of water was placed on top of it and was expanded with some drops of water. The activation tube was put in the air pressure tube, which leads to the reactor bottom first. The detailed setup is shown in Fig. 3.4. After activation, it was necessary to let the samples decay between 9 and 11 minutes in the air pressure tube before continuing the experiment. The following handling with the sample in the micro tube was done with tweezers and it was tried to keep the biggest possible distance between the active sample and the researcher's body. The micro tube was removed out of the activation tube and measured with the γ -spectrometer "Dicker Fritz".

It has proven that an irradiation time of just 30 s is enough for an efficient evaluation. The

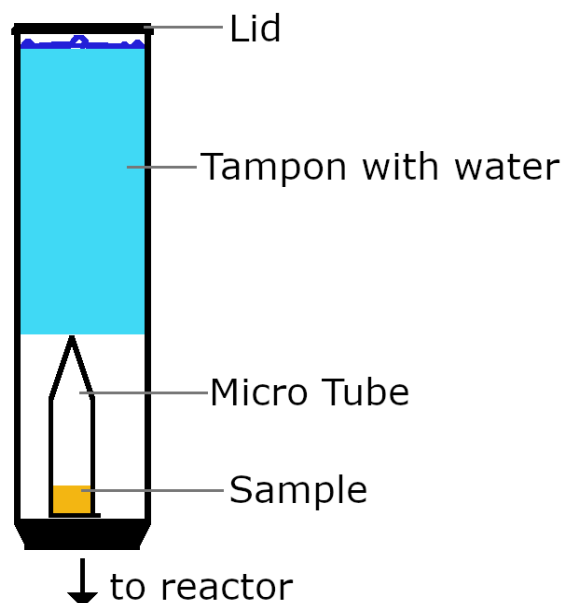


Figure 3.4: Position of the sample for the activation process.

zeolite and four Coal Fly Ash (CFA) samples were weighted in eight different micro tubes (Appendix Tab. A.4). Each zeolite sample was activated together with a Coal Fly Ash sample at the same time. This allows a very accurate analysis of the chemical components of the zeolites. The two micro tubes were loaded next to each other in the activation tube. The setup is as in Fig. 3.4 just with two micro tubes at the bottom.

Two unforeseen complications occurred. Due to building work at the ATI institute, the compressed air was turned off. The remaining air pressure was enough to send the first experiment with the sample A to the reactor for activation. But there was not enough air pressure left to push the activation tube back to the labour. The reactor was turned off to prevent to get a too hot zeolite and CFA powder. After the problem was figured out to be the turning off of the compressed air, it was turned on again. The activation tube was pushed out of the reactor and was not used for further experiments. For further use, the sample A and CFA were weighted again in two new separate micro tubes. Also, another sample C and corresponding CFA were activated and measured the next day because the first measurement was deleted accidentally.

It was necessary to let the samples decay in the air pressure tube only between 7 and 9 minutes before continuing the experiment due to the shorter irradiation time. The handling of the micro tube with tweezers was the same as in the pilot tests. The micro tube with the zeolite sample was always measured first with the γ -spectrometer "Dicker Fritz". Afterwards the micro tube with the CFA sample was measured. The times can be found in Tab. A.5. The spectra of the experiments can be looked up in the Appendix A. The details of the CFA are provided in Appendix H.

For analysis the net peak area of a specific γ -peak in the zeolite data $Zeolite_{Net\ Peak\ Area}$ was compared with the net peak area of the same peak $CFA_{Net\ Peak\ Area}$ and the corresponding mass for this element $mass_{CFA}$ in the CFA data. That way it was possible to calculate the amount of this element in the zeolite $mass_{Zeolite}$. For the calculation of $mass_{CFA}$ the radioactive decay of the CFA sample, which happens in the interval between the measurement of the zeolite and the CFA micro tube, have to be considered. The used ratio is shown in Equation 3.3.1 and the detailed procedure is to be found in the Appendix A.

$$Zeolite_{Net\ Peak\ Area} : CFA_{Net\ Peak\ Area} = mass_{Zeolite} : mass_{CFA} \quad (3.3.1)$$

Silicon cannot be determined directly with the spectra, because it does not have a detectable γ -peak. Georg Steinhauser of the Institute of Radioecology and Radiation Protection (IRS) of Leibniz Universität Hannover gave the input to determine the Si content of the samples with help of ^{29}Al . During the activation process the stable ^{29}Si can convert into ^{29}Al by undergoing a (n, p)-reaction. This means an entering neutron is forcing a proton to leave the atom nucleus. By detecting the γ -peak of ^{29}Al (Alfassi, 1994) the silicon content of the sample can be calculated the same way as the other element amounts were determined. The counts of the ^{29}Al peak in the CFA spectra are in correlation with the silicon content in the CFA, which can be calculated with the CFA data sheet.

3.3.1 NAA Results

The γ -peaks of the detected elements are listed in Tab. 2.5. The weight percent of the detected elements aluminium (Al), silicon (Si), calcium (Ca), magnesium (Mg), potassium (K), sodium (Na), titanium (Ti), manganese (Mn) and vanadium (V) are shown in Tab. 3.3. For the Mg, value the peak with the energy 843.76 10 keV was used because this peak has an intensity of 71.800 %. For the Na value the mean value of both Na peaks was calculated because the intensity for both is over 99 %. For the Mn value, the peak with the energy 846.7638 19 keV was used because this peak has an intensity of 98.85 %. Tab. 3.4 shows the results converted to the oxide form. The conversion factor c_{Al} for aluminium is shown in Equation 3.3.2. The molar mass of the element is divided by the molar mass of the elemental oxide. The NAA element results have to be divided by the conversion factor for the specific element to get the weight percentage of the oxide in the zeolite sample.

$$c_{Al} = \frac{M_{Al}}{M_{Al} + 2 \cdot M_O} \quad (3.3.2)$$

This allows to compare the gathered data in Tab. 3.4 to the literature data provided in Appendix D, which is summarised in Tab. 3.5. It is obvious that the silicon dioxide SiO_2 and the aluminium oxide Al_2O_3 content of sample A and B are in the same range as for different other clinoptilolite samples. For sample C the SiO_2 and the Al_2O_3 content is a bit lower. Sample D has a much higher SiO_2 content than the other clinoptilolite samples, but the Al_2O_3 content lies in the range. This is consistent because D is the external sample, which should only contain less than 60 % of clinoptilolite. The content of the other components can vary a lot. All the other results for the compounds lie in the range which can be found in the literature data. Only Appendix Tab. D.10 provides uncertainties of the values. Titanium dioxide TiO_2 and manganese(II) oxide MnO were not determined by all works.

The pie charts (Fig. 3.5) present the distribution of the main elements Si, Al, Ca, Mg, K, and Na in the four samples and provide a quick overview. The detailed occurrence of the detected elements compared of the four samples is illustrated in Fig. 3.6 and Fig. 3.7. It can be seen that the Al content decreases from sample A to C and is the highest for the external sample D (Fig. 3.6(a)). The Si content (Fig. 3.6(b)) is the lowest for sample C and the highest for sample D. For sample A and B it is around 30 %, which is compatible with the Al content for these samples, which is around 6 %. The chemical formula of clinoptilolite (Eq. 2.1.3) indicates 6 Al atoms and 30 Si atoms. The properties of the K content (Fig. 3.6(d)) are similar to the properties of the Ca content (Fig. 3.6(c)). The occurrence in sample B is a bit higher than in sample A. It is quite lower for sample C and is the smallest for sample D. The Na content decreases from sample A to C and is quite different for sample C (Fig. 3.6(e)). Fig. 3.7(a) (Mg content) and Fig. 3.7(b) (Ti content) show clearly that sample D was mined at an external site. The Mn content (Fig. 3.7(c)) and the V content (Fig. 3.7(d)) vary to the same amount. The occurrence decreases from sample A to C and increases again for sample D.

Fig. 3.8 allows to compare the components for all 4 zeolites. Fig. 3.9 zooms in to an max-

imum occurrence of 7 wt.%. It can be seen as a similarity of sample A (dark blue line) and B (light blue line). For the elements aluminium, potassium, calcium and sodium the red lines are nearly parallel to the blue ones. This can be due to a mining at the same or a nearby spot. This conclusion is consistent with the information provided by the company. Sample D is an external one, which can be concluded due the higher aluminium content and the distribution of the other elements. Also the silicon content is the highest for the external sample D. The content of magnesium, titanium, manganese and vanadium is each time less than 0.1 %. It would be interesting to analyse all the trace elements of the four zeolites exactly to learn more about the mining site.

The uncertainty of the Si and K values are higher than for the other elements. As described above, the ²⁹Al peak was used for the determination of Si, which only had about 2600 cts and an uncertainty of 5 % in average. Due to the small probability of a (n, p)-reaction, the uncertainty bars of the Si content are bigger. For K the cross section is also quite small and an activation of just 30 s was too short for a better determination.

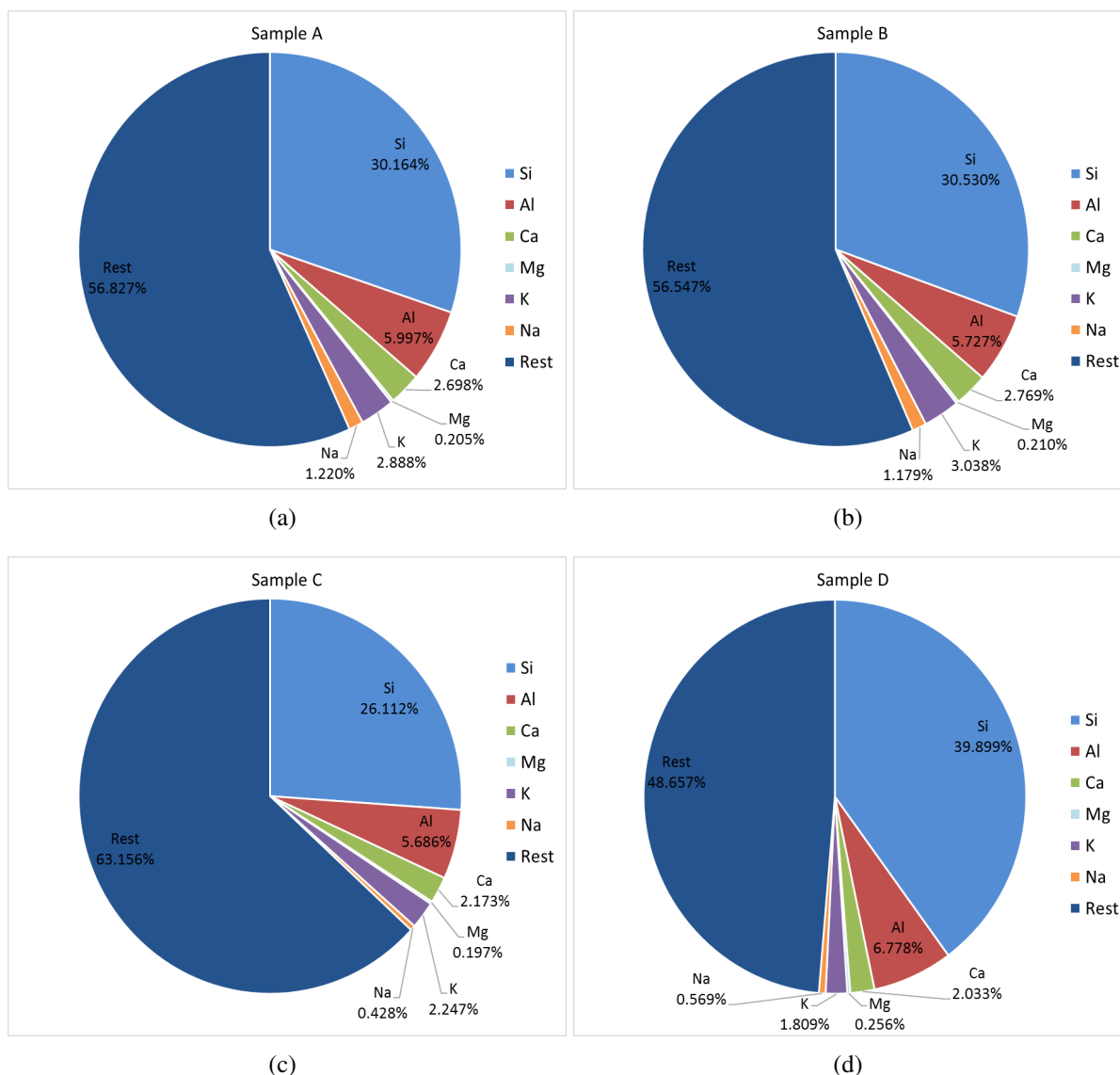


Figure 3.5: Distribution of the main elements Si, Al, Ca, Mg, K and Na in the four zeolites.

The NAA results show that samples A and B satisfy the chemical equation of clinoptilolite $Al_6Si_{30}O_{72} \cdot 21H_2O$ quite well. Both have a silicon content of about 30 wt.% and an aluminium content of about 6 wt.%. The silicon and aluminium content of sample C is a bit smaller. Sample D contains more silicon and aluminium, which indicates some additional mineral. The comparison with literature values substantiates these conclusions.

Element	A		B	
	wt. %	σ	wt. %	σ
Si	30.16	3.46	30.53	2.12
Al	6.00	0.12	5.73	0.11
Ca	2.70	0.15	2.77	0.14
Mg	0.21	0.01	0.21	0.01
K	2.89	0.42	3.04	0.72
Na	1.22	0.03	1.18	0.03
Ti	0.09	0.01	0.10	0.01
Mn	0.023	0.001	0.021	0.001
V	0.001	0.001	0.001	0.001
	C		D	
	wt. %	σ	wt. %	σ
Si	26.11	3.17	39.90	4.42
Al	5.69	0.12	6.78	0.14
Ca	2.17	0.12	2.03	0.10
Mg	0.20	0.01	0.256	0.01
K	2.25	0.30	1.81	0.10
Na	0.43	0.02	0.57	0.02
Ti	0.09	0.01	0.12984	0.01
Mn	0.017	0.001	0.020	0.001
V	0.001	0.001	0.001	0.001

Table 3.3: Element composition of the four zeolites.

Compound	A		B	
	wt. %	σ	wt. %	σ
SiO₂	64.53	7.39	65.31	4.52
Al₂O₃	11.33	0.22	10.82	0.20
CaO	3.78	0.20	3.87	0.20
MgO	0.34	0.01	0.35	0.01
K₂O	3.48	0.51	3.66	0.86
Na₂O	1.64	0.04	1.59	0.03
TiO₂	0.15	0.01	0.16	0.01
MnO	0.03	0.01	0.03	0.01
	C		D	
	wt. %	σ	wt. %	σ
SiO₂	55.86	6.77	85.36	9.45
Al₂O₃	10.74	0.21	12.81	0.25
CaO	3.04	0.17	2.84	0.14
MgO	0.33	0.01	0.43	0.02
K₂O	2.71	0.37	2.18	0.12
Na₂O	0.58	0.02	0.77	0.02
TiO₂	0.15	0.01	0.22	0.02
MnO	0.02	0.01	0.03	0.01

Table 3.4: Element composition of the four zeolites converted to the oxide form.

Compound	Range in wt. %	
SiO₂	60.13 (Tab. D.4)	to 72.75 (Tab. D.8)
Al₂O₃	10.88 (Tab. D.13)	to 16.12 (Tab. D.8)
CaO	0.1 (Tab. D.10)	to 4.17 (Tab. D.13)
MgO	0.0 (Tab. D.8)	to 1.46 (Tab. D.13)
K₂O	1.20 (Tab. D.13)	to 8.6 (Tab. D.10)
Na₂O	0.24 (Tab. D.14)	to 4.32 (Tab. D.1)
TiO₂	0.04 (Tab. D.2)	to 0.41 (Tab. D.9)
MnO	0.001 (Tab. D.14)	to 0.11 (Tab. D.15)

Table 3.5: Range of the chemical composition of clinoptilolite in wt. % after Appendix D.

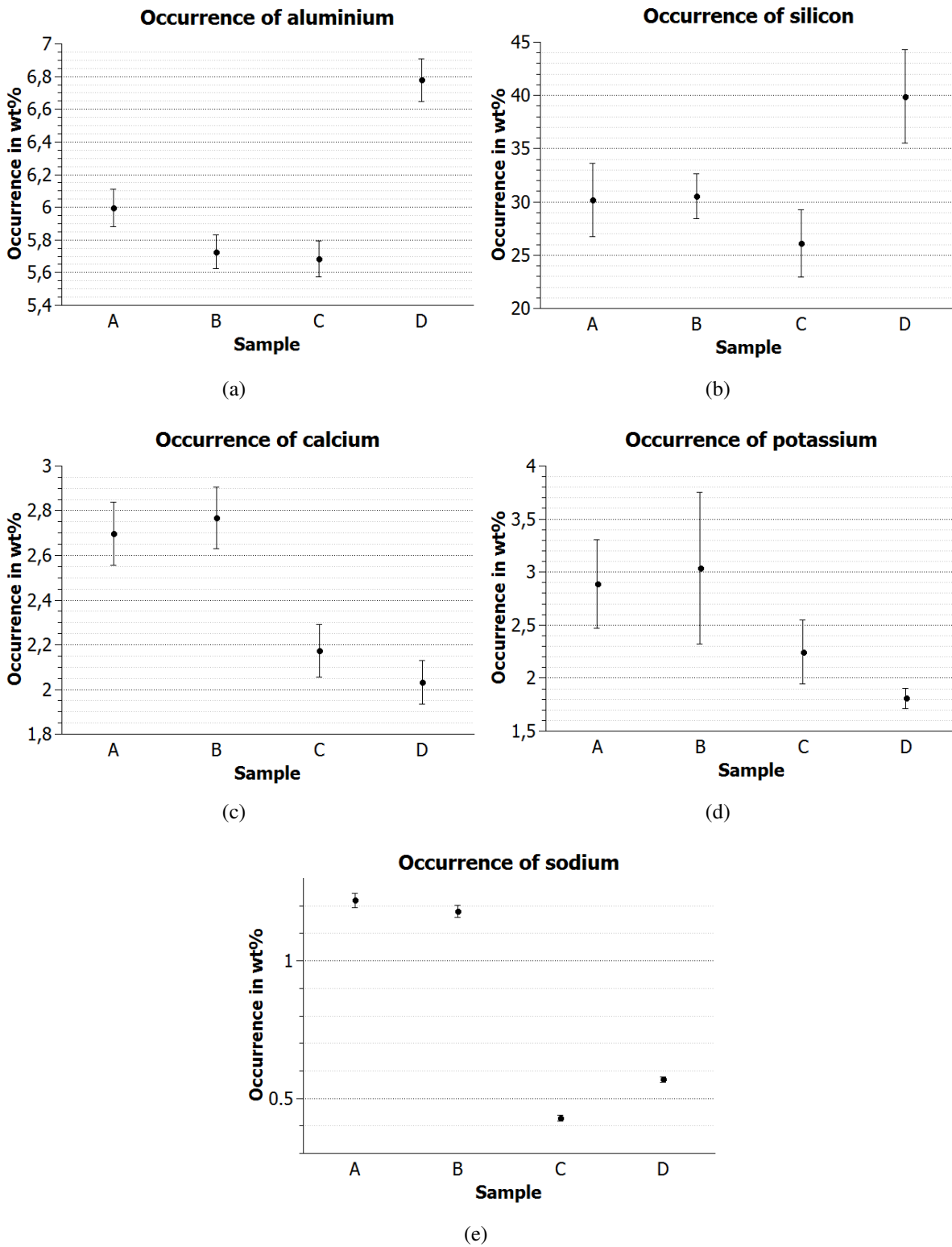


Figure 3.6: Occurrence in percent of Al, Si, Ca, K and Na in the zeolites.

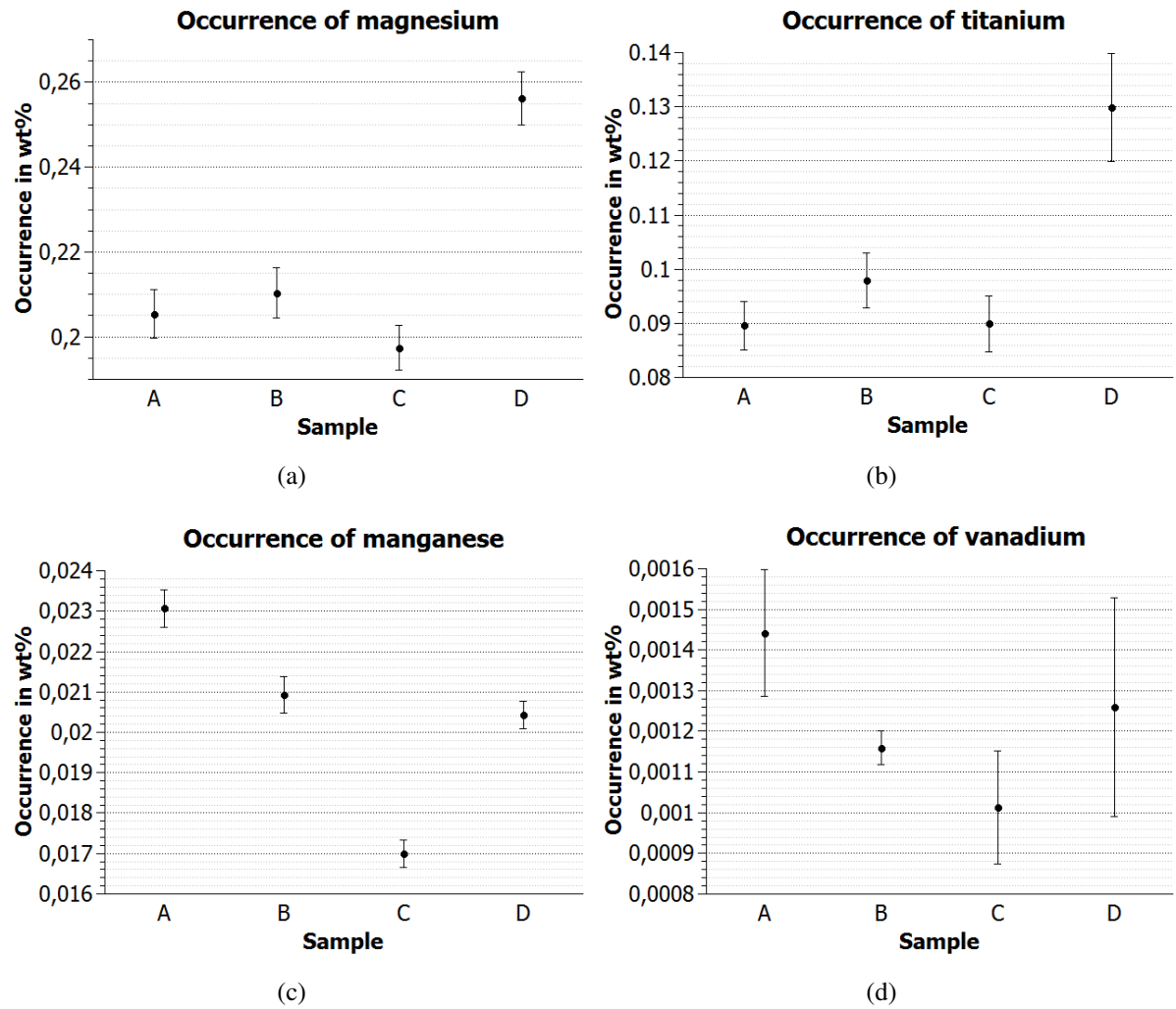


Figure 3.7: Occurrence in percent of Mg, Ti, Mn and V in the zeolites.

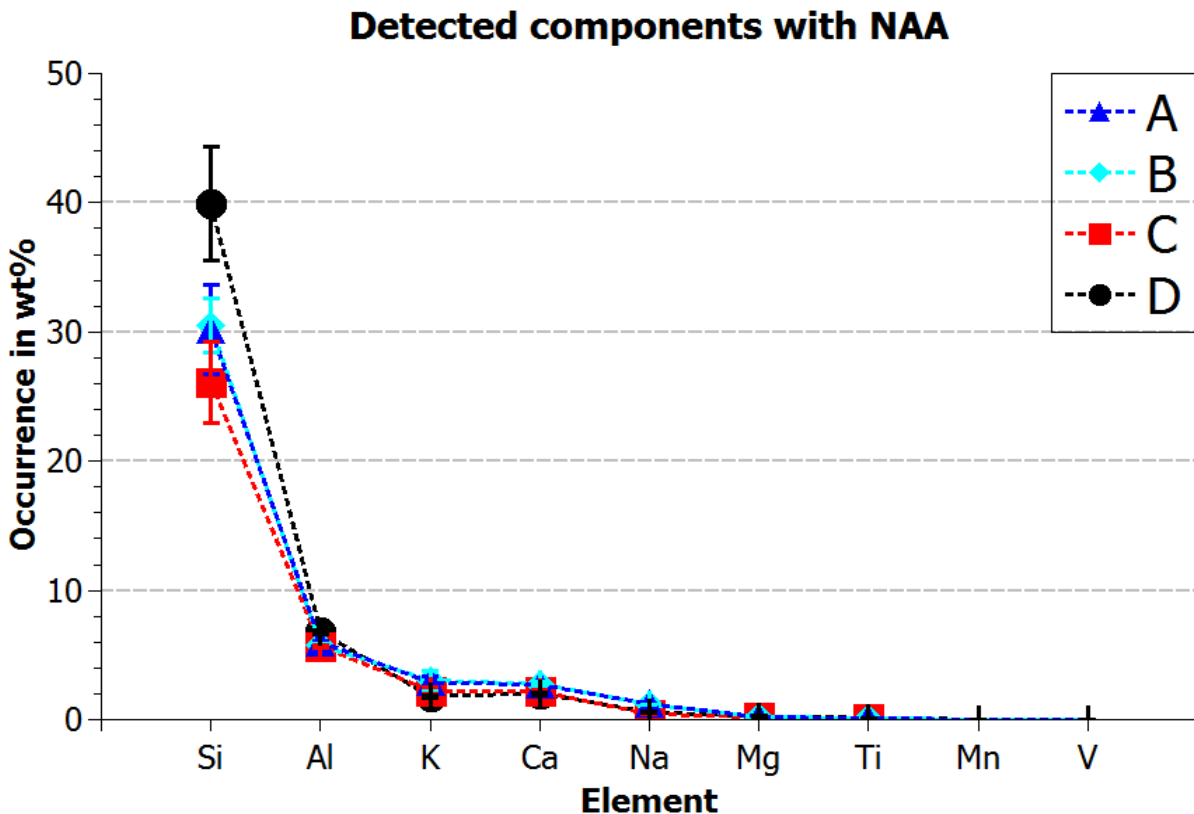


Figure 3.8: Occurrence in percent of all detected components in the zeolites.

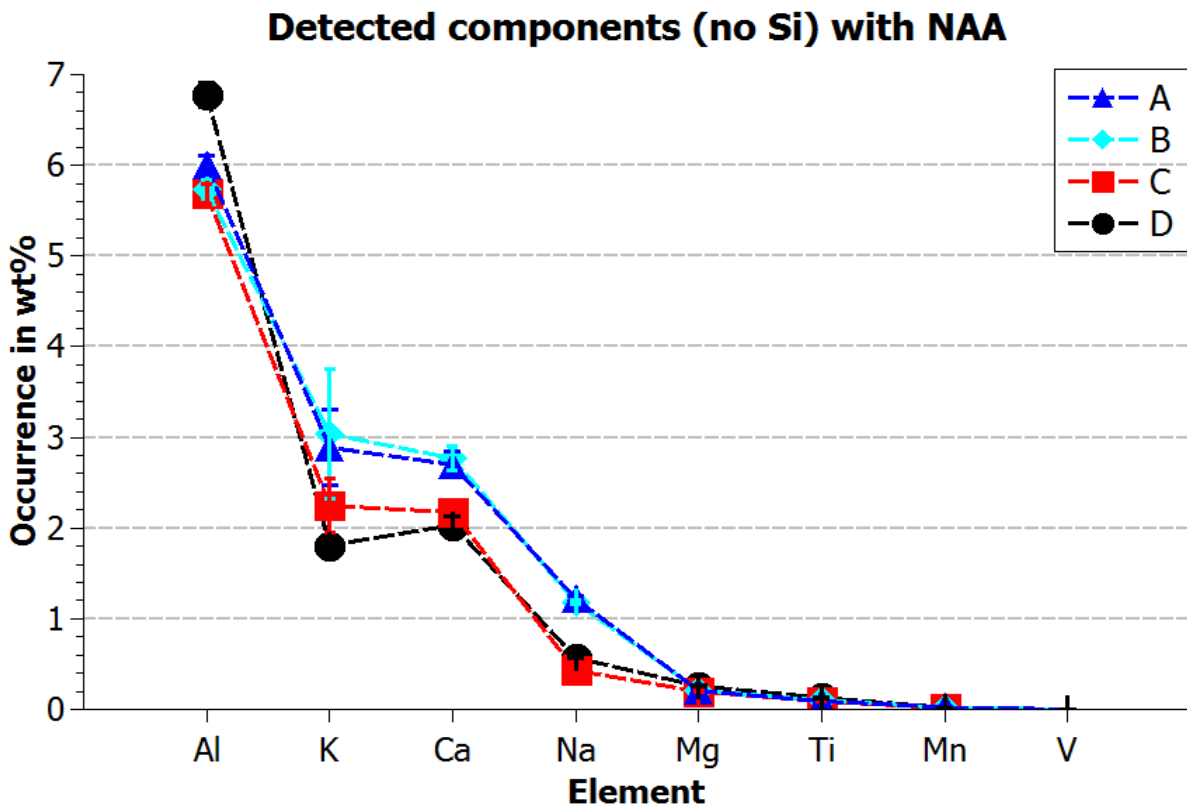


Figure 3.9: Occurrence in percent of all detected components except Si in the zeolites.

3.4 TXRF Experiment

The measurements and analysis were done by Thomas Bretschneider, who is part of the X-ray group of TU WIEN Atominstitut. The instrument Atomika 8030C was used. It works with W-L β -excitation and measures in a helium atmosphere. The helium atmosphere is suitable for the analyses of light elements, because it minimises the absorption of the radiation. For each zeolite sample five samples were prepared on carriers and measured separately. The same was done for a standard reference material. The zeolite C was milled for the TXRF measurements. The theory of TXRF can be reread in previous section 2.2.5 *Total External Reflection X-Ray Fluorescence Analysis (TXRF)*.

The characterisation of the zeolites by TXRF was carried out principally to gather complementary information about the silicon content of the samples. Furthermore, it was of interest to compare the TXRF results to the NAA results to validate the sampling procedure applied for TXRF.

The zeolite powder was applied to Plexiglas reflectors, which are mainly out of hydrogen, carbon and oxygen. The carriers were tapped vertically on the table so most of the powder had fallen off again. Only a very thin layer of the sample - optimally one particle layer - stayed on the reflectors and was used for the measurement. The Atomika 8030C calculates concentration proportional constants of the elements with the fundamental parameters of the experiment set-up and the thin film approximation. For the analysis the thin film approximation can be used, because of the way the samples were produced. The Atomika 8030C software requires the measurement of an internal standard or a specific element can be set as the internal standard. For the analysis in this work the element silicon was set to the internal standard. The quantification program of the Atomika 8030C calculates with this chosen internal standard the element specific concentration proportional constants. The proportional constant of silicon was set to 1000. These element proportional constants can be looked up in the Appendix B.

The mean element proportional constants of the detected elements aluminium (Al), silicon (Si), potassium (K), calcium (Ca), titanium (Ti), iron (Fe) and nickel (Ni) were calculated out of the data results, which Atomika 8030C had provided. This method does not allow to determine absolute values for the different element content, because the amount of the zeolite powder on the carriers was too low to determine with a scale. The mean element proportional constants can be used to calculate the ratios between the determined elements. These ratios were corrected with a quantification factor (Eq. 3.4.1) which was calculated due to the measurement of a standard reference material. The details of the used Coal Fly Ash (CFA) are provided in Appendix H. The ratios for the mean element proportional constants r_m were calculated and compared to the ratios of the weight percent of the CFA standard data sheet r_s . The quantification factor k (Eq. 3.4.1) is the quotient of the real ratios to the measured ratios. This quantification factor k was multiplied to the ratios of the mean element proportional constants of the zeolites to correct them.

$$k = \frac{r_s}{r_m} \quad (3.4.1)$$

The step-by-step procedure can be looked up in the Appendix B.

3.4.1 TXRF Results

The raw data and the mean element proportional constants can be looked up in the Appendix B. It can be seen, the data of the five different sample carriers is consistent. This shows, that the used TXRF procedure and analysis provides reliable data. The spectra of the first carrier of the CFA is shown in Fig. 3.11 and the first carrier of sample A is shown in Fig. 3.10. The element proportional constants of the different carriers were calculated by the Atomika 8030C software out of the intensities provided in the spectra.

The calculated corrected ratios for the four samples are given in Tab. 3.7, Tab. 3.9, Tab. 3.11 and Tab. 3.13. The ratios calculated with the NAA results are shown in Tab. 3.8, Tab. 3.10, Tab. 3.12 and Tab. 3.14. This allows a comparison of the TXRF and NAA method. It is clear that the ratios are quite the same for both methods (Tab. 3.6). This means the NAA and the TXRF results are comparable and both methods are reliable.

The ratios which consider K and result from the TXRF measurement are more reliable because for the NAA the zeolite samples were only activated 30 seconds and measured for 300 seconds with the γ -spectrometer. This is too short for a good determination of potassium. For sample A comparing the NAA data ratios in Tab. 3.8 and the TXRF data ratios in Tab. 3.7, it can be seen that there is a difference of about 21 % between the ratio of K to Al. This huge difference is nearly the same for sample B (Tab. 3.10). Sample C shows a difference of the K to Al and Ca to Al ratios smaller than 10 % but the difference for the Si to Al and Ti to Al ratio is over 30 %. This huge difference can be caused by milling the original zeolite for the TXRF measurements. The milled power might not have had the same grain size as the industrial milled zeolites. Due to a bigger grain size the thin film approximation might not be suitable for the analysis of the

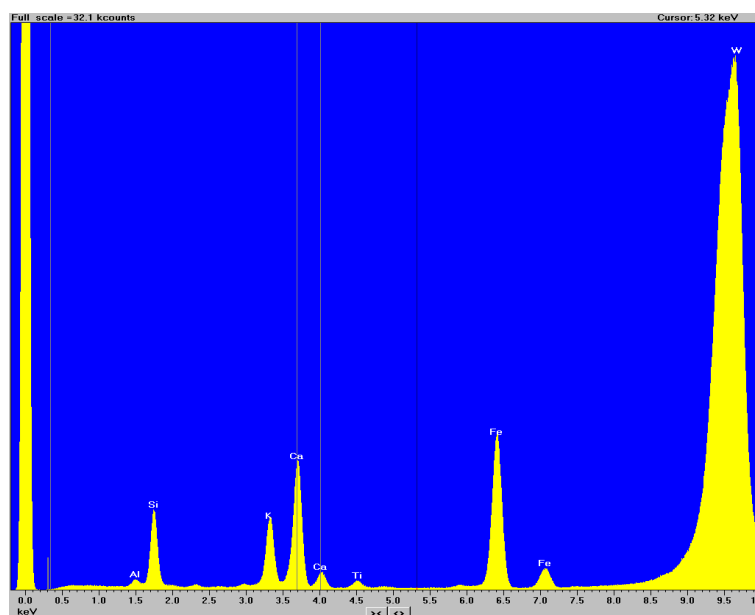


Figure 3.10: TXRF spectrum of sample A on carrier one (shortcut: A01). Element specific concentration proportional constants in Appendix Tab. B.1.

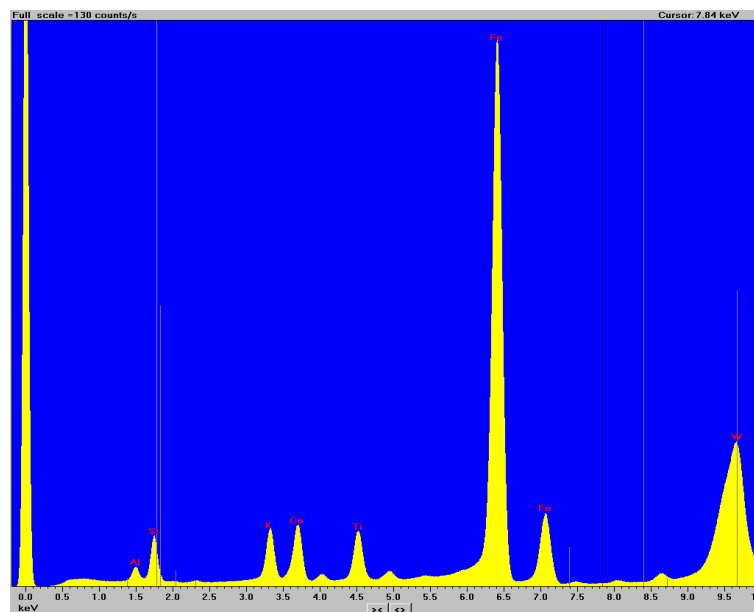


Figure 3.11: TXRF spectrum of the CFA on carrier one (shortcut: CFA01). Element specific concentration proportional constants in Appendix Tab. B.2.

TXRF data. The differences of the external sample D are completely different and for Ca to Al and Ti to Al also significantly higher than for the other samples (Tab. 3.14). This can be caused due a peak overlapping caused by the existent of different elements in the sample.

Sample		Si	K	Ca	Ti
A	Al	-6.61	20.90	5.39	-10.50
B	Al	-3.95	20.06	8.70	-2.18
C	Al	-33.61	3.81	5.66	-30.57
D	Al	-2.67	-6.04	20.78	-49.88

Table 3.6: Difference in per cent between the ratio of the TXRF data to the ratio of the NAA data.

As explained in previous section 2.1.1 *Clinoptilolite* the Si/Al ratio provides information about the zeolite type. It lies between 4.0 and 5.5 for clinoptilolite. The Si/Al ratio for sample A (Tab. 3.7 and 3.8) and B (Tab. 3.9 and 3.10) is in this range. This result also matches the information given by the company – A and B contain 90 % clinoptilolite. Fig. 2.2 indicates that both samples have a high Si content due to their ratio. The company also said C has a content of 90 % clinoptilolite. The calculated ratio with TXRF data is higher than 6 (Tab. 3.11), but the ratio of the more reliable NAA data is about 4.6 (Tab. 3.12). The NAA ratio compared with Fig. 2.2 indicates a clinoptilolite sample at the boarder of low and high silicon content. The Si/Al ratio of sample D (Tab. 3.13 and 3.14) is higher than 5.8 for both methods and this indicates some additional content next to clinoptilolite. For sample D this result matches the given information of an external sample. Appendix Tab. D.11 presents different elemental ratios for zeolites part of the heulandite-clinoptilolite group.

It is also possible to calculate the quantitative content of the detected elements with TXRF. A

device-specific sensitivity factor (Tab. 3.15) was calculated by division of the mean element proportional constant of CFA by the weight percentage content of CFA which is provided in the standard reference data sheet (H). The device-specific sensitivity factor depends on the detected element. The mean element proportional constants of the samples are divided by the corresponding device-specific sensitivity factor to obtain the quantitative content of a specific element. The results are shown in Tab. 3.16 and are also compared to the NAA results. Iron was not detectable by NAA due to short activation times. The TXRF values are always lower than the NAA values which can be explained by absorption effects. The difference between the TXRF and the NAA results are quite the same for sample A and B which just indicates again the similarity of those two samples. Sample D has a much higher difference and just for titanium the difference is a bit lower than before. For sample C the alignment is different and the cause might be the milling process in the labour. The particle might not have been so homogeneous than the industrial milled samples.

Summarised, it was shown that TXRF and NAA provide comparable results for the characterisation of zeolites. To classify the zeolite type, the Si/Al ratio is decisive. TXRF and NAA are complementary to each other and are, as such, effective tools to characterise zeolites. As expected sample A, B and C are clinoptilolite and the external sample D includes some additional non-clinoptilolite material.

	Al	Si	K	Ca	Ti	Fe
Al	1	5.36	0.38	0.43	0.02	0.31
Si	0.19	1	0.07	0.08	0.00	0.06
K	2.63	14.08	1	1.12	0.04	0.82
Ca	2.35	12.60	0.89	1	0.04	0.74
Ti	60.59	324.89	23.08	25.79	1	18.97
Fe	3.20	17.13	1.22	1.36	0.05	1

Table 3.7: Corrected ratios of the elements Al, Si, K, Ca, Ti and Fe for sample A.

	Al	Si	K	Ca	Ti
Al	1	5.03	0.48	0.45	0.01
Si	0.20	1	0.10	0.09	0.00
K	2.08	10.44	1	0.93	0.03
Ca	2.22	11.18	1.07	1	0.03
Ti	66.95	336.74	32.24	30.12	1

Table 3.8: Ratios of the elements Al, Si, K, Ca and Ti for sample A calculated with NAA data.

	Al	Si	K	Ca	Ti	Fe
Al	1	5.54	0.42	0.44	0.02	0.32
Si	0.18	1	0.08	0.08	0.00	0.06
K	2.36	13.07	1	1.04	0.04	0.75
Ca	2.27	12.55	0.96	1	0.04	0.72
Ti	57.26	317.24	24.28	25.28	1	18.12
Fe	3.16	17.51	1.34	1.39	0.06	1

Table 3.9: Corrected ratios of the elements Al, Si, K, Ca, Ti and Fe for sample B.

	Al	Si	K	Ca	Ti
Al	1	5.33	0.53	0.48	0.02
Si	0.19	1	0.10	0.09	0.00
K	1.89	10.05	1	0.91	0.03
Ca	2.07	11.03	1.10	1	0.04
Ti	58.51	311.86	31.03	28.29	1

Table 3.10: Ratios of the elements Al, Si, K, Ca and Ti for sample B calculated with NAA data.

	Al	Si	K	Ca	Ti	Fe
Al	1	6.14	0.38	0.36	0.02	0.35
Si	0.16	1	0.06	0.06	0.00	0.06
K	2.63	16.14	1	0.95	0.05	0.93
Ca	2.77	17.02	1.05	1	0.06	0.98
Ti	48.45	297.27	18.42	17.47	1	17.07
Fe	2.84	17.41	1.08	1.02	0.06	1

Table 3.11: Corrected ratios of the elements Al, Si, K, Ca, Ti and Fe for sample C.

	Al	Si	K	Ca	Ti
Al	1	4.59	0.40	0.38	0.02
Si	0.22	1	0.09	0.08	0.00
K	2.53	11.62	1	0.97	0.04
Ca	2.62	12.02	1.03	1	0.04
Ti	63.26	290.50	25.00	24.18	1

Table 3.12: Ratios of the elements Al, Si, K, Ca and Ti for sample C calculated with NAA data.

	Al	Si	K	Ca	Ti	Fe
Al	1	6.04	0.28	0.24	0.03	0.42
Si	0.17	1	0.05	0.04	0.00	0.07
K	3.53	21.35	1	0.84	0.10	1.47
Ca	4.21	25.44	1.19	1	0.12	1.75
Ti	34.83	210.49	9.86	8.27	1	14.50
Fe	2.40	14.52	0.68	0.57	0.07	1

Table 3.13: Corrected ratios of the elements Al, Si, K, Ca, Ti and Fe for sample D.

	Al	Si	K	Ca	Ti
Al	1	5.89	0.27	0.30	0.02
Si	0.17	1	0.05	0.05	0.00
K	3.75	22.05	1	1.12	0.07
Ca	3.33	19.63	0.89	1	0.06
Ti	52.20	307.28	13.93	15.65	1

Table 3.14: Ratios of the elements Al, Si, K, Ca and Ti for sample D calculated with NAA data.

	Proportional constants		CFA		Sensitivity factor	
	\bar{x}	σ	wt.%	σ	1/wt.%	σ
Al	1081.40	7.98	15.05	0.27	71.85	1.40
Si	1000.00	0.00	23.02	0.08	43.44	0.16
K	138.52	1.01	1.95	0.03	71.04	1.21
Ca	83.47	1.19	1.51	0.06	55.28	2.34
Ti	57.14	1.33	0.791	0.014	72.24	2.11
Fe	204.16	9.02	7.78	0.23	26.24	1.40

Table 3.15: Calculation of the device-specific sensitivity factors for the elements.

	TXRF		NAA		Difference
A	wt.%	σ	wt.%	σ	%
<i>Al</i>	4.29	0.15	6.00	0.12	28.41
<i>Si</i>	23.02	0.09	30.16	3.46	23.68
<i>K</i>	1.64	0.12	2.89	0.43	43.37
<i>Ca</i>	1.83	0.12	2.70	0.15	32.27
<i>Ti</i>	0.07	0.01	0.09	0.01	20.90
<i>Fe</i>	1.34	0.10			
B					
<i>Al</i>	4.15	0.09	5.73	0.11	27.46
<i>Si</i>	23.02	0.09	30.53	2.12	24.60
<i>K</i>	1.76	0.04	3.04	0.72	42.01
<i>Ca</i>	1.83	0.09	2.77	0.14	33.77
<i>Ti</i>	0.07	0.01	0.10	0.01	25.88
<i>Fe</i>	1.31	0.08			
C					
<i>Al</i>	3.75	0.10	5.69	0.12	34.02
<i>Si</i>	23.02	0.09	26.11	3.17	11.84
<i>K</i>	1.43	0.05	2.25	0.31	36.54
<i>Ca</i>	1.35	0.07	2.17	0.12	37.75
<i>Ti</i>	0.08	0.01	0.09	0.01	13.85
<i>Fe</i>	1.32	0.08			
D					
<i>Al</i>	3.81	0.08	6.78	0.14	43.80
<i>Si</i>	23.02	0.09	39.90	4.42	42.30
<i>K</i>	1.08	0.03	1.81	0.10	40.41
<i>Ca</i>	0.90	0.06	2.03	0.10	55.48
<i>Ti</i>	0.11	0.01	0.13	0.02	15.77
<i>Fe</i>	1.59	0.11			

Table 3.16: Results of the quantitative content of the elements determined with TXRF and NAA are compared.

3.5 PXRD Experiment and Results

The measurements were done with the help of Werner Artner and Danny Müller at the X-Ray Center of TU Wien. Sample C was milled for the performance. The analysis was performed by Klaudia Hradil.

PXRD is normally used to study the crystalline structure of zeolites principally by analysis of crystalline lattice parameters. In this work it was used to qualitatively assess the samples for clinoptilolite (and other mineral phases) content. A quantitative evaluation was not carried out, due to the presence of only relatively minor impurities and quality of the data acquired.

The measurements (Fig. 3.12 - 3.16) are the red curve. The vertical lines are the reflexes of the found phases. The used phases are listed in Tab. 3.17. The theory of PXRD is summarised in previous section 2.2.3 *Powder X-Ray Diffraction (PXRD)*.

The major crystalline phase for sample A, B and C (milled) is phase 1, which is clinoptilolite-Na. Fig. 3.12 shows the diffractogram for sample A just with the reflexes of phase 1. The alignment is quite high and it confirms graphically that the sample A, like B and C, is clinoptilolite. The first minor phase is number 3, which correspond to gismondine. This mineral occurs in basalt cavities, mostly nepheline basalt, and in combination with gonnardite and phillipsite (IZA (a)). The occurrence of gismondine is reasonable, because the mining site of the samples was in Upper Austria. The framework is built by "doubly connected 4-membered rings linked into double crankshaft chains" (IZA, a) and the chemical formula is $\text{CaAl}_2\text{Si}_2\text{O}_8 \cdot 4\text{H}_2\text{O}$. The second minor phase is phase 2, which is terranovaite. This mineral has a high silicon content and the framework "is characterised by chains of five-membered rings (pentasil chains) and by a two-dimensional ten-membered channel system parallel to (010)" (IZA (b)). The International Zeolite Association (IZA) provides detailed information about gismondine and terranovaite, which can be looked up on their database.

Phase 1 to 3 are part of the zeolite family and all three crystalline phases can be found in sample A, B and C. Sample D has an additional phase 4, which was defined as part of the Feldspar family. This just shows the contamination of the zeolite sample. All the detailed data of the four phases can be looked up in the Appendix C *PXRD*.

A small amount of sample A is present in its amorphous (non-crystalline) order, which is indicated by the minimal increase of the background (dark green curve in Fig. 3.13) between 17 and $35^\circ 2\theta$. Sample B and C do not really have this increase. The diffractogram of sample D clearly seems different, but has also an increase of the background (Fig. 3.16). Industrial milling of the mined material could have caused destruction of the long ranged order of the crystals, which can lead to the amorphous order. The particle size of A, B and D is in the micrometer range, which consolidates the theory.

It could be verified that samples A, B and C have clinoptilolite-Na as the major phase and sample D contains an additional non-clinoptilolite phase.

Phase	Mineral name	Family
1	Clinoptilolite-Na	Zeolite
2	Terranovaite	Zeolite
3	Gismondine	Zeolite
4	Anorthite, sodian, syn	Feldspar

Table 3.17: Explanation of phase numbers.

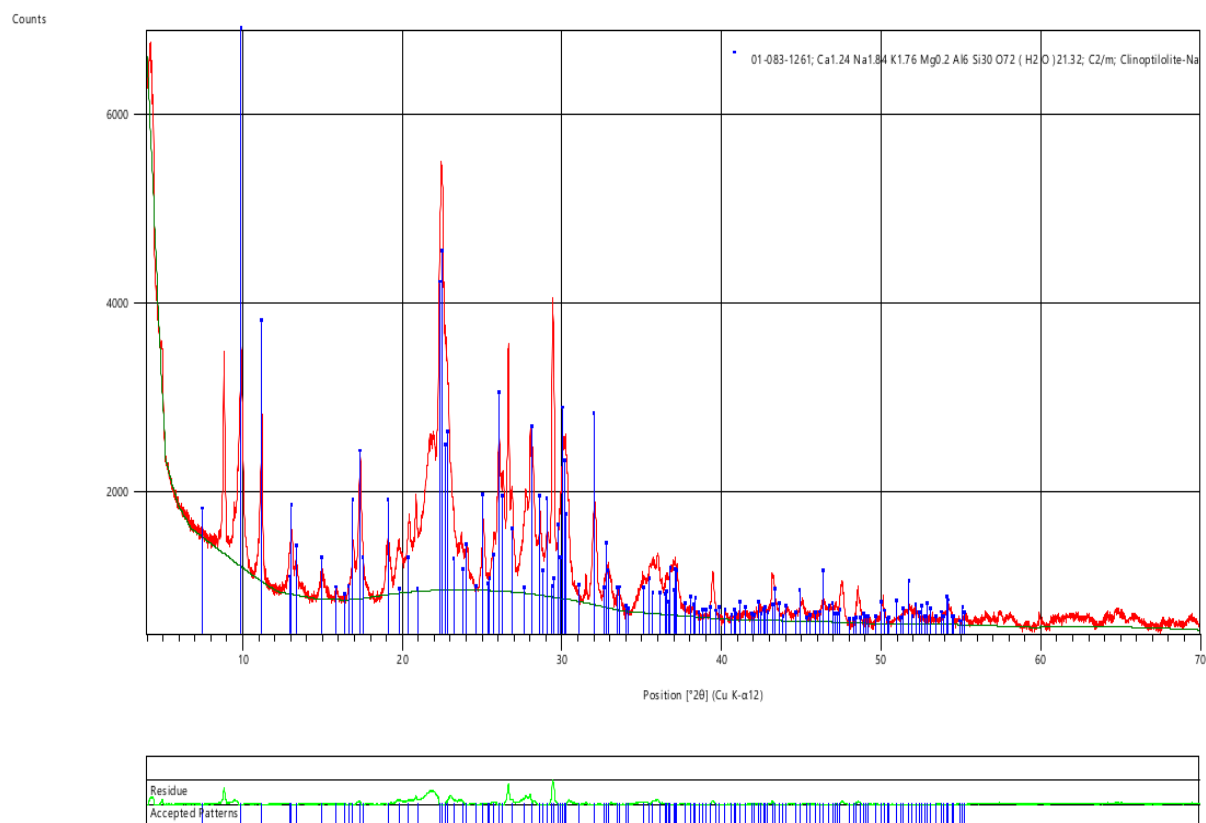


Figure 3.12: Diffractogram of sample A using the major phase 1.

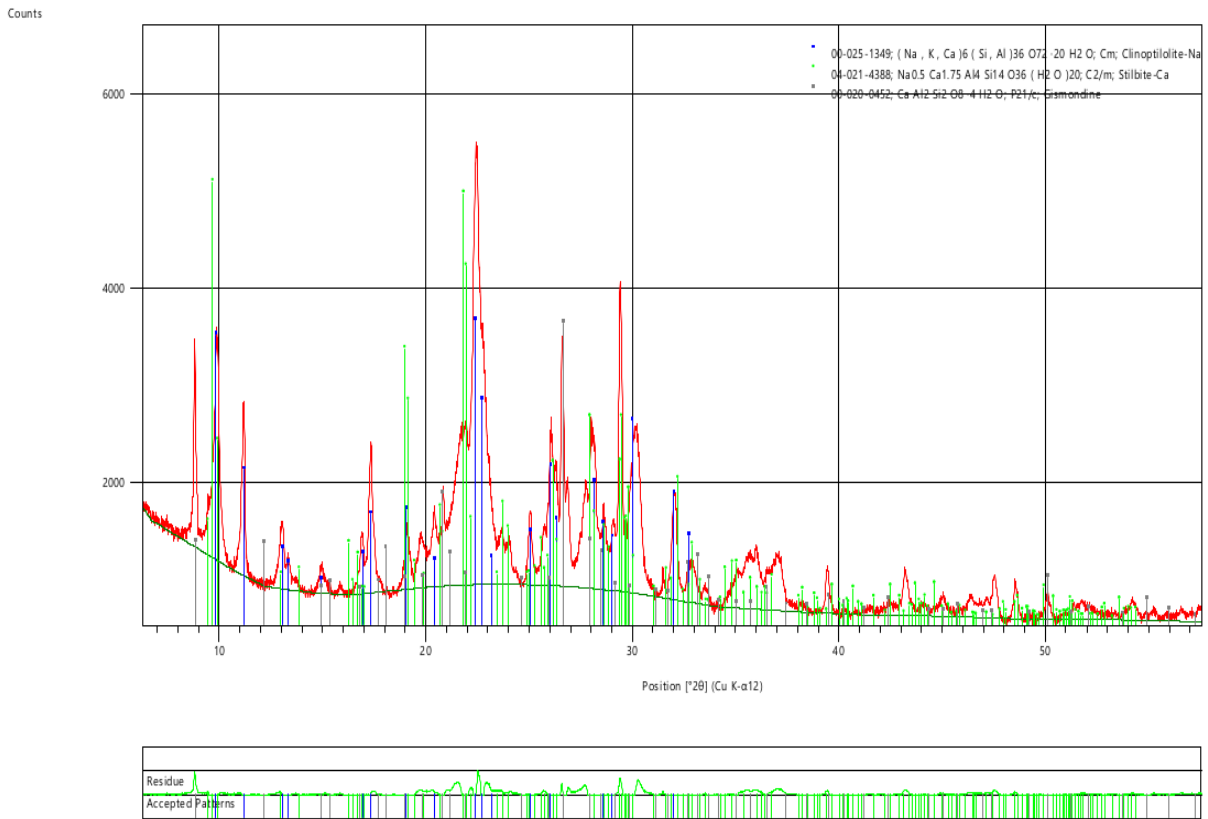


Figure 3.13: Diffractogram of sample A using phase 1 to 3.

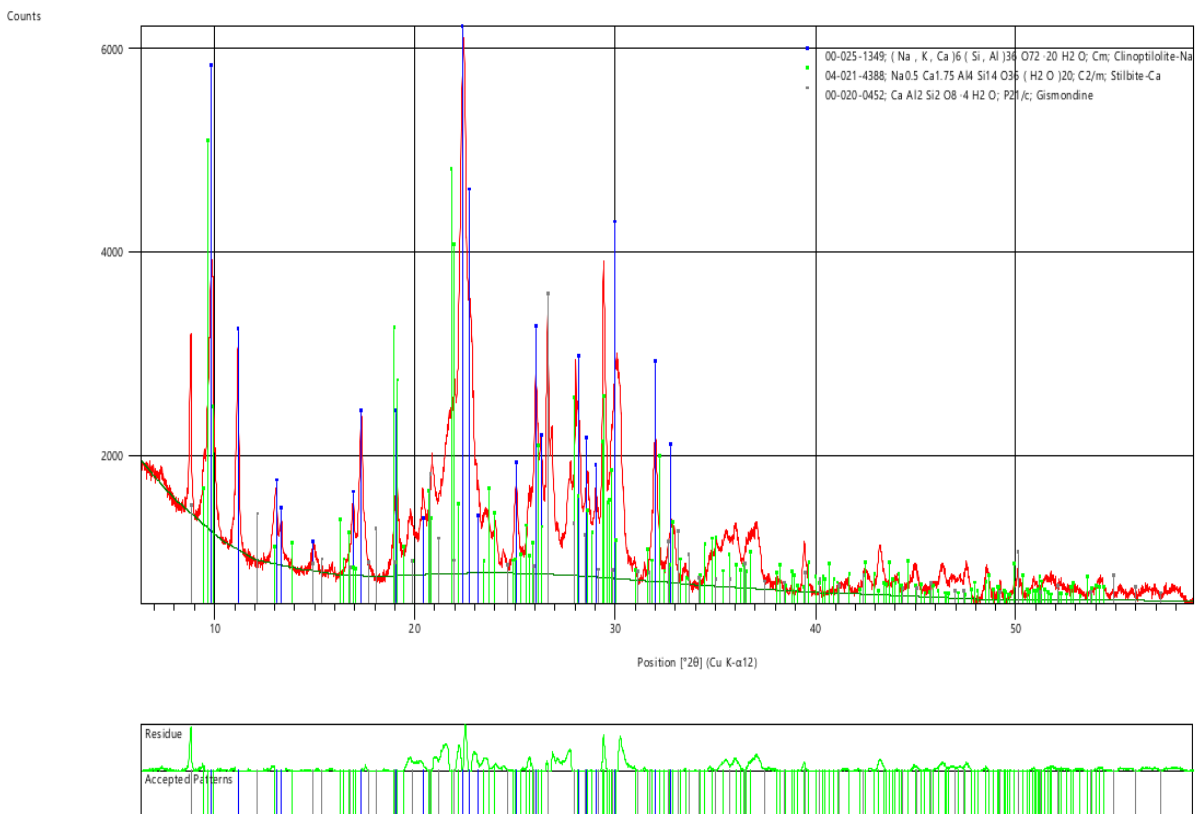


Figure 3.14: Diffractogram of sample B using phase 1 to 3.

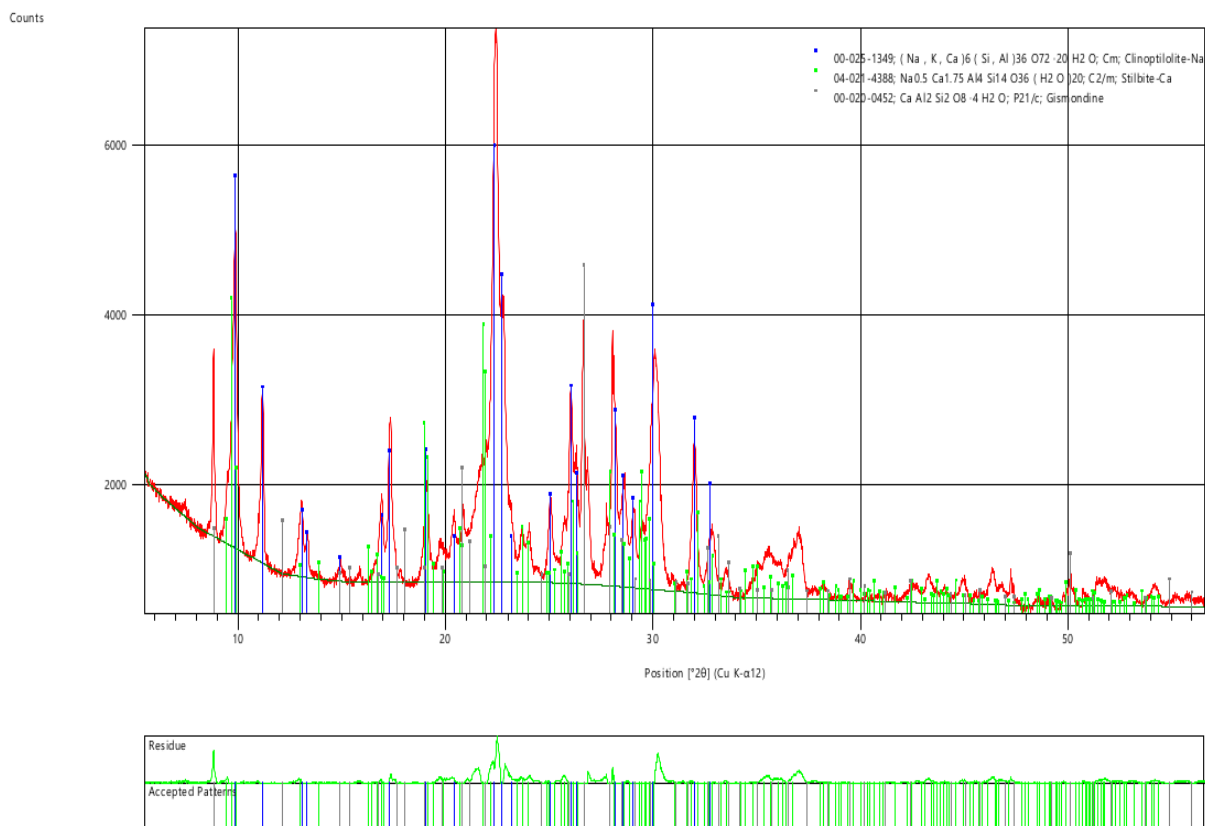


Figure 3.15: Diffractogram of sample C using phase 1 to 3.

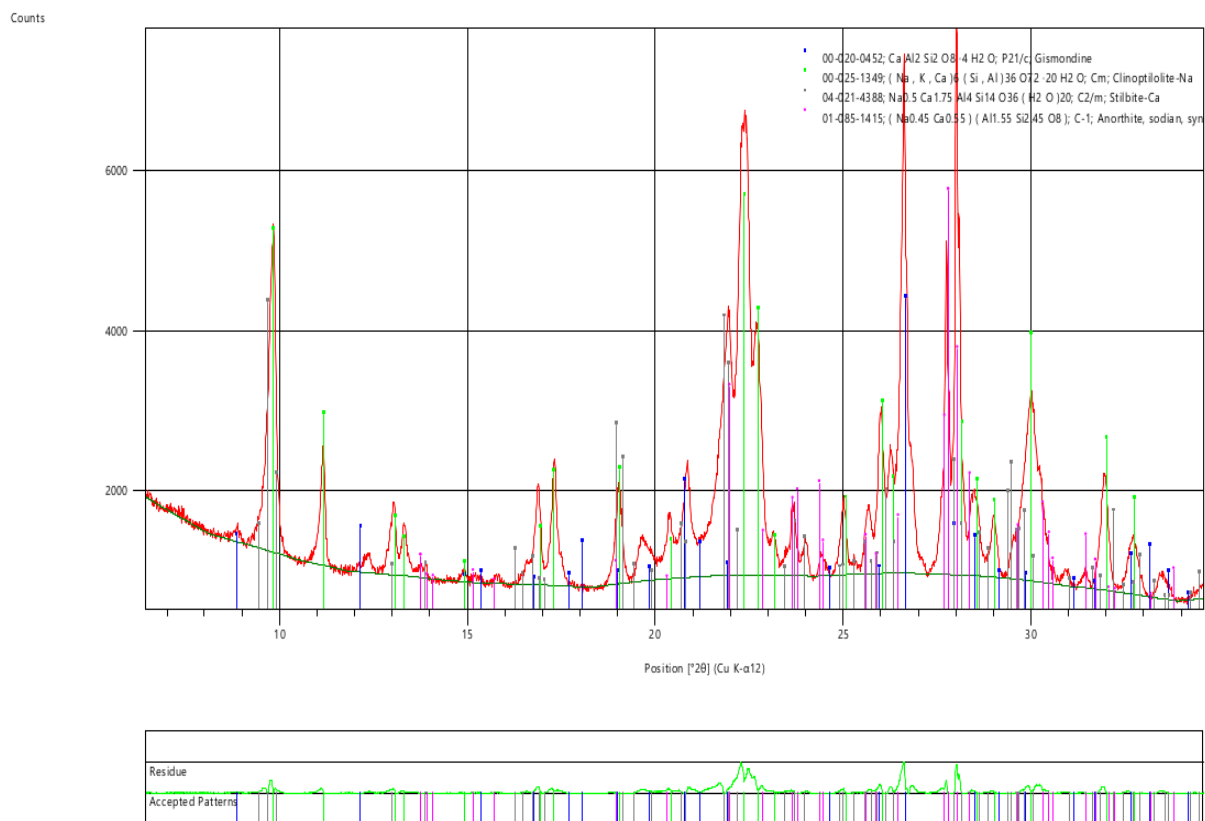


Figure 3.16: Diffractogram of sample D using phase 1 to 4.

4. Determination of the Capacity for Sr and Cs

As mentioned in previous section 2.1.1 *Clinoptilolite*, the analysed zeolite is used for decontamination of low and intermediate-level radioactive waste because of its great ion exchange selectivity for the isotopes ^{137}Cs and ^{90}Sr . Two previous theses did some separate research on the ^{137}Cs (Wallenko, 2013) and the ^{90}Sr (Sperrer, 2013) uptake. Different physical factors like competing ions, time and temperature were analysed and the results are concluded in the paper of Sterba et al. (2018). The saturation value for Sr or Cs ions was not analysed in detail.

In this thesis the maximal Sr or Cs uptake of the zeolite samples was of interest. The ion capacity of zeolites follows a saturation principle. The ions have fixed sites in the zeolite framework to exchange and if the sites are all occupied no more ions can be taken up by the zeolite (see 2.1.1 *Clinoptilolite*). A general saturation curve is illustrated in Fig. 4.1 and for this work the right side of it was of interest.

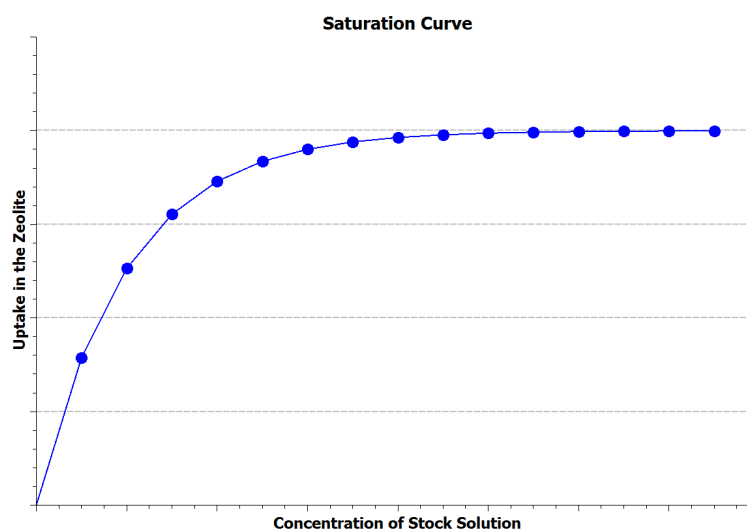


Figure 4.1: General saturation curve for the uptake of an ion into the zeolite.

4.1 Concept

The four zeolites A (LithoFill 100 “T”), B (LithoFill 100), C (LithoGran 2) and D (“Extern I”) were analysed for their maximal capacity for Sr or Cs ions. The isotopes $^{85}_{38}\text{Sr}$ and $^{134}_{55}\text{Cs}$ were used as radiotracers because of their ease of production by neutron activation in a reactor (see 2.2.6 *Capacity Analysis with Radiotracers Dilution Experiment*). For each tracer ion type, two different stock (analyte) solutions of different concentrations were prepared. The concentration of the first stock solution was chosen on the basis of the Al content of the zeolite samples as determined in section 3.3 *NAA Experiment*. Al was used to estimate zeolite capacity because Sr and Cs can ion exchange at different sites in the zeolite and cations compensate for the negatively charged sites in the framework caused by the presence of Al rather than Si (see 2.1 *Zeolites*). For the first caesium stock solution, the number of the Al sites in the sample of zeolite should be roughly equal to the number of Cs ions available in solution. For the first strontium stock solution the number of the Sr ions should be half as many as the number of the Al sites because of the divalent nature of Sr. The second stock solutions had ten-fold higher concentrations than the first solution to confirm saturation of the zeolite by the analyte.

From each zeolite four samples were taken which were mixed separately with each of the two strontium and two caesium stock solutions. Since four different zeolite samples were tested with four different stock solutions, 16 dilution experiments were done in total. The general theory of a dilution experiment is explained in the prior section 2.2.6 *Capacity Analysis with Radiotracers Dilution Experiment*.

To comparatively evaluate the maximum capacity of the zeolite samples for Sr and Cs, an fixed experimental procedure was devised for the dilution experiments. The flow diagram in Fig. 4.2 gives a more detailed overview of the experimental procedure described generally by the flow chart shown in Fig. 2.7. A short description of terminology is shown in Tab. 4.1.

Two different parent (tracer) solutions were produced by dissolving activated $\text{Sr}(\text{NO}_3)_2$ or CsNO_3 in triply distilled water. The activations were carried out in the TRIGA Mark II reactor at the Atominstitut in the same way as the the NAA analyses. The theory can be reread in prior section 2.2.4 *Neutron Activation Analysis (NAA)* and the experimental set up is described in section 3.3 *NAA Experiment*. The detailed procedure is also explained in section 4.2 *Parent (Tracer) Solution*.

Different amounts of the parent solution were used to mix the two 50 ml strontium stock (analyte) solutions and the two 50 ml caesium stock (analyte) solutions. The considerations for the concentrations of the stock solutions are described above. The first stock solution for the strontium ions is labelled with SL_1_Sr and the second stock solution with a ten-fold higher concentrations is labelled with SL_2_Sr. The first stock solution for the caesium ions is labelled with SL_1_Cs and the second stock solution with a ten-fold higher concentrations is labelled with SL_2_Cs. The stock solutions SL_Number_Ion are a mixture of an amount of the parent solution PS_Ion, an amount of the inactive ion nitrate and triply distilled water. The total volume of a stock solution was set to 50 ml to allow to use 10 ml of it for each of the four zeolite samples and to have a standard geometry for the measurements. This standard geometry was a

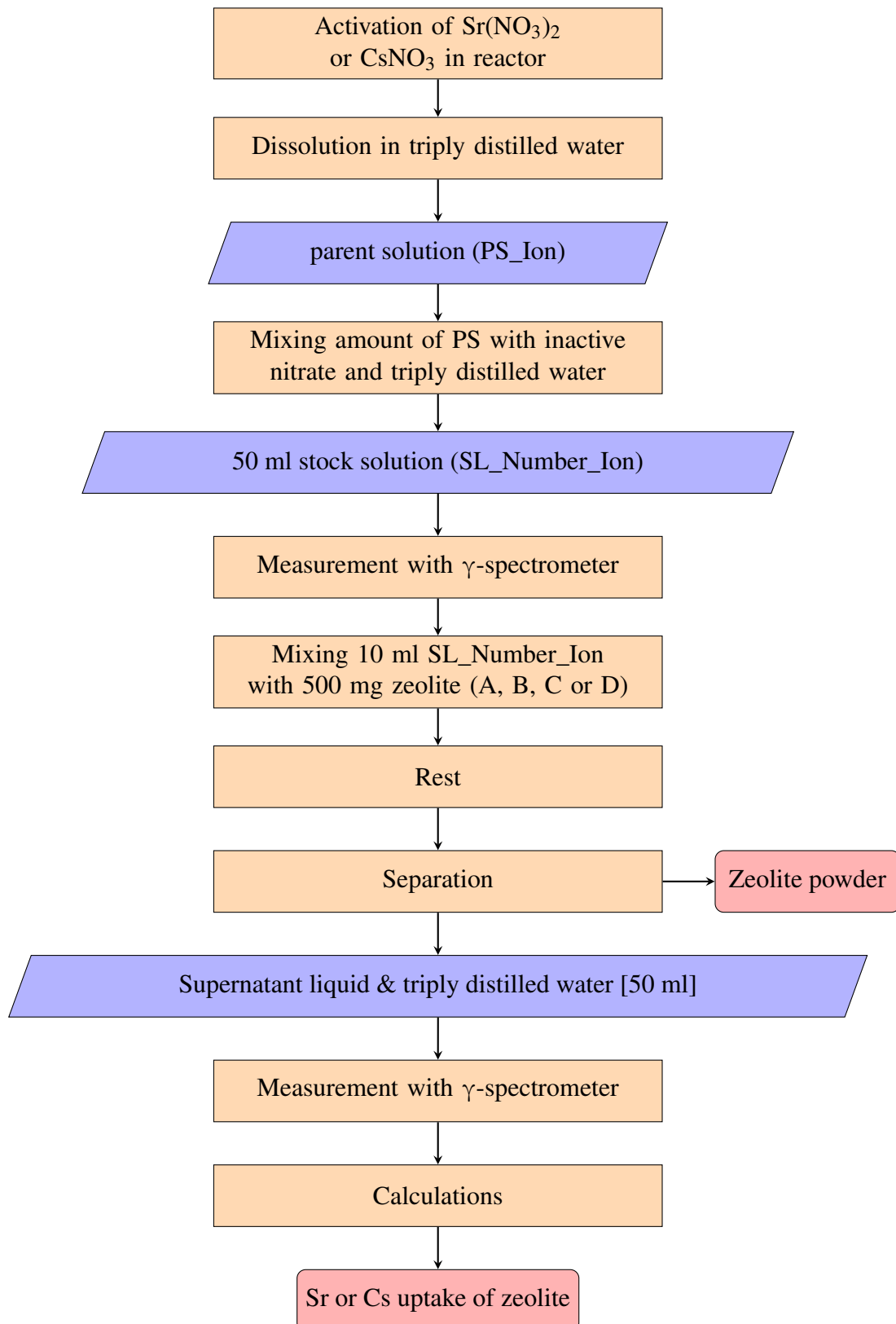


Figure 4.2: Flow chart of the experimental set up of the capacity determination. Two different stock solutions (Number = 1, 2) for each radiotracer (Ion = Sr, Cs) were prepared. The second stock solution had a ten-fold higher concentration than the first stock solution.

Name	Description
Ion	strontium (Sr) or caesium (Cs).
Ion uptake	Ions in the zeolite due to ion exchange after the capacity experiment.
parent solution	Activated nitrate dissolved in triply distilled water. Shortcut: PS_Ion
stock solution	Amount of parent solution mixed with an amount of inactive nitrate and triply distilled water which has a total volume of 50 ml. Second stock solution which is indicated with number 2 has a ten-fold higher concentration than first one which is represented with number 1. Shortcut: SL_Number_Ion
Supernatant liquid	Collected liquid after the ion exchange process via separation from the zeolite powder.
90 ml polypropylene sample vial	Plastic container with a volume of 90 ml and a white lid. Shortcut: vial

Table 4.1: Used terminology for the capacity experiment.

90 ml polypropylene sample vial which was filled up with 50 ml of a fluid. Each stock solution was measured right after its preparation in the γ -spectrometer "Dicker Fritz" at the Atominstitut of TU Wien.

10 ml of stock solution SL_Number_Ion was mixed with 500 mg of zeolite sample in centrifuge tubes. As described above, this was done for all four zeolites (A, B, C and D) and for the two strontium and the two caesium stock solutions. In total, 16 mixing experiments were carried out allowing about 17 hours for the ion exchange process to reach equilibrium. The experiments with the strontium stock solutions SL_Number_Sr were done at a temperature of about 53°C instead of room temperature because it had been shown previously that the ion exchange process for strontium is much slower than for caesium. This temperature was chosen due to results of [Sperrer \(2013\)](#) and the maximal temperature which the centrifuge tubes could tolerate. The experiment was done with two different concentrations of the stock solutions to determine the maximal Sr or Cs uptake of the zeolite samples.

After settling, the zeolite powder and the supernatant liquid were separated. The supernatant liquid was mixed with triply distilled water to achieve the same volume of 50 ml as the stock solutions during the measurement in the γ -spectrometer. This mixture of the supernatant liquid and triply distilled water was measured with the γ -spectrometer "Dicker Fritz". In order to compare the results of different experiments and the stock solutions, it is essential to measure in the same geometry. Therefore the collected zeolite powder after the separation could not be used to determine the Sr or Cs uptake of the zeolite sample directly. Measurements were done, but it was clear that the inhomogeneity in the samples results in incomparable sample geometries and exaggerated measured Cs and Sr contents.

The ion concentration in the supernatant liquid was calculated by comparison with the stock solution SL_Number_Ion measurements. By simple subtraction of the ion concentration in 10 ml of SL_Number_Ion from the ion concentration in the supernatant liquid, the Sr or Cs uptake of the zeolite samples could be determined. The analysis is explained in more detail in section 4.5 *Experiment Analysis*.

4.2 Parent (Tracer) Solution

First a parent solution was prepared for Sr and Cs. The step-by-step procedures can be looked up in the Appendix F. The nitrates were activated in the reactor for about 8 hours by a thermal neutron flux of about $10^{12} \text{ cm}^{-2}\text{s}^{-1}$. They were left for about 16 hours in the turned off reactor to allow the decay of the short-life elements.

For the parent solution strontium PS_Sr 7.09508 g of $\text{Sr}(\text{NO}_3)_2$ was activated in the reactor and then dissolved in a polypropylene sample vial with 15 ml of triply distilled water. The mixture was emptied into a 20 ml volumetric flask out of glass. The vial was washed with 2 ml of triply distilled water and the liquid was emptied again into the flask. The flask was filled up to the 20 ml mark with triply distilled water and then emptied into a new vial. The parent solution strontium had a concentration c_{PS_Sr} of $1.68 \frac{\text{mol Sr}}{\text{l solution}}$ (Appendix Eq. E.0.1) and an activity of the magnitude of 10^5 Bq.

The parent solution caesium PS_Cs was prepared with 0.01043 g of activated CsNO_3 and 10 ml of triply distilled water which was mixed together in a polypropylene sample vial. It had an activity of the magnitude of 10^5 Bq. The parent solution caesium had a concentration c_{PS_Cs} of $0.00535 \frac{\text{mol Cs}}{\text{l solution}}$ (Appendix Eq. E.0.9).

The whole work took place under a fume hood. The formula to calculate the concentration of the parent solution (4.2.1) depends on the mass of the activated nitrate m^* in g, the volume of the solution V in l and the molar mass of the nitrate M in $\frac{\text{g}}{\text{mol}}$. The concentrations of the parent solutions strontium c_{PS_Sr} and caesium c_{PS_Cs} and their uncertainties can be looked up in Tab. 4.6 and 4.14.

$$\frac{m^* \text{ in g}}{V \text{ in l}} \cdot \frac{1}{M \text{ in } \frac{\text{g}}{\text{mol}}} = x \frac{\text{mol element Sr or Cs}}{\text{l solution}} \quad (4.2.1)$$

4.3 Stock (Analyte) Solution

As described in section 4.1 *Concept*, two different stock solutions were prepared for the Sr and for the Cs capacity experiment. The second stock solution had a concentration ten-fold higher than the first one. Each stock solution had a volume of 50 ml, because for each of the four zeolite samples 10 ml of it were used for the experiment. It was calculated how much of the parent solution and how much inactive nitrate is necessary to achieve the desired concentrations for the stock solutions (Appendix E). The exact activity of the solutions is not necessary to know because for the calculations only ratios were used. The step-by-step procedures of the preparations can be looked up in the Appendix F. Work took place under a fume hood while

handling active material. The stock solutions 1 and 2 were measured with the γ -spectrometer "Dicker Fritz" to get measurement data about their concentrations. The spectra are in Appendix G.

The parent solution strontium had a concentration of $1.68 \frac{\text{mol Sr}}{\text{l solution}}$. To prepare the 50 ml stock solution 1 strontium SL_1_Sr with a concentration of $c_{SL_1_Sr} 0.055 \frac{\text{mol Sr}}{\text{l solution}}$ it is necessary to use 1.64 ml of the parent solution strontium (Appendix Eq. E.0.2 and E.0.3). For the experiment 1.6 ml of parent solution strontium was pipetted to a 50 ml volumetric flask out of glass. The flask was filled up to the 50 ml mark with triply distilled water and emptied in a new 90 ml polypropylene sample vial.

To prepare the 50 ml stock solution 2 strontium SL_2_Sr with a concentration $c_{SL_2_Sr}$ of $0.55 \frac{\text{mol Sr}}{\text{l solution}}$ it is necessary to use 2.1 ml of the parent solution strontium (Appendix Eq. E.0.5 and E.0.6) and dissolve additional inactive 5.07 g of strontium nitrate (Appendix Eq. E.0.8). The volume of the parent solution strontium was calculated under consideration of the lower activity of the parent solution strontium due to the time between the preparation of the parent solution strontium and the experiments with the second stock solution. The time span in between was about 24 days and the half-life time of ^{85}Sr is about 65 days. To know the mass of the inactive $\text{Sr}(\text{NO}_3)_2$ the total mass of nitrate (Appendix Eq. E.0.4) was calculated which is needed for a concentration of $0.55 \frac{\text{mol Sr}}{\text{l solution}}$ and the mass of $\text{Sr}(\text{NO}_3)_2$ in 2.1 ml of the parent solution strontium (Appendix Eq. E.0.7) was subtracted. For the experiment 5.09452 g of inactive $\text{Sr}(\text{NO}_3)_2$ was weighted in a vial and dissolved with 45 ml of triply distilled water while the closed vial was swivelled sideways under warm tap water. Afterwards 2.8 ml of triply distilled water and 2.2 ml of the parent solution strontium were added to the vial.

The parent solution caesium had a concentration of $5.35 \frac{\text{mmol Cs}}{\text{l solution}}$. To prepare the 50 ml stock solution 1 caesium SL_1_Cs with a concentration $c_{SL_1_Cs}$ of $0.11 \frac{\text{mol Cs}}{\text{l solution}}$ it is necessary to dissolve additional 1.07 g of caesium nitrate (Appendix Eq. E.0.14) and add 330 μl of the parent solution caesium (Appendix Eq. E.0.13). With the detector efficiency it was calculated how much active CsNO_3 is needed for a reliable measurement (Appendix Eq. E.0.10 and E.0.11). Due to the ratio of the volume of the parent solution caesium and the whole activated CsNO_3 dissolved in it, the volume of the parent solution caesium, which has to be added for stock solution 1 caesium, was calculated (Appendix Eq. E.0.12). This amount was so small that it was not subtracted from the added inactive nitrate. For the experiment 1.07780 g of inactive CsNO_3 was put into a vial and 50.04 g triply distilled water were added. Afterwards 40 μl and then 360 μl of parent solution caesium were pipetted to the vial. This was done in two steps because of an error in the calculation.

For the 50 ml stock solution 2 caesium SL_2_Cs a concentration $c_{SL_2_Cs}$ of $1.11 \frac{\text{mol Cs}}{\text{l solution}}$ was desired. It is necessary to dissolve additional 10.82 g of caesium nitrate (Appendix Eq. E.0.15) for that. The same volume of 330 μl of the parent solution caesium could have been used, because the half-life time of ^{134}Cs is about two years and a loss of activation does not need to be

considered for about 24 days. For the experiment 10.85546 g of inactive CsNO_3 was weighed in a vial and dissolved step-wise in 40 ml of triply distilled water. The closed vial was swivelled sideways under warm tap water for this process. Afterwards 8 ml of triply distilled water and 2000 μl of parent solution caesium were added. More of the active parent solution caesium was used to reduce the measuring time with the γ -spectrometer.

4.4 Experiment Setup

The capacity experiment was done with the same procedure for all four stock solutions. Each stock solution was mixed with all four zeolite samples. The exact step-by-step process can be looked up in Appendix *F*.

500 mg of the zeolite powder was given into a centrifuge tube. It was filled up with 10 ml of an active stock solution and mixed. The stock solution contains the activated caesium or strontium ions and triply distilled water. The detailed preparations of the stock solutions is explained in section 4.3 *Stock (Analyte) Solution*. The strontium experiment was heated up to 53°C in silicon oil on a hot plate, because the process of ion exchange is much slower for strontium than for caesium. The caesium experiment was done by room temperature. For the experiment with stock solution 1 strontium each centrifuge tube was closed with a stubble through which a thin cannula was pierced to allow steam to be released. For the experiment with stock solution 1 caesium each centrifuge tube was just closed with a stubble. For the experiment with the second stock solutions parafilm was used to seal the centrifuge tubes. After around 17 hours the zeolite powder was extracted from the supernatant liquid by centrifuging. The zeolite was washed twice, and all the liquid was collected in a vial with a volume of 90 ml. The centrifuge tube was always put directly into a titration flask after the centrifugation for the way to the labour desk. Due to the washing, the container contained 30 ml of active liquid which contained the Cs or Sr radioisotopes the zeolite could not uptake. The container was filled with additional 20 ml of triply distilled water to get the same volume as the stock solutions had after preparation. The containers were measured with the γ -spectrometer at the Atominstitut. Due to the same sample geometry of the vial filled with 50 ml of a water mixture, the data results can be compared with the data of the stock solutions. All the spectra can be looked up in the Appendix *G*.

The procedure of collecting the supernatant liquid after the last washing process was a bit different for sample A and stock solution 1 strontium. The centrifuge tube shattered while taking it out of the centrifuge for the last time. Some of the zeolite particles got lost with some liquid during the cleaning of the centrifuge but most of them were saved thanks to the centrifuge holder. The titration flask caught most of the leaking zeolite particles and triply distilled water. So the mixture was collected out of the titration flask. It was washed and the destroyed centrifuge tube was rinsed to collect all of the Sr ions. The step-by-step procedure for sample A and stock solution 1 strontium is explained in Appendix *F*.

Fig. 4.3 illustrates the main steps of the explained procedure. The stock solution was pipetted onto the zeolite sample. The Sr experiments were done at higher temperature and the Cs experi-

ments at room temperature. Afterwards the zeolite powder was extracted and the water mixture was collected in a container.

For sample C the first experiment was done with the provided material, but the experiment with the second stock solution was done with the milled material by mistake.

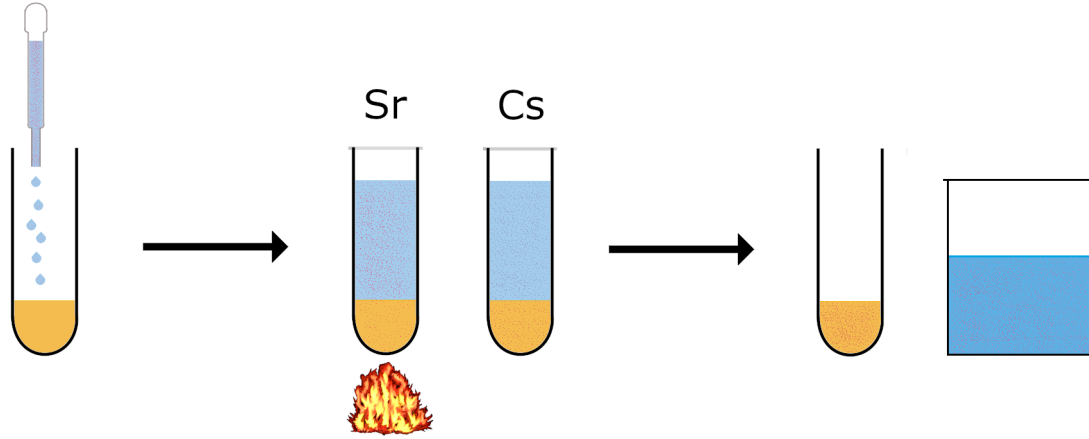


Figure 4.3: Procedure of main steps for the capacity experiments.

4.5 Experiment Analysis

The stock solution was measured with the γ -spectrometer right after its preparation. For each capacity experiment the supernatant water mixture was collected in the same geometry as the stock solutions were before the experiments. These vials were measured also with the γ -spectrometer. Each vial with a volume of 90 ml was filled with 50 ml of liquid. Due to the same geometry the results are comparable. The radioisotope concentration of the stock solutions $c_{SL_Number_Ion}$ and the Net Peak Area (NPA) of the isotope of the stock solution $NPA_{SL_Number_Ion}$ were known and could be set in relation to the counted Net Peak Area of the isotope in the collected supernatant water mixture $NPA_{Mixture}$. It is important to compensate for the difference of measurement time and this means to adjust the Net Peak Areas. So the leftover concentration of the ions in the liquid $c_{Sample_SL_Number_Ion_L}$ could be calculated (Eq. 4.5.1). Due to simple subtraction of the concentration of the ions in 10 ml of the stock solution $c_{SL_Number_Ion\ 10ml}$ (Eq. 4.5.2) and the concentration in the collected water mixture at the end of the capacity experiment, the Sr or Cs uptake of the zeolite samples $c_{Sample_SL_Number_Ion_Z}$ could be calculated (Eq. 4.5.3). The Sr or Cs uptake could not be measured directly, because the geometry of the zeolite powder mixed with 50 ml of triply distilled water is different to the geometry of the stock solutions. The zeolite powder settles to the ground of the vial and all the activated ions are right on top of the detector and not homogeneous distributed in the liquid. The uncertainties u_i of the functions $f(x_1, \dots, x_N)$ were calculated with the Gaussian propagation of uncertainty (Eq. 4.5.4) as for all the data in this work.

$$c_{SL_Number_Ion} : NPA_{SL_Number_Ion} = c_{Sample_SL_Number_Ion_L} : NPA_{Mixture} \quad (4.5.1)$$

$$c_{SL_Number_Ion\ 10ml} = \frac{c_{SL_Number_Ion}}{5} \quad (4.5.2)$$

$$c_{Sample_SL_Number_Ion_Z} = c_{SL_Number_Ion\ 10ml} - c_{Sample_SL_Number_Ion_L} \quad (4.5.3)$$

$$u_i = \sqrt{\sum_{n=1}^N \left(\frac{\partial f}{\partial x_n} \cdot u_n \right)^2} \quad (4.5.4)$$

It was tried to consider all the uncertainties of the used materials. For the pipetting the Pipette Socorex 5000, which allows the manual control of the pipetted volume, the Pipette Brand 100 μl and the Pipette Brand 20 μl were used. The uncertainties were already determined from Michaela Foster from the ATI Wien. The protocol for all used pipettes are shown in Appendix I. The Pipette Socorex 5000 was tested for volumes of 5000 μl , 2500 μl and 500 μl (Appendix Tab. I.1). The used pipetting volumes (Appendix Tab. I.2) were extrapolated with the program QTI Plot (Appendix Fig. I.1). The deviation d was calculated with the fitting Equation 4.5.5 and the uncertainty u_i^{Pip} of the pipetting volume V_i with Equation 4.5.6. Sometimes different small pipette volumes were used to reach a big liquid volume. This was considered for the calculations of the uncertainties. The experimental procedures for the capacity determination in the Appendix *F* explain the exact processes and with them it is clear when to consider different pipette volumes. The variable names are explained in Tab. 4.2.

$$d(x) = 0.666666667 - 0.00014x + 1.3333333333333 \cdot 10^{-08}x^2 \quad (4.5.5)$$

$$u_i^{Pip} = \frac{V_i \cdot d(V_i)}{100} \quad (4.5.6)$$

Symbol	Name
$c_{Sample_SL_Number_Ion_L}$	concentration of the $Ion = Sr, Cs$ in the leftover liquid after the experiment of $Sample = A, B, C, D$ and stock solution $Number = 1, 2$
$c_{Sample_SL_Number_Ion_Z}$	concentration of the $Ion = Sr, Cs$ in the zeolite after the experiment of $Sample = A, B, C, D$ and stock solution $Number = 1, 2$
$c_{SL_Number_Ion\ 10ml}$	concentration of the $Ion = Sr, Cs$ in 10 ml of the the stock solution $Number = 1, 2$
$d(x)$	deviation of a volume of the Pipette Socorex 5000
$NPA_{Mixture}$	Net Peak Area of the isotope Sr or Cs in the leftover liquid
$NPA_{SL_Number_Ion}$	Net Peak Area (NPA) of the $Ion = Sr, Cs$ in the stock solution $Number = 1, 2$
u_i	uncertainty of a function $f(x_1, \dots, x_N)$
u_i^{Pip}	uncertainty of a volume of the Pipette Socorex 5000
V_i	volume i of the Pipette Socorex 5000

Table 4.2: Variables for capacity experiment analysis.

4.5.1 Analysis of the Sr Capacity Experiments and Results

The concentration of the parent solution strontium c_{PS_Sr} was calculated as explained above in section 4.2. 1.6 ml of the parent solution was used to create the stock solution 1 strontium. The strontium concentration of stock solution 1 strontium $c_{SL_1_Sr}$ was calculated with the concentration of the parent solution strontium, its used volume and the total volume of the stock solution 1 strontium, which was 50 ml. Each 500 mg zeolite sample was mixed with 10 ml of the stock solution 1 strontium and the concentration of the strontium ions was 0.000536 ± 0.000004 mol Sr, which is equal to 47.00 ± 0.27 mg Sr. All the used values are listed in Tab. 4.4, the equations can be looked up in Tab. 4.5 and the calculated concentrations are in Tab. 4.6.

The strontium concentration of stock solution 2 strontium $c_{SL_2_Sr}$ was calculated with the mass of the strontium nitrate in 2.2 ml of the parent solution strontium, the mass of the added inactive strontium nitrate, the volume of the added parent solution strontium, the volume of the added triply distilled water and the molar mass of strontium nitrate. 10 ml of the stock solution 2 strontium had 0.00555 ± 0.00002 mol Sr in it, which is equal to 486.48 ± 1.68 mg Sr. The values for the calculations are shown in Tab. 4.8, the used equations are in Tab. 4.7 and the calculated values are listed in Tab. 4.9. It can be clearly seen the ten-fold higher concentration of the stock solution 2.

The used variable names are described in Tab. 4.3. The spectra are in Appendix G. The strontium uptake of the zeolite samples are presented in Tab. 4.10 and Fig. 4.4. Between the data results of sample C (red squares) is no line, because for the experiment with stock solution 1 the provided zeolite powder and for the experiment with stock solution 2 the milled material was used. The uptake was calculated as explained in section 4.5. The uptake of strontium is similar for samples A, B and C. The external sample D has the lowest concentration of strontium for both stock solutions. The uncertainty for the experiment with stock solution 2 is so high because the concentration was too big. The zeolites were not able to uptake much more strontium than for stock solution 1 and the uptake limit was reached. It would be interesting to do the experiment for a different stock solution just with a concentration five times higher than stock solution 1.

"A high selectivity for strontium is difficult to find when considering ordinary ion exchange because of the chemical similarity of strontium to the calcium which is found in the[] soils and minerals in their natural state." (Frysiner, 1962) Fedorova et al. modified clinoptilolite with the magnetite to study the sorption for ^{90}Sr and the influence of competing ions. The ion calcium Ca^{2+} is chemical similar to Sr^{2+} and effects the strontium sorption the most. The ions sodium Na^+ and potassium K^+ effect the Sr uptake less but quite the same comparing to each other.

Symbol	Description
$m_{Sr(NO_3)_2^*}$	mass of activated strontium nitrate
$m_{Sr(NO_3)_2}$	mass of inactivate strontium nitrate for stock solution 2 strontium
$m_{Sr(NO_3)_2^* 2.2ml PS_Sr}$	mass of activate strontium nitrate in 2.2 ml of the parent solution strontium
$M_{Sr(NO_3)_2}$	molar mass of strontium nitrate
M_{Sr}	molar mass of strontium
$V_{Bottle20ml}$	volume of the 20 ml bottle
$V_{Bottle50ml}$	volume of the 50 ml bottle
$Pip5000$	used pipette with maximal volume of 5000 μ l
c_{PS_Sr}	strontium concentration of parent solution strontium
$V_{PS_Sr in SL_1_Sr}$	volume of parent solution strontium in stock solution 1 strontium
$V_{PS_Sr in SL_2_Sr}$	volume of parent solution strontium in stock solution 2 strontium
$c_{SL_1_Sr}$	strontium concentration of stock solution 1 strontium
$c_{SL_2_Sr}$	strontium concentration of stock solution 2 strontium
$c_{SL_1_Sr 10ml}$	strontium concentration of 10 ml of stock solution 1 strontium
$c_{SL_2_Sr 10ml}$	strontium concentration of 10 ml of stock solution 2 strontium
$V_{SL_1_Sr on Z}$	volume of stock solution 1 strontium put upon the zeolite powder
$V_{SL_2_Sr on Z}$	volume of stock solution 2 strontium put upon the zeolite powder
$V_{H_2O in WH}$	volume of the water mixture in the vial
$V_{H_2O in SL_2_Sr}$	added volume of the triply distilled water for stock solution 2 strontium

Table 4.3: Description of the variable names for the strontium capacity experiment.

Name	Value	Uncertainty
$m_{Sr(NO_3)_2}^*$	7.09508 g	0.00001 g
$M_{Sr(NO_3)_2}$	211.63 g/mol	
M_{Sr}	87.62 g/mol	0.01 g/mol
$V_{Bottle20ml}$	0.02000 l	0.00004 l
$V_{Bottle50ml}$	0.05000 l	0.00005 l
$Pip5000$	5.000 ml	0.015 ml
	4.000 ml	0.013 ml
	1.600 ml	0.008 ml
	1.000 ml	0.005 ml
$V_{PS_Sr \text{ in } SL_1_Sr}$	0.0016000 l	7.7E-06 l
$V_{SL_1_Sr \text{ on } Z}$	0.010000 l	2.1E-05 l
$V_{H_2O \text{ in } WH}$	0.05000 l	1.5E-04 l

Table 4.4: Necessary values for the calculation of the concentrations for the strontium capacity experiment for SL_1_Sr.

Name	Formula
C_{PS_Sr}	$\frac{m_{Sr(NO_3)_2}^*}{V_{Bottle20ml} \cdot M_{Sr(NO_3)_2}}$
$C_{SL_1_Sr}$	$\frac{C_{PS_Sr} \cdot V_{PS_Sr \text{ in } SL_1_Sr}}{V_{Bottle50ml}}$
$C_{SL_1_Sr \text{ 10ml}}$	$C_{SL_1_Sr} \cdot V_{SL_1_Sr \text{ on } Z}$
$C_{SL_1_Sr \text{ 10ml in } \frac{g \text{ Sr}}{10 \text{ ml solution}}}$	$C_{SL_1_Sr \text{ 10ml}} \cdot M_{Sr}$

Table 4.5: Equations for the calculation of the concentrations for the strontium capacity experiment for SL_1_Sr.

Name	Value	Uncertainty
c_{PS_Sr}	$1.6763 \frac{\text{mol Sr}}{\text{l solution}}$	$3.4\text{E-}03 \frac{\text{mol Sr}}{\text{l solution}}$
$c_{SL_1_Sr}$	$0.05364 \frac{\text{mol Sr}}{\text{l solution}}$	$2.9\text{E-}04 \frac{\text{mol Sr}}{\text{l solution}}$
$c_{SL_1_Sr\ 10ml}$	$0.0005364 \frac{\text{mol Sr}}{10\ \text{ml solution}}$	$3.1\text{E-}06 \frac{\text{mol Sr}}{10\ \text{ml solution}}$
	$0.04700 \frac{\text{g Sr}}{10\ \text{ml solution}}$	$2.7\text{E-}04 \frac{\text{g Sr}}{10\ \text{ml solution}}$

Table 4.6: Calculated concentrations of the SL_1_Sr.

Name	Value	Uncertainty
$Pip5000$	2.800 ml	0.011 ml
	2.2000 ml	0.0094 ml
$V_{PS_Sr\ \text{in}\ SL_2_Sr}$	0.0022000 l	$9.4\text{E-}06\ \text{l}$
$m_{Sr(NO_3)_2}$	5.09452 g	0.00001 g
$V_{H_2O\ \text{in}\ SL_2_Sr}$	0.04780 l	$1.4\text{E-}04\ \text{l}$
$V_{SL_2_Sr\ \text{on}\ Z}$	0.010000 l	$2.1\text{E-}05\ \text{l}$

Table 4.7: Additional values for the calculation of the concentrations for the strontium capacity experiment for SL_2_Sr.

Name	Formula
$m_{Sr(NO_3)_2} \cdot 2.2\text{ml}\ PS_Sr$	$V_{PS_Sr\ \text{in}\ SL_2_Sr} \cdot c_{PS_Sr} \cdot M_{Sr(NO_3)_2}$
$c_{SL_2_Sr}$	$\frac{(m_{Sr(NO_3)_2} \cdot 2.2\text{ml}\ PS_Sr + m_{Sr(NO_3)_2}) \cdot (V_{PS_Sr\ \text{in}\ SL_2_Sr} + V_{H_2O\ \text{in}\ SL_2_Sr})}{M_{Sr(NO_3)_2}}$
$c_{SL_2_Sr\ 10ml}$	$c_{SL_2_Sr} \cdot V_{SL_2_Sr\ \text{on}\ Z}$
$c_{SL_2_Sr\ 10ml}\ \text{in}\ \frac{\text{g Sr}}{10\ \text{ml solution}}$	$c_{SL_2_Sr\ 10ml} \cdot M_{Sr}$

Table 4.8: Equations for the calculation of the concentrations for the strontium capacity experiment for SL_2_Sr.

Name	Value	Uncertainty
$m_{Sr(NO_3)_2} \text{ 2.2ml PS}_{Sr}$	0.7805 g	3.7E-03 g
$c_{SL_2_Sr}$	$0.5552 \frac{\text{mol Sr}}{\text{l solution}}$	$1.6E-03 \frac{\text{mol Sr}}{\text{l solution}}$
$c_{SL_2_Sr} \text{ 10ml}$	$0.005552 \frac{\text{mol Sr}}{10 \text{ ml solution}}$	$2.0E-05 \frac{\text{mol Sr}}{10 \text{ ml solution}}$
	$0.4865 \frac{\text{g Sr}}{10 \text{ ml solution}}$	$1.7E-03 \frac{\text{g Sr}}{10 \text{ ml solution}}$

Table 4.9: Calculated values for the strontium capacity experiment for SL_2_Sr.

Sample_solution	Sr Uptake in %	σ	Sr Uptake in mg	σ
A_1	28.49	3.60	13.39	1.71
B_1	28.54	3.60	13.41	1.71
C_1	27.59	3.65	12.97	1.73
D_1	14.96	4.28	7.03	2.02
A_2	6.81	4.68	33.14	22.73
B_2	8.07	4.61	39.25	22.43
C_2	3.37	4.85	16.42	23.57
D_2	2.56	4.89	12.48	23.76

Table 4.10: Uptake of Sr for stock solution 1 and stock solution 2.

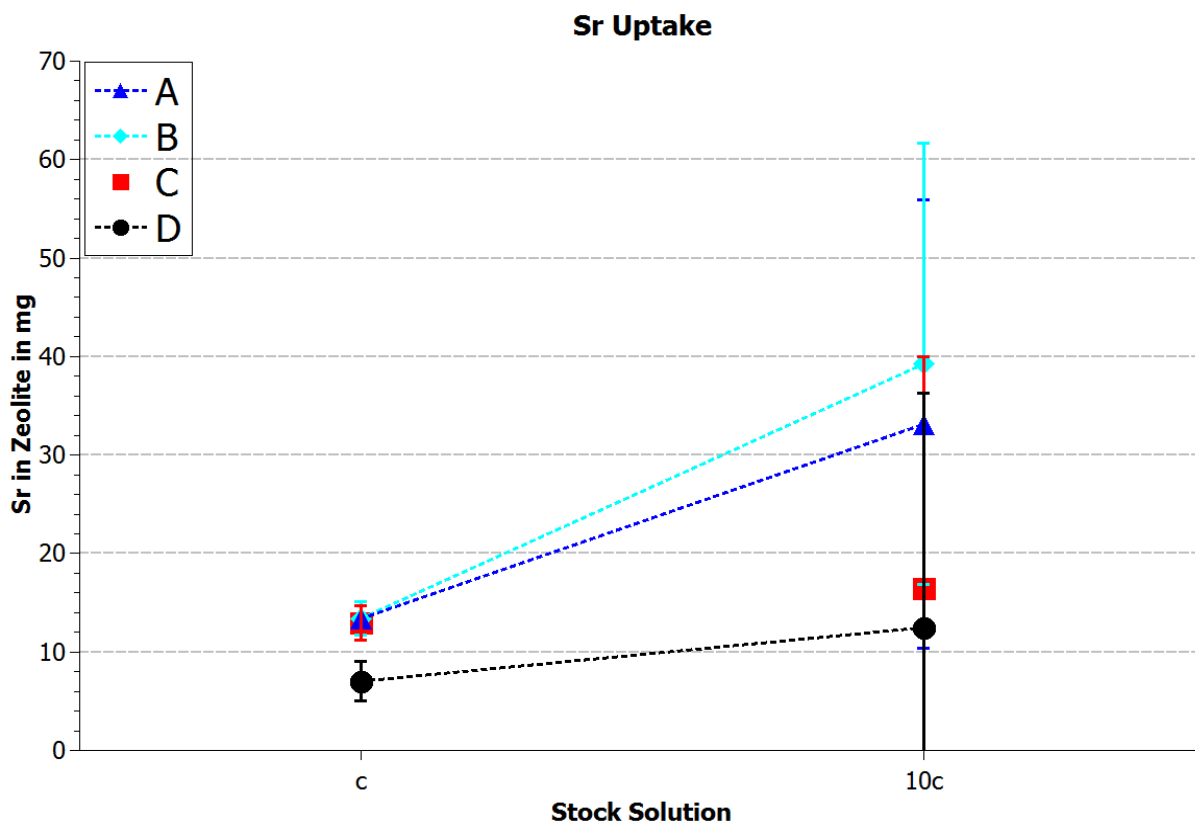


Figure 4.4: Uptake of Sr for the two different stock solutions.

4.5.2 Analysis of the Cs Capacity Experiments and Results

The concentration of the parent solution caesium c_{PS_Cs} was calculated as explained above in section 4.2. 400 μl of the parent solution was used to create the stock solution 1 caesium. The caesium concentration of stock solution 1 caesium $c_{SL_1_Cs}$ was calculated with the mass of the caesium nitrate in 400 μl of the parent solution caesium, the mass of the added inactive caesium nitrate, the volume of the added parent solution caesium, the volume of the added triply distilled water and the molar mass of caesium nitrate. Each 500 mg zeolite sample was mixed with 10 ml of the stock solution 1 caesium and the concentration of the caesium ions was 0.001105 ± 0.000003 mol Cs, which is equal to 146.93 ± 0.30 mg Cs. All the used calculations values are listed in Tab. 4.13 and with Tab. 4.12 the caesium concentration of stock solution 1 was calculated (Tab. 4.14).

The caesium concentration of the stock solution 2 caesium $c_{SL_2_Cs}$ was calculated the same way as $c_{SL_1_Cs}$ just the values changed. 10 ml of the stock solution 2 caesium had 0.01114 ± 0.00004 mol Cs in it, which is equal to 1480.71 ± 5.03 mg Cs. The additional values for the calculations are listed in Tab. 4.15, the equations can be looked up in Tab. 4.16 and the calculated values are in Tab. 4.17. The used variable names are described in Tab. 4.11. The tenfold higher concentration of the stock solution 2 can be clearly seen.

This caesium concentrations of the stock solutions were much higher than the strontium concentrations, because the better exchange process was considered. The spectra are in Appendix G. The caesium uptake of the zeolite samples are presented in Tab. 4.18 and Fig. 4.5. Between the data results of sample C (red squares) is no line, because for the experiment with the first stock solution the provided zeolite powder and for the experiment with the second stock solution the milled material was used. The γ -spectrometer detected peaks of two different energies for $^{134}_{55}\text{Cs}$. The uptake was calculated for each γ -peak as explained in section 4.5 and then the mean values were taken. The stock solution 1 caesium had a concentration of around 150 mg caesium per 10 ml. Sample B is the best material out of the four for trapping caesium particles. As explained in section 2.1 Si rich zeolites prefer to ion-exchange with Cs. Fig. 3.6(b) and Tab. 3.3 show that sample B has the most content of silicon in it from the 90 % clinoptilolite samples A, B and C. So the result is consistent with the theory. As expected, sample D is the worst. The three lines are parallel, and they just represent a short section of the specific saturation curve. The limit for the caesium uptake was nearly reached. The uptake is about 1.6 times higher at a ten-fold higher concentration. It can be seen that a line between the red squares would not be parallel to the others. This suggests that sample C can uptake more ions in its milled form. So, a smaller grain size favours the uptake of ions.

[Frysjnger](#) analysed the caesium-sodium ion exchange of clinoptilolite and found out that clinoptilolite prefers mostly other ions over sodium. The experiments in that work were done differently. The stock solutions flowed through a column which was filled with the clinoptilolite mineral. [He and Walling](#) studied the effects of the particle size on the adsorption of ^{137}Cs . The Cs uptake increases with a bigger surface area of the material, which is equivalent to a smaller grain size. The particle size has "a primary control on the concentrations adsorbed." ([He and](#)

Walling, 1996) In the research of Lihareva et al. a XRD was performed for clinoptilolite after an ion-exchange with Cs. The result was that Cs occupies first the M1 site where normally Na ions sit and then the M2 site where Ca sits. The M1 sites were mainly occupied by Cs, but some M2 sites were still filled with Ca. Furthermore, it was indicated that a longer sorption time increases the possibility of internal diffusion of Cs cations which allows them to occupy more inner M3 sites where K sits. The sites of clinoptilolite are explained in the previous section *2.1.1 Clinoptilolite*.

Symbol	Description
$m_{CsNO_3^*}$	mass of activated caesium nitrate
$m_{1_CsNO_3}$	mass of inactivate caesium nitrate for stock solution 1 caesium
$m_{2_CsNO_3}$	mass of inactivate caesium nitrate for stock solution 2 caesium
$m_{CsNO_3^* 400\mu l PS_Cs}$	mass of activate caesium nitrate in 400 μ l of the parent solution caesium
$m_{CsNO_3^* 2 ml PS_Cs}$	mass of activate caesium nitrate in 2 ml of the parent solution caesium
M_{CsNO_3}	molar mass of caesium nitrate
M_{Cs}	molar mass of caesium
$V_{H_2O in PS_Cs}$	volume of triply distilled water in parent solution caesium
$V_{Bottle50ml}$	volume of the 50 ml bottle
$Pip5000$	used pipette with maximal volume of 5000 μ l
$Pip20$	used pipette with volume of 20 μ l
$Pip100$	used pipette with volume of 100 μ l
c_{PS_Cs}	caesium concentration of parent solution caesium
$V_{PS_Cs in SL_1_Cs}$	volume of parent solution caesium in stock solution 1 caesium
V_{PS_40}	volume of parent solution caesium firstly added to stock solution 2 caesium
V_{PS_360}	volume of parent solution caesium secondly added to stock solution 2 caesium
$V_{PS_Cs in SL_2_Cs}$	volume of parent solution caesium in stock solution 2 caesium
$c_{SL_1_Cs}$	caesium concentration of stock solution 1 caesium
$c_{SL_2_Cs}$	caesium concentration of stock solution 2 caesium
$c_{SL_1_Cs 10ml}$	caesium concentration of 10 ml of stock solution 1 caesium
$c_{SL_2_Cs 10ml}$	caesium concentration of 10 ml of stock solution 2 caesium
$V_{SL_1_Cs on Z}$	volume of stock solution 1 caesium put upon the zeolite powder
$V_{SL_2_Cs on Z}$	volume of stock solution 2 caesium put upon the zeolite powder
$V_{H_2O in WH}$	volume of the water mixture in the vial
$V_{H_2O in SL_1_Cs}$	added volume of the triply distilled water for stock solution 1 caesium
$V_{H_2O in SL_2_Cs}$	added volume of the triply distilled water for stock solution 2 caesium

Table 4.11: Description of the variable names for the caesium capacity experiment.

Name	Value	Uncertainty
$m_{CsNO_3^*}$	0.01043 g	0.00001 g
$m_{1_CsNO_3}$	1.07780 g	0.00001 g
M_{CsNO_3}	194.91 g/mol	
M_{Cs}	132.9100000 g/mol	0.00000002 g/mol
$Pip5000$	5.000 ml	0.015 ml
$Pip20$	20.00 μ l	0.08 μ l
$Pip100$	100.0 μ l	0.5 μ l
$V_{H_2O \text{ in } PS_Cs}$	0.010000 l	3.0E-05 l
$V_{H_2O \text{ in } SL_1_Cs}$	50.04 g	0.01 g
V_{PS_40}	0.00004000 l	1.6E-07 l
V_{PS_360}	0.0003600 l	1.5E-06 l
$V_{SL_1_Cs \text{ on } Z}$	0.010000 l	2.1E-05 l
$V_{H_2O \text{ in } WH}$	0.05000 l	1.5E-04 l

Table 4.12: Values for the calculation of the concentrations for the caesium capacity experiment for SL_1_Cs.

Name	Formula
c_{PS_Cs}	$\frac{m_{CsNO_3^*}}{V_{H_2O \text{ in } PS_Cs} \cdot M_{CsNO_3}}$
$V_{PS_Cs \text{ in } SL_1_Cs}$	$V_{PS_40} + V_{PS_360}$
$m_{CsNO_3^*} \text{ 400}\mu\text{l } PS_Cs$	$V_{PS_Cs \text{ in } SL_1_Cs} \cdot c_{PS_Cs} \cdot M_{CsNO_3}$
$c_{SL_1_Cs}$	$\frac{m_{1_CsNO_3} + m_{CsNO_3^*} \text{ 400}\mu\text{l } PS_Cs}{V_{H_2O \text{ in } PS_Cs} \cdot 10^{-3} \cdot M_{CsNO_3}}$
$c_{SL_1_Cs} \text{ 10ml}$	$c_{SL_1_Cs} \cdot V_{SL_1_Cs \text{ on } Z}$
$c_{SL_1_Cs} \text{ 10ml in } \frac{\text{g Cs}}{10 \text{ ml solution}}$	$c_{SL_1_Cs} \text{ 10ml} \cdot M_{Cs}$

Table 4.13: Equations for the calculation of the concentrations for the caesium capacity experiment for SL_1_Cs.

Name	Value	Uncertainty
c_{PS_Cs}	$0.005351 \frac{\text{mol Cs}}{\text{l solution}}$	$1.7\text{E-}05 \frac{\text{mol Cs}}{\text{l solution}}$
$V_{PS_Cs \text{ in } SL_1_Cs}$	0.0004000 l	1.6E-06 l
$m_{CsNO_3^*} 400\mu\text{l } PS_Cs$	0.0004172 g	1.4E-06 g
$c_{SL_1_Cs}$	$0.110549 \frac{\text{mol Cs}}{\text{l solution}}$	$2.3\text{E-}05 \frac{\text{mol Cs}}{\text{l solution}}$
$c_{SL_1_Cs} 10\text{ml}$	$0.0011055 \frac{\text{mol Cs}}{10 \text{ ml solution}}$	$2.3\text{E-}06 \frac{\text{mol Cs}}{10 \text{ ml solution}}$
	$0.14693 \frac{\text{g Cs}}{10 \text{ ml solution}}$	$3.1\text{E-}04 \frac{\text{g Cs}}{10 \text{ ml solution}}$

Table 4.14: Calculated values for the caesium capacity experiment for SL_1_Cs.

Name	Value	Uncertainty
$m_{2_CsNO_3}$	10.85546 g	0.00001 g
$Pip5000$	2.000 ml	0.009 ml
	3.000 ml	0.011 ml
$V_{H_2O \text{ in } SL_2_Cs}$	0.04800 l	1.4E-04 l
$V_{PS_Cs \text{ in } SL_2_Cs}$	0.0020000 l	8.8E-06 l
$V_{SL_2_Cs \text{ on } Z}$	0.010000 l	2.1E-05 l

Table 4.15: Additional values for the calculation of the concentrations for the caesium capacity experiment for SL_2_Cs.

Name	Formula
$m_{CsNO_3^*} 2 \text{ ml } PS_Cs$	$V_{PS_Cs \text{ in } SL_2_Cs} \cdot c_{PS_Cs} \cdot M_{CsNO_3}$
$c_{SL_2_Cs}$	$\frac{(m_{2_CsNO_3} + m_{CsNO_3^*} 2 \text{ ml } PS_Cs)}{(V_{PS_Cs \text{ in } SL_2_Cs} + V_{H_2O \text{ in } SL_2_Cs}) \cdot M_{CsNO_3}}$
$c_{SL_2_Cs} 10\text{ml}$	$c_{SL_2_Cs} \cdot V_{SL_2_Cs \text{ on } Z}$
$c_{SL_2_Cs} 10\text{ml} \text{ in } \frac{\text{g Cs}}{10 \text{ ml solution}}$	$c_{SL_2_Cs} 10\text{ml} \cdot M_{Cs}$

Table 4.16: Equations for the calculation of the concentrations for the caesium capacity experiment for SL_2_Cs.

Name	Value	Uncertainty
$m_{CsNO_3^*} 2 \text{ ml } PS_Cs$	0.002100 g	1.2E-05 g
$C_{SL_2_Cs}$	$1.1141 \frac{\text{mol Cs}}{\text{l solution}}$	$3.1E-03 \frac{\text{mol Cs}}{\text{l solution}}$
$C_{SL_2_Cs} 10\text{ml}$	$0.011141 \frac{\text{mol Cs}}{10 \text{ ml solution}}$	$3.8E-05 \frac{\text{mol Cs}}{10 \text{ ml solution}}$
	$1.4807 \frac{\text{g Cs}}{10 \text{ ml solution}}$	$5.1E-03 \frac{\text{g Cs}}{10 \text{ ml solution}}$

Table 4.17: Calculated values for the caesium capacity experiment for SL_2_Cs.

Sample_solution	Cs Uptake in %	σ	Cs Uptake in mg	σ
A_1	32.37	0.53	47.55	0.79
B_1	40.40	0.49	59.36	0.73
C_1	38.36	0.50	56.35	0.76
D_1	18.12	0.64	26.62	0.94
A_2	4.70	0.60	69.53	8.93
B_2	5.54	0.60	82.10	8.89
C_2	5.67	0.60	83.91	8.83
D_2	3.52	0.60	52.07	8.85

Table 4.18: Uptake of Cs for stock solution 1 and stock solution 2.

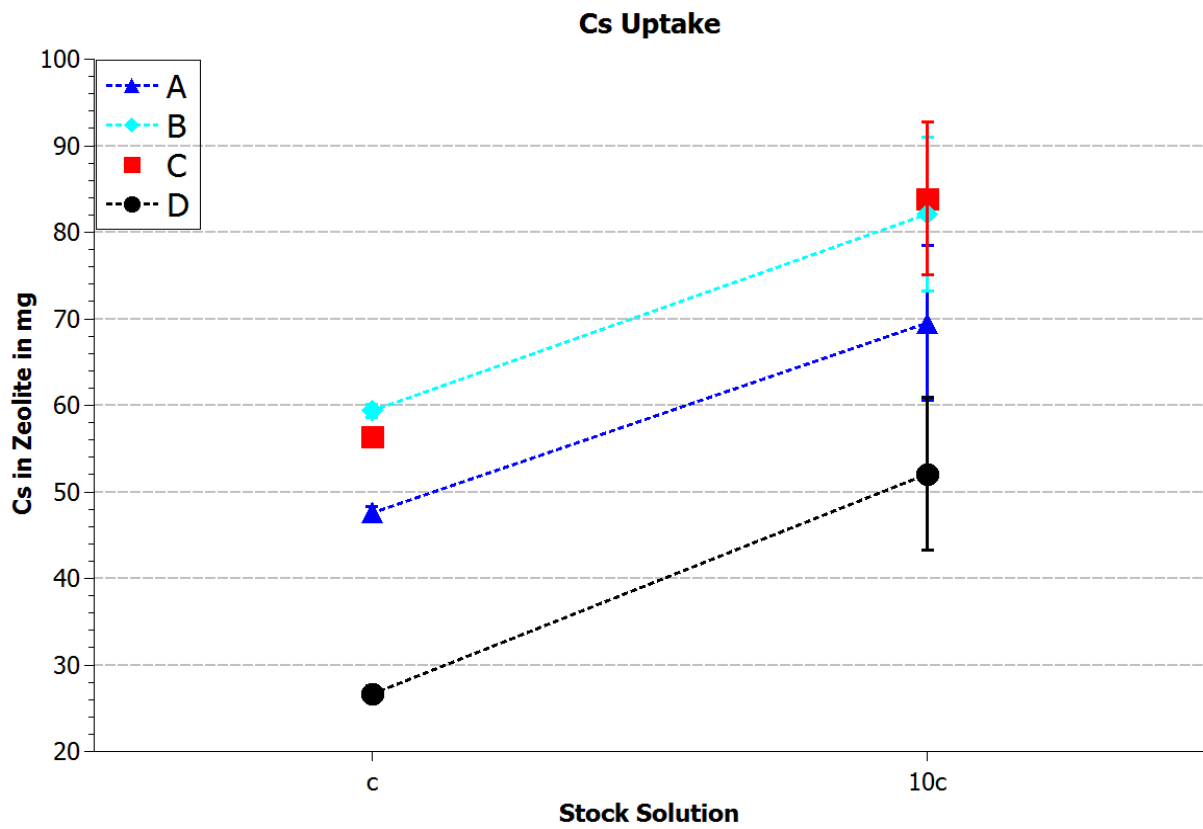


Figure 4.5: Uptake of Cs for the two different stock solutions.

4.6 Capacity for Stock Solution Containing Sr and Cs

For this work no experiment for a stock solution containing strontium and caesium ions was done.

[Ádám et al.](#) investigated the decontamination of radioactive waste water with low activity, which can be proceeded directly in the storage containers. Different ground materials like clinoptilolite was analysed. During this study it was ascertained only little bit less Sr was combined by using a stock solution containing both radioisotopes. The Cs uptake was much lesser than for a stock solution only containing caesium. So it can be said, more " Sr^{2+} ions were combined at the cost of Cs^+ adsorption" ([Ádám et al., 1971](#)). Furthermore, a smaller grain size of the ground material benefits the "ion combining capacity" ([Ádám et al., 1971](#)). But in general zeolites are more selective for monovalent cations like Cs than for divalent cations like Sr ([Misaelides, 2011](#)). The influence of clinoptilolite rich ground on the ^{90}Sr and ^{137}Cs uptake by bean plants was determined by [Nishita et al.](#). Additional added clinoptilolite to the soil increases the ^{137}Cs uptake and decreases the ^{90}Sr uptake into the plant. This result is consistent with the data of [Ádám et al.](#) because, as described above, clinoptilolite prefers to ion-exchange with Sr ions, if both radioisotopes ^{90}Sr and ^{137}Cs are available. A more recent work on the Cs and Sr uptake was done by [Dyer et al.](#). The uptake was analysed in the presence of the competing cations Na^+ , K^+ , Ca^{2+} and Mg^{2+} . The experimental set-up by [Rajec et al.](#) was quite the same as for this work. Furthermore, the results are comparable to the findings of this thesis. "[T]he uptake of strontium and the other bivalent cations is not as effective as of the monovalent cations." ([Rajec et al., 1998](#)) Furthermore, the kinetic factor of the strontium exchange could be quite important for the exchange process.

4.7 Analysis of the Absorbed Sr or Cs Particles

It was checked next, if there is an obvious correlation between the exchangeable ions in the zeolite and the Sr or Cs particles, which were uptaken in the zeolite after the capacity experiment. The zeolite mass for the different capacity experiments is shown in Tab. 4.20 and for the following calculations the mean values of the four samples were taken. For example, to get the mean value $m_{\bar{A}}$ for the experiments with sample A Eq. 4.7.1 was used. The other mean values $m_{\bar{B}}$, $m_{\bar{C}}$ and $m_{\bar{D}}$ were calculated identically.

$$m_{\bar{A}} = \frac{m_{A_SL_1_Sr_Z} + m_{A_SL_2_Sr_Z} + m_{A_SL_1_Cs_Z} + m_{A_SL_2_Cs_Z}}{4} \quad (4.7.1)$$

Tab. 4.21 presents the conversion of Tab. 3.3 into particles. The data was calculated with the mean value of the zeolite sample mass m_Z ($Z = m_{\bar{A}}, m_{\bar{B}}, m_{\bar{C}}, m_{\bar{D}}$), the molar mass of a specific element M_X ($X = Si, Al, Ca, Mg, K, Na, Ti, Mn, V$), the Avogadro constant N_{Av} and the percentage amount of the specific element i in the zeolite powder A_i^{NAA} , which was determined by Neutron Activation Analysis (NAA) (Eq. 4.7.2). The Sr or Cs particles in the zeolites after the experiment were calculated similarly (Eq. 4.7.3 and 4.7.4). The mass of the ions in the zeolite $m_{Ion\ in\ Z}$ ($Ion = Sr, Cs$) was divided through the molar mass of the ion M_{Ion} and multiplied with the Avogadro constant N_{Av} . Tab. 4.22 shows the Sr and Cs particles, which were exchanged into the zeolite during the experiment. Tab. 4.19 explains the variable names.

$$Particles_{NAA} = \frac{m_Z \cdot A_i^{NAA}}{M_X} \cdot N_{Av} \quad (4.7.2)$$

$$Particles_{Sr} = \frac{m_{Sr\ in\ Z}}{M_{Sr}} \cdot N_{Av} \quad (4.7.3)$$

$$Particles_{Cs} = \frac{m_{Cs\ in\ Z}}{M_{Cs}} \cdot N_{Av} \quad (4.7.4)$$

As explained in the previous section 2.1.1 Cs ions exchange mainly with Na and K ions and Sr ions can exchange with two Na ions. From the calculated data it appears that the amounts of Sr or Cs taken up by the zeolite are smaller than the number of exchangeable ions present in the zeolite lattice. Repetition of the capacity experiment with inactive stock solutions followed by subsequent NAA of the zeolite powder could elucidate which ions and how many are exchanged for Sr or Cs.

Symbol	Name
A_i^{NAA}	percentage amount of an element i in the zeolite powder
M_{Ion}	molar mass of $Ion = X, Sr, Cs$
$m_{Ion\ in\ Z}$	mass of $Ion = Sr, Cs$ in zeolite
m_Z	mean mass of the zeolite samples $Z = \bar{A}, \bar{B}, \bar{C}, \bar{D}$
N_{Av}	Avogadro constant
X	element Si, Al, Ca, Mg, K, Na, Ti, Mn or V

Table 4.19: variable names for the analysis of the absorbed Sr or Cs particles.

Sample	Mass of Zeolite Sample in g	Uncertainty in g
A_SL_1_Sr_Z	0.50085	0.00001
B_SL_1_Sr_Z	0.50077	0.00001
C_SL_1_Sr_Z	0.50008	0.00001
D_SL_1_Sr_Z	0.50009	0.00001
A_SL_2_Sr_Z	0.50010	0.00001
B_SL_2_Sr_Z	0.50092	0.00001
C_SL_2_Sr_Z	0.50081	0.00001
D_SL_2_Sr_Z	0.50093	0.00001
A_SL_1_Cs_Z	0.50064	0.00001
B_SL_1_Cs_Z	0.50077	0.00001
C_SL_1_Cs_Z	0.50020	0.00001
D_SL_1_Cs_Z	0.50038	0.00001
A_SL_2_Cs_Z	0.50083	0.00001
B_SL_2_Cs_Z	0.50022	0.00001
C_SL_2_Cs_Z	0.50035	0.00001
D_SL_2_Cs_Z	0.50032	0.00001
Mean values		
A	0.500605	0.00002
B	0.50067	0.00002
C	0.50036	0.00002
D	0.50043	0.00002

Table 4.20: Mass of the zeolite powder used for the capacity experiments.

Elements	Particles	σ	Particles	σ
	A		B	
Al	67E+19	2E+19	64E+19	2E+19
Si	32E+20	4E+20	33E+20	3E+20
Ca	20E+19	2E+19	21E+19	2E+19
Mg	30E+18	8E+18	18E+18	2E+18
K	22E+19	4E+19	23E+19	6E+19
Na	160E+18	8E+18	155E+18	6E+18
Ti	56E+17	3E+17	62E+17	4E+17
Mn	13E+17	1E+17	117E+16	9E+16
V	9E+16	1E+16	69E+15	3E+15
	C		D	
Al	64E+19	2E+19	76E+19	2E+19
Si	28E+20	4E+20	43E+20	5E+20
Ca	163E+18	9E+18	153E+18	8E+18
Mg	25E+18	5E+18	21E+18	3E+18
K	17E+19	3E+19	139E+18	8E+18
Na	56E+18	3E+18	75E+18	3E+18
Ti	57E+17	4E+17	82E+17	7E+17
Mn	94E+16	6E+16	116E+16	9E+16
V	60E+15	9E+15	7E+16	2E+16

Table 4.21: Number of particles calculated with the NAA results for the elements Al, Si, Ca, Mg, K, Na, Ti, Mn and V.

Sample	Sr particles	σ	Cs particles	σ
A_1	9E+19	2E+19	215E+18	4E+18
B_1	9E+19	2E+19	269E+18	4E+18
C_1	9E+19	2E+19	255E+18	4E+18
D_1	5E+19	2E+19	121E+18	5E+18
A_2	23E+19	16E+19	32E+19	5E+19
B_2	27E+19	16E+19	37E+19	5E+19
C_2	11E+19	17E+19	38E+19	4E+19
D_2	9E+19	20E+19	24E+20	4E+19

Table 4.22: Absorbed Sr or Cs particles for stock solution 1 and stock solution 2.

5. Conclusion and Outlook

The Si/Al ratio for samples A and B lies between 4.0 and 5.5 as is characteristic for clinoptilolite. For sample C the ratio is also in this range, if calculated from the NAA data. It can be concluded that sample A, B and C are mainly clinoptilolite. Sample D has a higher value for the Si/Al ratio, which indicates the presence of some additional non-clinoptilolite material.

It has been demonstrated that NAA and TXRF analyses of finely powdered zeolites are comparable. While NAA has been previously applied to the analysis of zeolitic materials, it has also been demonstrated that TXRF analyses of finely powdered zeolites are also possible using a very simple sampling method. Nonetheless, TXRF seems to systematically underestimate the quantitative element content of the zeolites. This can be explained by absorption effects and the inadequacy of the thin film approximation to the sampling method applied.

IR spectroscopy confirmed that sample A, B, C and D contain mostly clinoptilolite and the water loss due to heating during the STA measurements also validates this conclusion. PXRD showed that sample D contains an additional phase compared to the other samples, which is consistent with D as the external sample and the analytical results.

To clarify that sample A and B are just the material C with smaller grain size, it would be interesting to perform a trace element analysis for the samples. Currently this is only an assumption that is not born out by the NAA or TXRF results. This theory may be tested by a longer activation of the samples directly in the TRIGA reactor central irradiation channel where a higher neutron flux is present during operation. A longer decay time subsequent to activation would be necessary before γ -spectroscopic analysis in this case, but should reveal elements present in far lower concentrations.

Comparable capacity determination experiments were performed for both Sr and Cs on the basis of the elemental compositions determined for the materials to be tested. For strontium the uptake (saturation) limit was reached, which lies for sample A and B at around 13.40 ± 1.71 mg Sr per 500 mg zeolite powder. The concentration of stock solution 2 strontium was too high for an accurate determination of the maximum capacity. It would be necessary to try out a stock solution with a concentration of 250 mg strontium per 10 ml for more precise determination of the uptake limit.

For caesium, sample B has a slightly higher capacity with 82.10 ± 8.89 mg Cs per 500 mg zeolite than sample A. The uptake limit was nearly reached and it would be interesting to use a stock solution with a concentration of 2250 mg caesium per 10 ml for the next experiment.

The milled version of sample C has even a higher capacity for Cs than sample B. This can be explained by the importance of the grain size for the ion adsorption ([He and Walling, 1996](#)). The external sample D has the lowest capacity for Sr and Cs as expected because it is less pure clinoptilolite. Sample A and B are about six times more selective for caesium than for strontium. This preference is for example confirmed by [Misaelides \(2011\)](#).

It would be interesting to do a further capacity experiment using a stock solution containing a mixture of both caesium and strontium ions. A PXRD after such a capacity experiment would allow a better understanding of the ion exchange processes involved and would reveal the exchange sites for Sr and Cs.

Appendices

A. NAA

Tables

Element	$T_{1/2}$		σ [b]	H in %	mass in u
Al ₂₈	2.246 min	134.76 s	0.23	100	27.981910350
Ca ₄₉	8.72 min	523.2 s	1.09	0.187	48.955674430
Ca ₄₇	4.54 d	392256 s	0.7	0.004	46.954546140
Mg ₂₇	9.458 min	567.48 s	0.038	11.01	26.984341280
Na ₂₄	14.96 h	53856 s	0.43	100	23.990962910
K ₄₂	12.36 h	44496 s	1.46	6.7302	41.962402760

Table A.1: Parameters for the calculation of the specific activity to choose the right irradiation time for the NAA.

Element	Specific activity in Bq				
	t in s				
	30	60	90	120	180
Al ₂₈	7.34E+08	1.36E+09	1.90E+09	2.36E+09	3.10E+09
Ca ₄₉	9.97E+05	1.96E+06	2.88E+06	3.76E+06	5.43E+06
Ca ₄₇	1.94E+01	3.89E+01	5.83E+01	7.78E+01	1.17E+02
Mg ₂₇	3.49E+06	6.85E+06	1.01E+07	1.32E+07	1.91E+07
Na ₂₄	4.35E+06	8.69E+06	1.30E+07	1.74E+07	2.61E+07
K ₄₂	6.75E+05	1.35E+06	2.02E+06	2.70E+06	4.04E+06

Table A.2: Calculation of the specific activity for different irradiation times for the NAA.

Sample	Mass m in mg	Uncertainty of m in mg	Irradiation time t in s
A	276.38	0.01	60
B	297.29	0.01	60
C	370.14	0.01	60
D	395.30	0.01	60

Table A.3: Mass and irradiation time of the samples for the qualitative NAA measurements.

Sample	Mass m in mg	Uncertainty of m in mg	Irradiation time t in s
A	96.53	0.01	30
CFA_A	107.29	0.01	30
B	99.17	0.01	30
CFA_B	105.35	0.01	30
C	101.32	0.01	30
CFA_C	103.23	0.01	30
D	100.84	0.01	30
CFA_D	92.16	0.01	30

Table A.4: Mass and irradiation time of the samples and the standard Coal Fly Ash (CFA) for the quantitative NAA measurements.

Sample	Acquisition time	Measured time in s	Interval in s
A	19.11.2018 14:33:29	300	389
CFA_A	19.11.2018 14:39:58	300	
B	19.11.2018 14:59:55	300	367
CFA_B	19.11.2018 15:06:02	300	
C	20.11.2018 14:59:25	300	416
CFA_C	20.11.2018 15:06:21	300	
D	19.11.2018 15:57:48	300	350
CFA_D	19.11.2018 16:03:38	300	

Table A.5: Acquisition and measured time of the samples and the standard Coal Fly Ash (CFA) for the quantitative NAA measurements.

Procedure of the Analysis

1. Assign the right elements to the specific energies of the γ peaks.
2. Calculate the error of the Net Peak Area, which is given in per cent, in counts.
3. Do steps 1 and 2 for the zeolite spectra and the CFA spectra.
4. Calculate for the CFA the mass $mass_{CFA}$ of the elements, which are corresponding to the Net Peak Areas, with help of the provided CFA Standard data sheet. Consider the radioactive decay of the CFA sample, which happens in the interval between the measurement of the zeolite and the CFA micro tube.
5. Solve the ratio $Zeolite_{Net\ Peak\ Area} : CFA_{Net\ Peak\ Area} = mass_{Zeolite} : mass_{CFA}$ (Eq. 3.3.1) to get the mass of the specific element in the zeolite sample.
6. Do step 5 for all elements.
7. Calculate the percentage of the elements in the zeolite.
8. Do not forget to calculate the uncertainties.

Spectra

	Peak No.	Energy [keV]	Net Peak Area [cts]	Bkgnd [cts]	FWHM [keV]	Counts/sec	Error [%]	
F	1	6.90	2300	16739	1.289	7.6656E+00	4.40	
F	2	74.85	3556	16118	1.180	1.1852E+01	13.30	
F	3	84.53	686	15132	1.123	2.2857E+00	13.04	
F	4	94.43	1846	15832	1.315	6.1529E+00	17.99	
M	5	165.38	3300	14276	1.294	1.1001E+01	10.66	
m	6	170.25	1020	15250	1.300	3.3989E+00	12.50	Mg-27
F	7	319.43	2011	11772	1.425	6.7031E+00	4.48	Ti-51
F	8	387.75	1131	9717	1.504	3.7710E+00	7.13	
F	9	510.29	6228	10708	2.672	2.0759E+01	7.25	β^* annihilation
F	10	755.87	5154	8211	1.987	1.7180E+01	5.84	Al-28
M	11	842.81	18596	7690	1.869	6.1988E+01	1.85	Mg-27
m	12	845.83	77896	7519	1.870	2.5965E+02	1.17	Mn-56
F	13	1013.62	6484	8068	1.969	2.1612E+01	5.37	Mg-27
M	14	1267.28	6658	9422	2.971	2.2193E+01	6.15	Al-28
m	15	1272.71	2692	11886	2.973	8.9726E+00	6.07	Al-29
F	16	1292.82	579	6416	1.841	1.9312E+00	82.77	
F	17	1368.04	43892	10030	2.275	1.4631E+02	1.16	Na-24
F	18	1433.56	3012	10883	2.385	1.0042E+01	10.60	V-52
F	19	1524.33	2275	14429	2.539	7.5836E+00	4.94	K-42
F	20	1731.45	2563	2612	3.136	8.5430E+00	2.60	Na-24
F	21	1778.71	223258	3236	2.651	7.4419E+02	0.36	Al-28
F	22	1810.50	10729	1446	2.620	3.5764E+01	2.09	Mn-56
F	23	2061.84	455	1061	2.793	1.5170E+00	28.00	Ca-49
F	24	2113.15	5209	1178	2.900	1.7362E+01	3.67	Mn-56
F	25	2243.05	3804	1352	3.878	1.2681E+01	1.80	Na-24
F	26	2573.88	717	1204	4.056	2.3893E+00	5.95	Ca-49
F	27	2658.09	269	505	2.547	8.9584E-01	9.97	Mn-56
F	28	2754.48	23066	625	3.479	7.6886E+01	0.66	Na-24
F	29	3084.97	3236	169	3.856	1.0788E+01	1.80	Ca-49

Table A.6: NAA spectrum data for A. Errors quoted at 1.00 sigma.

	Peak No.	Energy [keV]	Net Peak Area [cts]	Bkgnd [cts]	FWHM [keV]	Counts/sec	Error [%]	
F	1	47.50	2033	9885	1.350	6.7758E+00	17.51	
M	2	53.92	950	8566	1.176	3.1683E+00	7.32	
m	3	58.61	1672	8815	1.186	5.5719E+00	4.70	
F	4	74.76	4833	11690	1.151	1.6111E+01	5.73	
F	5	94.51	12490	12291	1.195	4.1634E+01	4.08	
F	6	104.11	4451	11226	1.213	1.4836E+01	8.02	
F	7	121.49	3938	9974	1.227	1.3128E+01	2.34	
M	8	165.46	2890	7066	1.204	9.6340E+00	13.91	
m	9	170.19	1065	7502	1.210	3.5485E+00	15.07	Mg-27
F	10	231.40	375	6417	0.954	1.2515E+00	17.97	
F	11	279.29	1407	6768	1.497	4.6904E+00	19.28	
F	12	319.53	9046	6813	1.408	3.0155E+01	1.23	Ti-51
F	13	343.64	873	6281	1.432	2.9109E+00	28.8	
F	14	361.11	1803	6726	1.504	6.0105E+00	3.98	
F	15	387.89	2203	7009	1.399	7.3425E+00	3.31	
F	16	416.25	631	5891	1.449	2.1040E+00	9.62	
F	17	510.31	3090	6648	2.661	1.0300E+01	2.58	β^* annihilation
F	18	558.46	1004	5045	1.469	3.3451E+00	6.50	
F	19	632.78	684	5873	1.588	2.2795E+00	10.07	
F	20	714.64	574	3473	1.715	1.9125E+00	9.77	
F	21	755.96	1777	4184	1.907	5.9237E+00	12.30	Al-28
F	22	833.21	536	3699	1.694	1.7868E+00	30.71	
M	23	842.81	30163	3845	1.797	1.0054E+02	1.26	Mg-27
m	24	845.89	48057	4130	1.799	1.6019E+02	1.04	Mn-56
F	25	962.46	1821	3296	1.790	6.0699E+00	9.54	
F	26	1013.57	10233	3863	2.001	3.4110E+01	1.08	Mg-27
F	27	1096.64	719	3415	2.176	2.3972E+00	29.78	
M	28	1267.19	2689	4082	2.918	8.9634E+00	9.66	Al-28
m	29	1272.67	1151	5129	2.920	3.8369E+00	9.70	Al-29
F	30	1292.94	1453	3879	2.173	4.8433E+00	14.35	
F	31	1368.03	8007	4072	2.253	2.6690E+01	3.26	Na-24
F	32	1433.50	20666	4602	2.305	6.8888E+01	1.70	V-52
F	33	1524.32	1697	6172	2.218	5.6572E+00	13.59	K-42
F	34	1731.49	479	916	2.976	1.5955E+00	7.26	Na-24
F	35	1778.63	84134	1019	2.596	2.8045E+02	0.60	Al-28
F	36	1810.42	6271	490	2.632	2.0902E+01	2.62	Mn-56
F	37	2113.11	3040	305	2.881	1.0133E+01	4.14	Mn-56
F	38	2242.90	747	314	4.162	2.4886E+00	4.13	Na-24
F	39	2657.78	216	151	2.829	7.2129E-01	8.46	Mn-56
F	40	2754.43	4199	141	3.464	1.3998E+01	1.56	Na-24
F	41	3084.83	1202	39	3.764	4.0066E+00	2.93	Ca-49

Table A.7: NAA spectrum data for CFA_A. Errors quoted at 1.00 sigma.

	Peak No.	Energy [keV]	Net Peak Area [cts]	Bkgnd [cts]	FWHM [keV]	Counts/sec	Error [%]	
F	1	7.40	7788	18795	2.205	2.5961E+01	10.58	
F	2	74.71	5087	36968	1.125	1.6956E+01	13.29	
F	3	84.54	1324	35036	0.927	4.4132E+00	35.00	
F	4	94.28	1766	36601	1.559	5.8861E+00	29.10	
F	5	165.14	3164	35608	1.291	1.0546E+01	14.31	
F	6	319.31	3434	24328	1.546	1.1448E+01	3.72	Ti-51
F	7	387.84	1150	18640	1.521	3.8326E+00	9.66	
F	8	510.09	13332	22546	2.865	4.4439E+01	5.32	β^* annihilation
F	9	755.91	14345	19311	1.966	4.7815E+01	2.53	Al-28
M	10	842.84	25133	17461	1.940	8.3775E+01	1.93	Mg-27
m	11	845.88	75143	17508	1.942	2.5048E+02	1.34	Mn-56
F	12	1013.71	9104	19844	2.092	3.0345E+01	5.07	Mg-27
M	13	1267.30	21138	27054	3.149	7.0461E+01	3.34	Al-28
m	14	1272.76	4048	30199	3.151	1.3492E+01	4.45	Al-29
F	15	1368.14	43738	28951	2.329	1.4579E+02	1.70	Na-24
F	16	1433.69	4959	28459	2.202	1.6530E+01	3.16	V-52
F	17	1524.10	2513	37180	2.522	8.3772E+00	7.11	K-42
F	18	1731.55	2663	5963	2.940	8.8769E+00	3.09	Na-24
F	19	1778.84	678680	11975	2.723	2.2623E+03	0.22	Al-28
F	20	1810.65	10688	2580	2.756	3.5626E+01	2.49	Mn-56
F	21	2062.46	690	1560	2.844	2.3012E+00	24.77	Ca-49
F	22	2113.35	4907	1709	2.845	1.6355E+01	4.16	Mn-56
F	23	2243.10	3896	1793	3.979	1.2988E+01	1.84	Na-24
F	24	2573.68	981	1701	4.386	3.2712E+00	4.96	Ca-49
F	25	2657.71	440	740	3.052	1.4655E+00	7.55	Mn-56
F	26	2754.57	23255	1011	3.554	7.7515E+01	0.66	Na-24
F	27	3085.06	4534	322	3.710	1.5112E+01	1.53	Ca-49

Table A.8: NAA spectrum data for B. Errors quoted at 1.00 sigma.

	Peak No.	Energy [keV]	Net Peak Area [cts]	Bkgnd [cts]	FWHM [keV]	Counts/sec [%]	Error	
F	1	6.62	2974	17827	1.369	9.9145E+00	3.72	
F	2	47.40	1796	18396	1.410	5.9879E+00	21.92	
M	3	53.96	928	15636	1.096	3.0935E+00	15.17	
m	4	58.65	2188	20325	1.106	7.2944E+00	12.75	
F	5	74.73	6424	22470	1.250	2.1412E+01	6.86	
F	6	84.56	948	23256	0.964	3.1614E+00	37.89	
F	7	94.44	13009	20668	1.226	4.3365E+01	3.86	
F	8	103.95	5048	21427	1.332	1.6828E+01	8.65	
F	9	121.40	3861	20708	1.179	1.2871E+01	2.92	
M	10	165.41	2811	15146	1.223	9.3688E+00	3.76	
m	11	170.07	1389	14809	1.228	4.6292E+00	6.73	Mg-27
F	12	279.13	923	12476	0.969	3.0764E+00	9.52	
F	13	319.41	14119	15490	1.407	4.7062E+01	3.17	Ti-51
F	14	343.70	995	11304	1.504	3.3153E+00	8.75	
F	15	360.97	1921	13506	1.426	6.4045E+00	10.52	
F	16	387.79	2143	9579	1.297	7.1428E+00	4.20	
F	17	416.20	602	8319	1.201	2.0077E+00	12.89	
F	18	510.21	6804	12430	2.856	2.2680E+01	6.92	β^* annihilation
F	19	558.32	1292	10115	1.931	4.3068E+00	6.67	
F	20	632.65	675	9920	1.355	2.2501E+00	12.35	
F	21	755.91	6010	8896	1.886	2.0034E+01	1.76	Al-28
M	22	842.81	39089	8718	1.833	1.3030E+02	1.20	Mg-27
m	23	845.85	48920	9476	1.835	1.6307E+02	1.03	Mn-56
F	24	962.56	1783	9170	2.014	5.9428E+00	16.85	
F	25	1013.62	13554	9093	2.011	4.5179E+01	1.01	Mg-27
M	26	1267.27	8216	12182	3.091	2.7387E+01	1.49	Al-28
m	27	1272.51	1699	13468	3.094	5.6642E+00	5.28	Al-29
F	28	1292.96	1316	9061	2.000	4.3855E+00	6.70	
F	29	1368.01	7671	11223	2.260	2.5569E+01	1.60	Na-24
F	30	1433.56	43278	14301	2.378	1.4426E+02	1.24	V-52
F	31	1524.26	1704	17314	1.997	5.6800E+00	22.31	K-42
F	32	1778.72	286628	2957	2.644	9.5543E+02	0.31	Al-28
F	33	1810.53	6470	846	2.669	2.1565E+01	2.71	Mn-56
F	34	2113.15	3235	339	3.005	1.0785E+01	4.20	Mn-56
F	35	2243.05	829	370	4.167	2.7644E+00	3.96	Na-24
F	36	2658.14	219	201	3.083	7.3047E-01	9.01	
F	37	2754.56	4308	198	3.410	1.4358E+01	1.55	Na-24
F	38	3084.94	1615	76	3.649	5.3842E+00	2.54	Ca-49

Table A.9: NAA spectrum data for CFA_B. Errors quoted at 1.00 sigma.

	Peak No.	Energy [keV]	Net Peak Area [cts]	Bkgnd [cts]	FWHM [keV]	Counts/sec [%]	Error	
F	1	74.83	3405	14575	1.173	1.1348E+01	12.95	
F	2	94.46	1867	13018	1.055	6.2241E+00	17.57	
M	3	165.38	4940	11013	1.244	1.6466E+01	7.87	
m	4	170.16	708	9725	1.250	2.3601E+00	13.43	Mg-27
F	5	319.48	2094	9323	1.358	6.9798E+00	4.07	Ti-51
F	6	387.87	1699	10338	1.602	5.6627E+00	4.72	
F	7	510.27	4864	9183	2.595	1.6212E+01	8.26	β^* annihilation
F	8	755.91	4991	7240	1.953	1.6638E+01	1.87	Al-28
M	9	842.83	19219	6795	1.850	6.4065E+01	1.73	Mg-27
m	10	845.83	61522	6119	1.852	2.0507E+02	1.17	Mn-56
F	11	1013.62	6654	6921	1.961	2.2181E+01	4.53	Mg-27
M	12	1267.21	6591	9092	2.931	2.1969E+01	5.88	Al-28
m	13	1272.57	2534	8568	2.933	8.4461E+00	6.23	Al-29
F	14	1293.00	751	5266	2.038	2.5037E+00	10.01	
F	15	1368.03	16750	9667	2.325	5.5832E+01	2.32	Na-24
F	16	1433.59	2247	10168	2.173	7.4897E+00	13.57	V-52
F	17	1524.32	2015	14746	2.621	6.7169E+00	5.48	K-42
F	18	1731.42	997	1994	2.825	3.3229E+00	5.00	Na-24
F	19	1778.66	227415	2554	2.654	7.5805E+02	0.36	Al-28
F	20	1810.47	8486	899	2.652	2.8286E+01	2.44	Mn-56
F	21	2113.13	4013	586	2.871	1.3376E+01	3.88	Mn-56
F	22	2243.02	1518	715	3.925	5.0589E+00	2.97	Na-24
F	23	2657.94	289	312	3.289	9.6189E-01	8.12	Mn-56
F	24	2754.43	8979	393	3.472	2.9930E+01	1.07	Na-24
F	25	3084.93	2552	94	3.711	8.5073E+00	2.01	Ca-49

Table A.10: NAA spectrum data for C. Errors quoted at 1.00 sigma.

	Peak No.	Energy [keV]	Net Peak Area [cts]	Bkgnd [cts]	FWHM [keV]	Counts/sec [%]	Error	
F	1	47.44	1908	9421	1.324	6.3611E+00	18.92	
M	2	53.95	978	7255	1.134	3.2613E+00	13.74	
m	3	58.66	1753	10248	1.144	5.8448E+00	11.78	
F	4	74.78	4596	10853	1.138	1.5319E+01	6.06	
F	5	94.52	12520	11736	1.192	4.1733E+01	1.04	
F	6	104.07	4334	10473	1.203	1.4446E+01	7.56	
F	7	121.52	4055	9499	1.244	1.3516E+01	2.26	
M	8	165.44	2953	8472	1.263	9.8450E+00	9.22	
m	9	170.30	1026	8387	1.269	3.4194E+00	10.58	Mg-27
F	10	279.26	1166	7897	1.278	3.8876E+00	18.16	
F	11	319.53	8151	6870	1.346	2.7169E+01	3.65	Ti-51
F	12	343.82	702	4351	0.939	2.3389E+00	25.44	
F	13	361.08	1850	5746	1.471	6.1664E+00	3.79	
F	14	387.95	2042	5335	1.355	6.8070E+00	12.09	
F	15	416.35	656	4768	1.448	2.1851E+00	9.07	
F	16	486.38	347	5114	1.077	1.1559E+00	14.91	
F	17	510.26	3231	6243	2.846	1.0772E+01	2.41	β^* annihilation
F	18	558.45	966	6487	1.601	3.2190E+00	6.62	
F	19	632.62	780	4734	1.280	2.5998E+00	8.34	
F	20	714.71	733	4241	2.194	2.4422E+00	7.61	
F	21	755.96	1615	3802	1.974	5.3820E+00	3.77	Al-28
F	22	833.32	553	3390	1.445	1.8429E+00	27.91	
M	23	842.82	28762	3506	1.775	9.5874E+01	1.28	Mg-27
m	24	845.90	47134	3836	1.777	1.5711E+02	1.06	Mn-56
F	25	962.44	1783	2952	1.976	5.9431E+00	3.35	
F	26	1013.58	9875	3265	2.028	3.2917E+01	2.84	Mg-27
F	27	1096.34	665	3071	2.131	2.2179E+00	7.95	
M	28	1267.16	2251	3630	2.937	7.5020E+00	11.25	Al-28
m	29	1272.56	1094	5264	2.940	3.6460E+00	10.37	Al-29
F	30	1292.92	1234	2718	2.216	4.1145E+00	4.78	
F	31	1367.97	7975	3545	2.279	2.6583E+01	3.22	Na-24
F	32	1433.48	18519	4081	2.365	6.1730E+01	1.78	V-52
F	33	1524.25	1770	4977	2.315	5.9003E+00	12.06	K-42
F	34	1731.39	494	811	2.682	1.6459E+00	9.48	Na-24
F	35	1778.61	72107	883	2.600	2.4036E+02	0.65	Al-28
F	36	1810.43	6244	574	2.659	2.0813E+01	1.29	Mn-56
F	37	2113.06	3085	349	3.009	1.0285E+01	1.86	Mn-56
F	38	2242.63	792	272	4.359	2.6402E+00	3.88	Na-24
F	39	2754.38	4262	163	3.414	1.4207E+01	1.55	Na-24
F	40	3084.89	1041	41	3.819	3.4696E+00	3.15	Ca-49

Table A.11: NAA spectrum data for CFA_C. Errors quoted at 1.00 sigma.

	Peak No.	Energy [keV]	Net Peak Area [cts]	Bkgnd [cts]	FWHM [keV]	Counts/sec [%]	Error	
F	1	74.79	2156	7473	1.194	7.1863E+00	11.99	
F	2	94.53	2809	7915	1.175	9.3642E+00	2.77	
F	3	104.02	997	7666	1.494	3.3240E+00	27.16	
F	4	121.46	744	5982	1.227	2.4807E+00	8.57	
F	5	165.43	3287	7224	1.167	1.0956E+01	7.68	
F	6	319.58	1367	5346	1.258	4.5563E+00	4.67	Ti-51
F	7	387.89	1005	3845	1.364	3.3510E+00	5.84	
F	8	510.22	1888	5520	2.486	6.2920E+00	14.48	β^* annihilation
F	9	755.84	826	2149	1.918	2.7538E+00	6.06	Al-28
M	10	842.85	14244	2866	1.843	4.7478E+01	1.80	Mg-27
m	11	845.89	70308	2631	1.844	2.3436E+02	1.04	Mn-56
F	12	1013.56	4924	2402	1.936	1.6414E+01	5.32	Mg-27
M	13	1267.18	903	2117	2.201	3.0104E+00	5.18	Al-28
m	14	1272.65	1117	2097	2.203	3.7223E+00	4.45	Al-29
F	15	1368.01	21590	2360	2.287	7.1968E+01	1.40	Na-24
F	16	1433.33	853	2430	2.407	2.8439E+00	21.17	V-52
F	17	1524.17	1531	3372	2.288	5.1043E+00	4.00	K-42
F	18	1731.26	1348	950	3.088	4.4937E+00	10.61	Na-24
F	19	1778.60	37989	1097	2.608	1.2663E+02	0.95	Al-28
F	20	1810.44	9636	761	2.643	3.2119E+01	2.17	Mn-56
F	21	2113.15	4550	597	2.739	1.5168E+01	3.69	Mn-56
F	22	2242.94	1880	725	3.808	6.2676E+00	2.60	Na-24
F	23	2657.81	397	234	3.635	1.3238E+00	6.06	Mn-56
F	24	2754.41	11286	298	3.468	3.7619E+01	0.95	Na-24
F	25	2960.41	169	70	3.243	5.6459E-01	8.92	Mn-56
F	26	3084.90	1520	59	3.635	5.0683E+00	2.61	Ca-49

Table A.12: NAA spectrum data for D. Errors quoted at 1.00 sigma.

	Peak No.	Energy [keV]	Net Peak Area [cts]	Bkgnd [cts]	FWHM [keV]	Counts/sec [%]	Error	
F	1	47.40	1674	5413	1.452	5.5796E+00	14.65	
M	2	53.96	980	4466	1.114	3.2670E+00	13.85	
m	3	58.72	941	5458	1.123	3.1358E+00	13.35	
F	4	74.83	3253	6422	1.128	1.0842E+01	7.12	
F	5	94.57	10423	6666	1.184	3.4744E+01	3.10	
F	6	104.13	3158	5528	1.199	1.0526E+01	8.99	
F	7	121.56	3232	4813	1.143	1.0773E+01	11.17	
M	8	165.49	2440	4336	1.256	8.1344E+00	2.79	
m	9	170.22	565	4268	1.262	1.8828E+00	8.78	Mg-27
F	10	279.33	1148	4227	1.438	3.8280E+00	17.62	
F	11	319.62	3772	3691	1.387	1.2575E+01	6.03	Ti-51
F	12	343.72	573	2846	1.168	1.9106E+00	8.24	
F	13	361.18	1464	2924	1.343	4.8801E+00	12.05	
F	14	388.00	1781	3155	1.352	5.9379E+00	3.24	
F	15	416.33	549	2451	1.507	1.8316E+00	8.46	
F	16	510.27	1764	3326	2.563	5.8806E+00	14.58	β^* annihilation
F	17	558.41	869	2954	1.503	2.8975E+00	5.94	
F	18	632.86	496	3398	1.433	1.6532E+00	10.52	
F	19	714.79	469	2009	1.570	1.5642E+00	8.8	
F	20	755.99	235	1380	1.491	7.8408E-01	14.73	Al-28
F	21	833.28	439	1399	1.885	1.4637E+00	29.9	
M	22	842.82	15966	1524	1.768	5.3221E+01	1.64	Mg-27
m	23	845.99	40378	1822	1.770	1.3459E+02	1.27	Mn-56
F	24	962.56	1532	1246	1.900	5.1080E+00	8.70	
F	25	1013.61	5688	1233	1.992	1.8962E+01	3.18	Mg-27
F	26	1096.64	496	1134	2.736	1.6545E+00	7.47	
F	27	1272.79	318	1099	1.729	1.0612E+00	10.12	Al-29
F	28	1292.87	1197	1089	2.175	3.9915E+00	3.67	
F	29	1368.02	6933	977	2.252	2.3109E+01	2.63	Na-24
F	30	1433.52	6214	1024	2.332	2.0712E+01	2.96	V-52
F	31	1524.26	1500	1331	2.326	5.0000E+00	3.30	K-42
F	32	1731.50	398	430	2.553	1.3260E+00	20.99	Na-24
F	33	1778.66	12729	420	2.576	4.2431E+01	1.68	Al-28
F	34	1810.48	5272	284	2.605	1.7574E+01	2.85	Mn-56
F	35	2113.18	2484	280	2.687	8.2807E+00	4.74	Mn-56
F	36	2242.96	586	235	4.099	1.9544E+00	4.65	Na-24
F	37	2523.59	112	156	2.061	3.7274E-01	14.48	Mn-56
F	38	2754.45	3636	125	3.407	1.2121E+01	1.68	Na-24
F	39	3084.90	649	15	3.564	2.1619E+00	3.97	Ca49

Table A.13: NAA spectrum data for CFA_D. Errors quoted at 1.00 sigma.

B. TXRF

Procedure of the Analysis

1. Measure five Plexiglas reflectors with zeolite powder for each sample. Calculate the mean element proportional constants for the elements out of the five data results from the experiment. Do this for all measured zeolite samples.
2. Calculate all the ratios for the determined elements with the mean proportional constants of the zeolite data. Call this x .
3. Calculate the mean proportional constants for the elements out of the five data results from the CFA measurements.
4. Calculate all the ratios for the elements with the mean proportional constants of the CFA data. Call this r_m .
5. Calculate the same ratios again with the data in wt% from the CFA data sheet. Call this r_s .
6. Calculate a quantification factor k by dividing z and y . The formula is $k = \frac{r_s}{r_m}$ (Eq. 3.4.1).
7. Multiply the k with x to get the corrected result because of formula $k \cdot x = \text{true } x$.

TXRF Data

	CFA01	CFA02	CFA03	CFA04	CFA05	\bar{x}	σ
Al	1088	1083	1080	1065	1090	1081	8
Si	1000	1000	1000	1000	1000	1000	0
K	140	137	139	138	139	139	2
Ca	83	82	85	83	85	83	2
Ti	58	56	56	56	59	57	2
Fe	200	191	216	199	215	204	10
Ni	0.639	0.631	0.707	0.625	0.679	0.656	0.029

Table B.1: Element specific concentration proportional constants (corrected intensities for fundamental parameters) and their mean values for CFA with TXRF. The values are given by Atomika 8030C and the element silicon was set to the internal standard. This means, that the proportional constant for silicon was set to 1000.

	A01	A02	A03	A04	A05	\bar{x}	σ
Al	316	303	315	315	293	308	9
Si	1000	1000	1000	1000	1000	1000	0
K	112	106	110	128	125	116	9
Ca	111	98	98	99	99	101	5
Ti	5	5	6	5	6	5	1
Fe	34	33	38	35	36	35	2
Ni	0.158	0.176	0.119	0.117	0.07	0.128	0.034

Table B.2: Element specific concentration proportional constants (corrected intensities for fundamental parameters) and their mean values for A with TXRF. The values are given by Atomika 8030C and the element silicon was set to the internal standard. This means, that the proportional constant for silicon was set to 1000.

	B01	B02	B03	B04	B05	\bar{x}	σ
Al	301	299	298	300	294	299	3
Si	1000	1000	1000	1000	1000	1000	0
K	125	127	125	124	124	125	1
Ca	102	103	99	105	98	101	3
Ti	5	5	5	5	5	5	1
Fe	34	35	35	34	34	35	1
Ni	0.035	0.044	0.036	0.022	0.041	0.036	0.007

Table B.3: Element specific concentration proportional constants (corrected intensities for fundamental parameters) and their mean values for B with TXRF. The values are given by Atomika 8030C and the element silicon was set to the internal standard. This means, that the proportional constant for silicon was set to 1000.

	C01	C02	C03	C04	C05	\bar{x}	σ
Al	264	274	274	271	265	270	4
Si	1000	1000	1000	1000	1000	1000	0
K	103	105	97	102	100	101	3
Ca	77	76	71	75	74	75	2
Ti	6	6	5	6	6	6	1
Fe	35	35	33	35	36	35	1
Ni	0.034	0.03	0.026	0.021	0.077	0.038	0.019

Table B.4: Element specific concentration proportional constants (corrected intensities for fundamental parameters) and their mean values for C with TXRF. The values are given by Atomika 8030C and the element silicon was set to the internal standard. This means, that the proportional constant for silicon was set to 1000.

	D01	D02	D03	D04	D05	\bar{x}	σ
Al	272	273	275	273	276	274	2
Si	1000	1000	1000	1000	1000	1000	0
K	76	79	75	78	74	77	2
Ca	50	53	49	51	48	50	2
Ti	8	8	8	8	8	8	1
Fe	40	45	41	42	40	42	2
Ni	0.022	0.026	0.026	0.028	0.019	0.024	0.003

Table B.5: Element specific concentration proportional constants (corrected intensities for fundamental parameters) and their mean values for D with TXRF. The values are given by Atomika 8030C and the element silicon was set to the internal standard. This means, that the proportional constant for silicon was set to 1000.

C. PXRD

Phases

The following section is presenting the different crystalline phases which were determined in the samples.

Four phases were found:

- Phase 1:
 - Reference code: 01-083-1261
 - Mineral name: Clinoptilolite-Na
- Phase 2:
 - Reference code: 00-050-1714
 - Mineral name: Terranovaite
- Phase 3:
 - Reference code: 00-020-0452
 - Mineral name: Gismondine
- Phase 4:
 - Reference code: 01-085-1415
 - Mineral name: Anorthite, sodian, syn

Date: 23.01.2019 Time: 09:43:54 File: HighScore Plus - 4-120°_24min_A_LithoFill_T

User: hradii

Name and formula

Reference code: 01-083-1261

Mineral name: Clinoptilolite-Na
 Compound name: Sodium Potassium Magnesium Calcium Hydrate Aluminum Silicate
 Common name: Clinoptilolite, sodium potassium magnesium calcium hydrate aluminosilicate *

Empirical formula: $\text{Al}_6\text{Ca}_{1.24}\text{H}_{42.64}\text{K}_{1.76}\text{Mg}_{0.2}\text{Na}_{1.84}\text{O}_{93.32}\text{Si}_{30}$
 Chemical formula: $\text{Ca}_{1.24}\text{Na}_{1.84}\text{K}_{1.76}\text{Mg}_{0.2}\text{Al}_6\text{Si}_{30}\text{O}_{72}(\text{H}_2\text{O})_{21.32}$
 Mineral classification: Zeolite (Family), heulandite (Supergroup)
 Zeolite classification: HEU(Heulandite)

Crystallographic parameters

Crystal system: Monoclinic
 Space group: C2/m
 Space group number: 12

a (Å): 17,6620
 b (Å): 17,9110
 c (Å): 7,4070
 Alpha (°): 90,0000
 Beta (°): 116,4000
 Gamma (°): 90,0000

Volume of cell (10^6 pm^3): 2098,80
 Z: 1,00

RIR: 0,95

Status, subfiles and quality

Status: Alternate Pattern
 Subfiles: ICSD Pattern, Inorganic, Micro & Mesoporous, Mineral, Mineral - Mineral, Mineral - Natural, Zeolite
 Quality: Blank (B)

Comments

ANX: AB7C8D9X467
 ICSD collection code: 100096
 Creation Date: 01.09.1998
 Modification Date: 01.09.2017
 Cross-References: ICSD:100096, ICDD:01-083-1261, ICDD:04-013-6125 (related phase)
 Additional Patterns: See PDF 04-013-6125
 ANX: AB7C8D9X467
 Analysis: $\text{H}_{42.64}\text{Al}_6\text{Ca}_{1.24}\text{K}_{1.76}\text{Mg}_{0.2}\text{Na}_{1.84}\text{O}_{93.32}\text{Si}_{30}$
 Formula from original source: $\text{Ca}_{1.24}\text{Na}_{1.84}\text{K}_{1.76}\text{Mg}_{0.2}\text{Al}_6\text{Si}_{30}\text{O}_{72}(\text{H}_2\text{O})_{21.32}$
 ICSD Collection Code: 100096
 Sample Source or Locality: Specimen from Agoura, USA
 Test from external database: Deviation of the charge sum from zero tolerable
 Minor Warning: Density calculated using chemical formula and refined composition differ by 1.4019%. Minor test comments from ICSD exist
 Significant Warning: Reported displacement parameters on non H atoms are outside the range $0.001 < U < 0.1$. $U_{eq} = 0.012$ used in the calculation
 Wyckoff Sequence: j13 i8 h2 g d c(C12/M1)
 Unit Cell Data Source: Single Crystal.

References

Primary reference: Koyama, K., Takeuchi, Y., *Z. Kristallogr., Kristallgeom., Kristallphys., Kristallchem.*, **145**, 216, (1977)
 Structure: Koyama, K., Takeuchi, Y., *Z. Kristallogr., Kristallgeom., Kristallphys., Kristallchem.*, **145**, 216, (1977)

Peak list

No.	h	k	l	d [Å]	2θ [°]	I [%]	
1	1	1	1	0	11,85710	7,450	4,2
2	0	2	0	0	8,95550	9,869	100,0
3	2	0	0	0	7,91003	11,177	40,9
4	-1	1	1	1	6,84247	12,928	2,4
5	-2	0	1	1	6,77974	13,048	13,7
6	0	0	1	1	6,63454	13,335	7,4

Date: 23.01.2019 Time: 09:43:54 File: HighScore Plus - 4-120°_24min_A_LithoFill_T

User: hradil

7	2	2	0	5,92857	14,931	6,2
8	1	3	0	5,58580	15,853	1,7
9	-2	2	1	5,40545	16,386	0,7
10	0	2	1	5,33099	16,616	1,8
11	-3	1	1	5,24298	16,897	15,4
12	1	1	1	5,10951	17,342	23,1
13	3	1	0	5,05866	17,517	6,0
14	-1	3	1	4,64759	19,081	14,6
15	0	4	0	4,47775	19,812	0,2
16	-4	0	1	4,35367	20,382	5,1
17	2	0	1	4,23919	20,939	0,1
18	1	3	1	3,97649	22,339	48,5
19	3	3	0	3,95238	22,477	53,3
20	4	0	0	3,95238	22,477	53,3
21	-4	2	1	3,91550	22,692	22,6
22	2	4	0	3,89671	22,803	24,8
23	2	2	1	3,83159	23,195	4,7
24	-2	4	1	3,73638	23,795	3,0
25	-2	0	2	3,70203	24,019	6,9
26	0	4	1	3,70203	24,019	6,9
27	4	2	0	3,61791	24,586	0,4
28	-3	1	2	3,55523	25,027	14,8
29	-1	1	2	3,51274	25,334	0,8
30	1	5	0	3,49375	25,474	1,5
31	-5	1	1	3,46348	25,701	5,3
32	-2	2	2	3,42123	26,024	31,1
33	-4	0	2	3,38987	26,269	14,9
34	3	1	1	3,38987	26,269	14,9
35	0	0	2	3,31727	26,854	9,8
36	-1	5	1	3,22462	27,641	0,5
37	-4	2	2	3,17034	28,124	26,3
38	5	1	0	3,12146	28,574	15,3
39	-4	4	1	3,12146	28,574	15,3
40	-3	3	2	3,10007	28,775	3,5
41	-1	3	2	3,07178	29,046	15,0
42	2	4	1	3,07178	29,046	15,0
43	-5	3	1	3,03868	29,369	1,3
44	-5	1	2	3,02675	29,488	2,5
45	-3	5	1	2,99893	29,767	11,3
46	3	3	1	2,98517	29,908	6,1
47	0	6	0	2,98517	29,908	6,1
48	1	5	1	2,97330	30,030	29,9
49	3	5	0	2,96318	30,135	21,5
50	4	4	0	2,96318	30,135	21,5
51	1	1	2	2,94971	30,276	13,1
52	4	0	1	2,88030	31,024	2,3
53	-6	2	1	2,79569	31,987	29,9
54	5	3	0	2,79569	31,987	29,9
55	-6	0	2	2,74158	32,636	2,7
56	4	2	1	2,74158	32,636	2,7
57	-5	3	2	2,73206	32,753	9,8
58	-2	6	1	2,73206	32,753	9,8
59	0	6	1	2,72230	32,874	5,6
60	1	3	2	2,67386	33,487	3,2
61	2	0	2	2,66550	33,595	3,3
62	0	4	2	2,66550	33,595	3,3
63	6	0	0	2,63668	33,973	0,5
64	-6	2	2	2,62149	34,176	0,2
65	2	2	2	2,55475	35,097	3,7
66	6	2	0	2,52933	35,462	5,1
67	1	7	0	2,52933	35,462	5,1
68	-5	5	1	2,51438	35,680	2,9
69	-7	1	1	2,48432	36,126	3,0
70	3	5	1	2,48432	36,126	3,0
71	-4	6	1	2,46201	36,465	2,8
72	-6	4	1	2,45737	36,536	3,4
73	-4	0	3	2,44906	36,665	1,6
74	2	6	1	2,44074	36,794	7,1
75	5	1	1	2,44074	36,794	7,1
76	-2	0	3	2,42812	36,992	3,5
77	4	4	1	2,42241	37,083	7,0
78	-1	7	1	2,41712	37,167	6,7
79	-7	1	2	2,41712	37,167	6,7
80	4	6	0	2,38266	37,724	1,7
81	-4	2	3	2,36232	38,062	2,9
82	3	1	2	2,35189	38,237	1,6
83	-5	1	3	2,35189	38,237	1,6
84	-2	2	3	2,34351	38,379	2,6
85	-5	5	2	2,33147	38,585	0,4

Date: 23.01.2019 Time: 09:43:54 File: HighScore Plus - 4-120°_24min_A_LithoFill_T

User: hradil

86	-3	7	1	2,31868	38,806	0,8
87	-1	1	3	2,31868	38,806	0,8
88	-7	3	1	2,30677	39,015	0,9
89	1	7	1	2,30677	39,015	0,9
90	2	4	2	2,29042	39,305	1,3
91	6	4	0	2,27204	39,636	0,9
92	5	3	1	2,27204	39,636	0,9
93	-7	3	2	2,25991	39,858	1,4
94	-6	0	3	2,25991	39,858	1,4
95	-4	6	2	2,24032	40,221	1,1
96	0	8	0	2,24032	40,221	1,1
97	0	6	2	2,21898	40,625	0,3
98	0	0	3	2,21151	40,768	1,2
99	3	3	2	2,20474	40,899	0,5
100	-6	2	3	2,19122	41,163	2,5
101	-8	0	2	2,17649	41,454	1,6
102	-1	3	3	2,17649	41,454	1,6
103	2	8	0	2,15425	41,902	0,5
104	0	2	3	2,14702	42,050	0,3
105	6	0	1	2,14702	42,050	0,3
106	-2	4	3	2,13449	42,309	2,5
107	-2	8	1	2,12595	42,487	0,6
108	-8	2	1	2,11960	42,620	1,4
109	4	0	2	2,11960	42,620	1,4
110	7	3	0	2,11364	42,746	1,7
111	-8	2	2	2,11364	42,746	1,7
112	-7	1	3	2,10611	42,907	0,8
113	-3	7	2	2,09088	43,235	2,1
114	-1	7	2	2,08576	43,347	4,6
115	6	2	1	2,08576	43,347	4,6
116	4	6	1	2,07276	43,632	2,4
117	-5	7	1	2,07276	43,632	2,4
118	4	2	2	2,06261	43,858	0,3
119	1	1	3	2,05482	44,033	2,0
120	3	7	1	2,05482	44,033	2,0
121	5	5	1	2,02902	44,623	1,0
122	-3	5	3	2,02902	44,623	1,0
123	-6	4	3	2,01752	44,891	4,5
124	-7	5	2	2,01752	44,891	4,5
125	-7	3	3	1,99847	45,343	0,3
126	5	7	0	1,98956	45,557	0,6
127	2	6	2	1,98956	45,557	0,6
128	6	6	0	1,97619	45,883	1,1
129	1	9	0	1,97619	45,883	1,1
130	-5	7	2	1,96578	46,140	1,2
131	-8	4	2	1,95750	46,346	7,8
132	-1	5	3	1,95750	46,346	7,8
133	1	7	2	1,94210	46,736	2,2
134	-9	1	2	1,94210	46,736	2,2
135	8	2	0	1,93430	46,935	2,7
136	6	4	1	1,93430	46,935	2,7
137	-8	2	3	1,92696	47,125	1,0
138	-1	9	1	1,92190	47,256	1,0
139	2	0	3	1,92190	47,256	1,0
140	-2	8	2	1,91578	47,417	1,7
141	-9	1	1	1,91578	47,417	1,7
142	5	1	2	1,89454	47,981	0,4
143	-4	6	3	1,89454	47,981	0,4
144	-2	6	3	1,88367	48,276	0,3
145	2	2	3	1,87728	48,451	0,6
146	-3	9	1	1,86819	48,702	0,6
147	-4	8	2	1,86819	48,702	0,6
148	3	9	0	1,86193	48,876	1,1
149	1	9	1	1,86193	48,876	1,1
150	-9	3	2	1,85674	49,022	0,8
151	0	8	2	1,85674	49,022	0,8
152	-4	0	4	1,85101	49,184	0,7
153	-5	1	4	1,83478	49,648	0,8
154	-3	1	4	1,82300	49,991	3,1
155	-7	5	3	1,82300	49,991	3,1
156	5	3	2	1,81505	50,225	1,8
157	-6	0	4	1,81505	50,225	1,8
158	8	4	0	1,80895	50,406	0,4
159	7	3	1	1,80895	50,406	0,4
160	-8	4	3	1,80564	50,505	0,6
161	-7	7	1	1,79110	50,944	3,3
162	0	10	0	1,79110	50,944	3,3
163	-6	8	1	1,78111	51,250	0,6
164	-3	7	3	1,77635	51,398	2,2

Date: 23.01.2019 Time: 09:43:54 File: HighScore Plus - 4-120°_24min_A_LithoFill_T

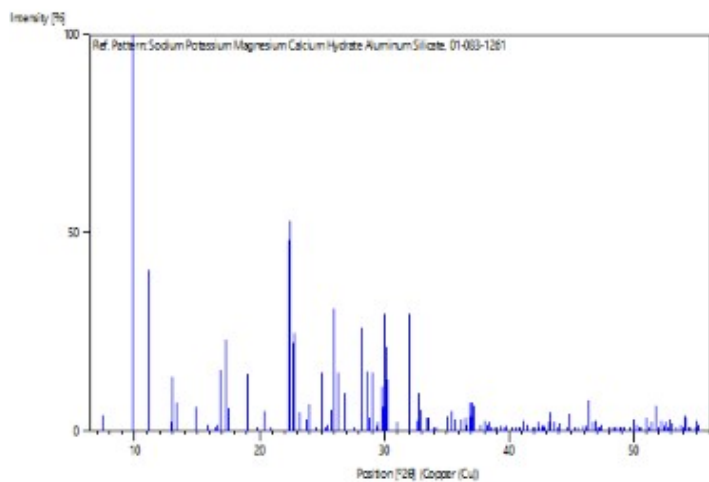
User: hradi

165	5	7	1	1,77635	51,398	2,2
166	4	8	1	1,76560	51,734	6,5
167	-7	7	2	1,76560	51,734	6,5
168	-8	6	2	1,75886	51,947	0,8
169	-8	6	1	1,75886	51,947	0,8
170	9	1	0	1,75186	52,170	2,7
171	-3	3	4	1,75186	52,170	2,7
172	-3	9	2	1,74477	52,398	1,5
173	2	10	0	1,74477	52,398	1,5
174	-5	7	3	1,74075	52,528	2,6
175	-1	9	2	1,74075	52,528	2,6
176	-5	9	1	1,73411	52,745	0,8
177	-6	8	2	1,73411	52,745	0,8
178	4	6	2	1,72919	52,907	2,9
179	0	10	1	1,72919	52,907	2,9
180	3	9	1	1,72366	53,090	2,2
181	6	0	2	1,72366	53,090	2,2
182	-9	5	2	1,71437	53,400	1,0
183	2	8	2	1,71437	53,400	1,0
184	3	3	3	1,70317	53,779	1,7
185	8	0	1	1,69951	53,904	1,0
186	-8	0	4	1,69388	54,098	4,1
187	7	7	0	1,69388	54,098	4,1
188	-10	0	3	1,69067	54,209	3,5
189	-10	2	1	1,69067	54,209	3,5
190	9	3	0	1,68459	54,421	0,9
191	5	9	0	1,68459	54,421	0,9
192	-6	4	4	1,68104	54,546	0,9
193	5	5	2	1,68104	54,546	0,9
194	-5	9	2	1,67008	54,934	0,3
195	8	2	1	1,67008	54,934	0,3
196	-8	2	4	1,66537	55,102	2,5
197	-1	3	4	1,66285	55,193	1,6
198	-10	2	3	1,66285	55,193	1,6

Structure

No.	Name	Element	X	Y	Z	Biso	sof	Wyck.
1	SI1	Si	0,17906	0,16943	0,09630	0,5000	0,8333	8j
2	AL1	Al	0,17906	0,16943	0,09630	0,5000	0,1667	8j
3	SI2	Si	0,21334	0,41099	0,50400	0,5000	0,8333	8j
4	AL2	Al	0,21334	0,41099	0,50400	0,5000	0,1667	8j
5	SI3	Si	0,20846	0,19034	0,71530	0,5000	0,8333	8j
6	AL3	Al	0,20846	0,19034	0,71530	0,5000	0,1667	8j
7	SI4	Si	0,06623	0,29837	0,41480	0,5000	0,8333	8j
8	AL4	Al	0,06623	0,29837	0,41480	0,5000	0,1667	8j
9	SI5	Si	0,00000	0,21651	0,00000	0,5000	0,8333	4g
10	AL5	Al	0,00000	0,21651	0,00000	0,5000	0,1667	4g
11	O1	O	0,19590	0,50000	0,45740	0,5000	1,0000	4i
12	O2	O	0,23360	0,12040	0,61440	0,5000	1,0000	8j
13	O3	O	0,18500	0,15510	0,85590	0,5000	1,0000	8j
14	O4	O	0,23330	0,10410	0,25090	0,5000	1,0000	8j
15	O5	O	0,00000	0,32320	0,50000	0,5000	1,0000	4h
16	O6	O	0,08080	0,16270	0,05550	0,5000	1,0000	8j
17	O7	O	0,12680	0,23170	0,54920	0,5000	1,0000	8j
18	O8	O	0,01220	0,27020	0,18560	0,5000	1,0000	8j
19	O9	O	0,21230	0,25200	0,18600	0,5000	1,0000	8j
20	O10	O	0,11880	0,37180	0,41480	0,5000	1,0000	8j
21	O11	O	0,21100	0,50000	0,96700	0,5000	0,3800	4i
22	O12	O	0,08400	0,00000	0,88800	0,5000	0,4400	4i
23	O13	O	0,07770	0,42060	0,96400	0,5000	1,0000	8j
24	O14	O	0,00000	0,50000	0,50000	0,5000	1,0000	2d
25	O15	O	0,00000	0,09500	0,50000	0,5000	0,7600	4h
26	O16	O	0,07300	0,00000	0,24900	0,5000	0,8300	4i
27	O17	O	0,09600	0,00000	0,75600	0,5000	0,4200	4i
28	NA1	Na	0,14280	0,00000	0,66700	0,5000	0,3600	4i
29	CA1	Ca	0,14280	0,00000	0,66700	0,5000	0,0600	4i
30	NA2	Na	0,03930	0,50000	0,21000	0,5000	0,1000	4i
31	CA2	Ca	0,03930	0,50000	0,21000	0,5000	0,2500	4i
32	K1	K	0,24130	0,50000	0,04900	0,5000	0,4400	4i
33	MG1	Mg	0,00000	0,00000	0,50000	0,5000	0,1000	2c

Stick Pattern



Date: 23.01.2019 Time: 09:45:16 File: HighScore Plus - 4-120°_24min_A_LithoFill_T

User: hradii

Name and formula

Reference code: 00-050-1714

Mineral name: Terranovaite
 Compound name: Potassium Sodium Calcium Magnesium Aluminum Silicate Hydrate
 Common name: Terranovaite

Empirical formula: $\text{Al}_{12.3}\text{Ca}_{3.7}\text{H}_{58}\text{K}_{0.2}\text{Mg}_{0.2}\text{Na}_{4.2}\text{O}_{189}\text{Si}_{67.7}$
 Chemical formula: $(\text{Na}_{4.2}\text{K}_{0.2}\text{Mg}_{0.2}\text{Ca}_{3.7})(\text{Al}_{12.3}\text{Si}_{67.7}\text{O}_{160})'_{29}\text{H}_2\text{O}$

Mineral classification: Zeolite (Family), other zeolites
 Zeolite classification: TER(Terranovaite)
 IMA number: 1995-026

Crystallographic parameters

Crystal system: Orthorhombic
 Space group: Cmcn
 Space group number: 63

a (Å): 9,7470
 b (Å): 23,8800
 c (Å): 20,0680
 Alpha (°): 90,0000
 Beta (°): 90,0000
 Gamma (°): 90,0000

Volume of cell (10^6 pm^3): 4670,99
 Z: 1,00

RIR:: -

Subfiles and quality

Subfiles: Inorganic, Micro & Mesoporous, Mineral, Mineral - Mineral, Mineral - Natural, Zeolite
 Quality: Calculated (C)

Comments

Creation Date: 01.09.2000
 Sample Source or Locality: Specimen from Ferrar dolerites, Mount Adamson, Northern Victoria Land, Antarctica.

References

Primary reference: Galli, E., Alberti, A., Vezzalini, G., Quartieri, S., *Am. Mineral.*, **82**, 423, (1997)

Peak list

No.	h	k	l	d [Å]	2θ [°]	I [%]
1	0	0	2	11,94000	7,398	21,5
2	0	0	2	10,26110	8,610	74,0
3	0	0	2	10,03400	8,806	41,0
4	1	1	0	9,02420	9,793	13,9
5	1	1	1	8,23040	10,741	6,1
6	0	2	2	7,68170	11,510	3,3
7	1	1	2	6,70980	13,184	6,2
8	1	3	0	6,16530	14,355	9,2
9	0	4	0	5,97000	14,827	4,7
10	1	3	1	5,89340	15,021	1,9
11	0	2	3	5,83590	15,170	12,4
12	0	4	1	5,72220	15,473	3,0
13	1	1	3	5,37390	16,482	1,7
14	1	3	2	5,25290	16,865	0,2
15	0	4	2	5,13060	17,270	13,9
16	0	0	4	5,01700	17,664	4,4
17	2	0	0	4,87350	18,188	24,8
18	0	2	4	4,62530	19,173	0,6
19	2	2	0	4,51210	19,659	2,2
20	2	2	1	4,40220	20,155	0,6
21	1	1	4	4,38490	20,235	1,8
22	2	0	2	4,38380	20,241	5,8
23	1	5	0	4,28880	20,694	0,6

Date: 23.01.2019 Time: 09:45:16 File: HighScore Plus - 4-120°_24min_A_LithoFill_T

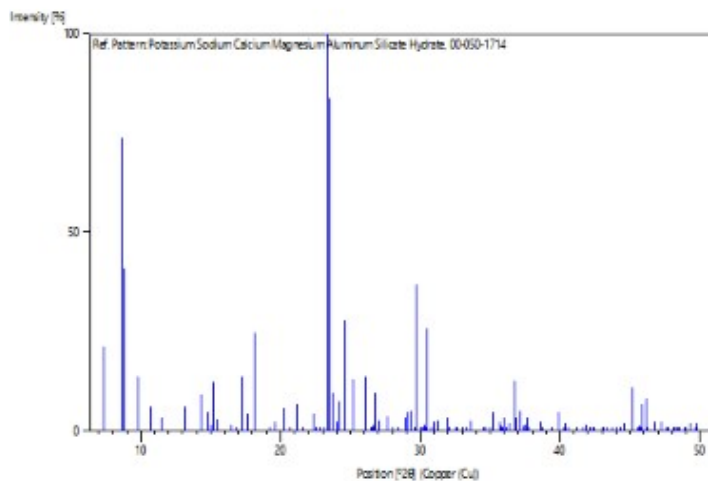
User: hradil

24	1	5	1	4,19410	21,166	7,0
25	2	2	2	4,11520	21,577	0,7
26	0	6	0	3,98000	22,319	4,5
27	1	5	2	3,94370	22,527	0,6
28	1	3	4	3,89140	22,834	0,8
29	0	4	4	3,84080	23,139	0,2
30	0	2	5	3,80440	23,364	100,0
31	2	4	0	3,77530	23,546	83,8
32	2	2	3	3,74070	23,767	9,4
33	0	6	2	3,69960	24,035	2,6
34	1	1	5	3,66720	24,251	7,5
35	1	5	3	3,61050	24,637	28,0
36	2	4	2	3,53350	25,183	13,2
37	0	6	3	3,42040	26,030	13,6
38	1	3	5	3,36360	26,478	0,4
39	2	2	4	3,35490	26,548	0,3
40	0	0	6	3,34470	26,630	1,5
41	0	4	5	3,33080	26,743	9,6
42	2	4	3	3,28780	27,100	2,7
43	0	2	6	3,22070	27,675	0,2
44	1	7	0	3,21990	27,682	3,6
45	3	1	0	3,21930	27,688	0,2
46	1	7	1	3,17920	28,044	0,2
47	3	1	1	3,17870	28,048	1,2
48	1	1	6	3,13620	28,436	0,7
49	2	6	0	3,08260	28,942	3,3
50	1	7	2	3,06590	29,103	1,1
51	3	1	2	3,06540	29,108	4,7
52	2	6	1	3,04690	29,288	5,1
53	2	4	4	3,01660	29,589	1,0
54	3	3	0	3,00810	29,675	36,9
55	3	3	1	2,97480	30,015	0,7
56	0	8	1	2,95250	30,247	0,9
57	2	6	2	2,94670	30,308	1,8
58	1	3	6	2,93990	30,379	1,0
59	1	5	5	2,93050	30,479	26,0
60	1	7	3	2,90130	30,793	1,1
61	3	1	3	2,90090	30,798	0,6
62	3	3	2	2,88140	31,011	2,3
63	0	8	2	2,86110	31,237	2,5
64	2	6	3	2,79970	31,940	3,3
65	0	2	7	2,78760	32,083	1,0
66	2	4	5	2,74990	32,535	0,4
67	3	3	3	2,74350	32,613	0,3
68	1	7	4	2,70980	33,030	0,4
69	2	2	6	2,68700	33,318	0,5
70	3	5	1	2,66260	33,633	2,8
71	3	5	2	2,59500	34,536	0,4
72	3	3	4	2,57990	34,744	0,2
73	1	9	0	2,56020	35,020	1,0
74	2	8	0	2,54550	35,229	4,7
75	3	1	5	2,51130	35,725	2,4
76	0	0	8	2,50850	35,766	1,2
77	2	4	6	2,50350	35,840	1,0
78	3	5	3	2,49280	35,999	3,5
79	1	9	2	2,48070	36,181	0,2
80	2	8	2	2,46730	36,384	2,0
81	2	6	5	2,44480	36,731	12,8
82	4	0	0	2,43670	36,857	3,3
83	2	2	7	2,41970	37,126	5,3
84	1	1	8	2,41690	37,170	0,3
85	3	3	5	2,40710	37,327	1,2
86	1	9	3	2,39100	37,588	1,6
87	0	10	0	2,38800	37,637	3,6
88	4	2	0	2,38750	37,645	1,4
89	1	5	7	2,38340	37,712	1,1
90	2	8	3	2,37910	37,783	0,6
91	0	6	7	2,32620	38,676	2,3
92	0	10	2	2,32310	38,730	0,6
93	2	4	7	2,28320	39,434	0,1
94	4	4	0	2,25610	39,928	4,8
95	3	3	6	2,23660	40,291	0,8
96	3	5	5	2,23240	40,370	0,6
97	2	0	8	2,23040	40,408	1,9
98	3	7	3	2,21940	40,617	0,3
99	0	2	9	2,19190	41,150	0,4
100	1	5	8	2,16530	41,678	0,3
101	1	9	5	2,15840	41,818	1,7
102	3	1	7	2,14100	42,174	0,3

Date: 23.01.2019 Time: 09:45:16 File: HighScore Plus - 4-120°_24min_A_LithoFill_T

User: hradil

103	2	10	1	2,13230	42,354	0,3
104	3	7	4	2,13010	42,400	0,2
105	2	6	7	2,09930	43,053	0,4
106	2	10	2	2,09700	43,103	1,0
107	2	4	8	2,08930	43,269	0,4
108	0	8	7	2,06770	43,745	0,7
109	4	4	4	2,05760	43,970	0,3
110	3	9	0	2,05510	44,027	0,4
111	3	9	1	2,04440	44,269	0,2
112	2	10	3	2,04200	44,324	0,2
113	3	7	5	2,02970	44,607	2,2
114	0	0	10	2,00680	45,144	10,9
115	0	12	0	1,99000	45,546	1,1
116	4	6	3	1,98460	45,677	1,3
117	0	12	1	1,98030	45,782	0,5
118	1	7	8	1,97890	45,816	6,8
119	3	9	3	1,96450	46,172	8,2
120	3	5	7	1,96020	46,279	0,2
121	5	1	0	1,94290	46,715	2,1
122	0	8	8	1,92040	47,296	2,3
123	1	9	7	1,90960	47,580	0,1
124	5	1	2	1,90750	47,635	0,3
125	2	8	7	1,90340	47,744	0,4
126	0	4	10	1,90220	47,776	0,4
127	4	8	0	1,88770	48,166	0,2
128	5	3	1	1,88510	48,237	0,2
129	4	8	1	1,87940	48,393	0,2
130	1	11	5	1,87390	48,544	0,2
131	5	3	2	1,86060	48,913	0,6
132	2	0	10	1,85560	49,054	0,5
133	4	6	5	1,84550	49,340	2,0
134	0	10	7	1,83480	49,647	0,2
135	3	9	5	1,82920	49,810	2,0

Stick Pattern

Date: 23.01.2019 Time: 10:05:31 File: HighScore Plus - 4-120°_24min_A_LithoFill_T

User: hradil

Name and formula

Reference code: 00-020-0452
 Mineral name: Gismondine
 Compound name: Calcium Aluminum Silicate Hydrate
 Common name: Gismondine
 Empirical formula: $\text{Al}_2\text{CaH}_8\text{O}_{12}\text{Si}_2$
 Chemical formula: $\text{CaAl}_2\text{Si}_2\text{O}_8 \cdot 4\text{H}_2\text{O}$
 Mineral classification: Zeolite (Family), gismondine (Supergroup)
 Zeolite classification: GIS(Gismondine)

Crystallographic parameters

Crystal system: Monoclinic
 Space group: P21/c
 Space group number: 14

a (Å): 10,0240
 b (Å): 10,6140
 c (Å): 9,8410
 Alpha (°): 90,0000
 Beta (°): 92,4800
 Gamma (°): 90,0000

Calculated density (g/cm³): 2,22
 Measured density (g/cm³): 2,20
 Volume of cell (10⁶ pm³): 1046,05
 Z: 4,00

RIR:: -

Subfiles and quality

Subfiles: Cement and Hydration Product, Inorganic, Micro & Mesoporous, Mineral, Mineral - Mineral, Mineral - Natural, Zeolite
 Quality: Indexed (I)

Comments

Color: White
 Creation Date: 01.09.1970
 Cross-References: ICDD:04-011-6565
 Additional Diffraction Lines: Plus 7 additional reflections to 0.7681
 Sample Source or Locality: White crystals from Hohenburg, Buhue, Westphalia, Germany
 Warning: One or more lines are unindexed
 Unit Cell Data Source: Powder Diffraction.

References

Primary reference: Department of Geology and Mineralogy, University of Oxford, Oxford, England, UK., *Private Communication*, (1967)
 Optical data: Deer, W., Howie, R., Zussman, J., *Rock Forming Minerals*, **4**, 351, (1966)

Peak list

No.	h	k	l	d [Å]	2θ [°]	I [%]
1	1	0	0	9,99000	8,845	2,0
2	1	1	0	7,28000	12,148	16,0
3	-1	1	1	5,93000	14,927	2,0
4	1	1	1	5,76000	15,371	4,0
5	0	2	0	5,28000	16,778	2,0
6	2	0	0	5,01000	17,689	4,0
7	0	0	2	4,91000	18,052	16,0
8	0	2	1	4,67000	18,988	4,0
9	0	1	2	4,47000	19,846	4,0
10	-1	2	1	4,27000	20,786	35,0
11	1	2	1	4,19000	21,187	12,0
12	2	1	1	4,05000	21,929	4,0
13	0	2	2	3,61000	24,641	2,0
14	-1	2	2	3,43000	25,956	2,0
15	3	0	0	3,34000	26,668	100,0

Date: 23.01.2019 Time: 10:05:31 File: HighScore Plus - 4-120°_24min_A_LithoFill_T

User: hradi

16	3	1	0	3,19000	27,947	18,0
17	0	1	3	3,13000	28,494	14,0
18	-3	1	1	3,06000	29,160	2,0
19	3	1	1	2,99000	29,858	2,0
20	0	3	2	2,87000	31,138	2,0
21	-3	0	2	2,82000	31,704	2,0
22	1	3	2	2,74000	32,655	14,0
23	-2	1	3	2,70000	33,153	18,0
24	1	2	3	2,66000	33,666	10,0
25	3	1	2	2,62000	34,196	2,0
26	0	4	1	2,56000	35,023	2,0
27	4	0	0	2,51000	35,744	2,0
28	0	0	4	2,46000	36,496	8,0
29	2	2	3	2,40000	37,442	2,0
30	3	3	1	2,34000	38,439	2,0
31	-1	4	2	2,28000	39,492	6,0
32	3	1	3	2,24000	40,227	4,0
33	4	2	1	2,19000	41,187	2,0
34	-2	4	2	2,13000	42,402	6,0
35	-3	4	1	2,04000	44,370	2,0
36	1	4	3	2,01000	45,068	2,0
37	-3	3	3	1,98100	45,765	4,0
38	0	1	5	1,93300	46,969	2,0
39	4	1	3	1,91600	47,411	2,0
40	2	3	4	1,85000	49,212	2,0
41	4	4	0	1,81900	50,108	16,0
42	0	5	3	1,78200	51,223	2,0
43	-2	2	5	1,75400	52,101	4,0
44	-1	3	5	1,70400	53,751	2,0
45	3	5	2	1,67100	54,901	8,0
46	2	6	1	1,64100	55,992	4,0
47	-3	4	4	1,60800	57,246	2,0
48	-2	5	4	1,54200	59,940	8,0
49	-6	1	3	1,49900	61,845	2,0
50	-6	2	3	1,45400	63,981	2,0
51	-2	7	1	1,43800	64,779	2,0
52	6	4	0	1,41300	66,070	2,0
53	0	4	6	1,39400	67,089	2,0
54	-5	2	5	1,38400	67,638	4,0
55	2	5	5	1,37500	68,142	1,0
56	2	1	7	1,32800	70,907	1,0
57	-6	1	5	1,29100	73,263	1,0
58	-2	7	4	1,25600	75,656	1,0
59	3	8	0	1,23300	77,326	1,0
60	0	7	5	1,20100	79,790	1,0
61	1	2	8	1,18300	81,255	1,0
62	2	2	8	1,15400	83,749	1,0
63	-8	3	4	1,08100	90,890	1,0
64	-9	2	3	1,04700	94,736	1,0

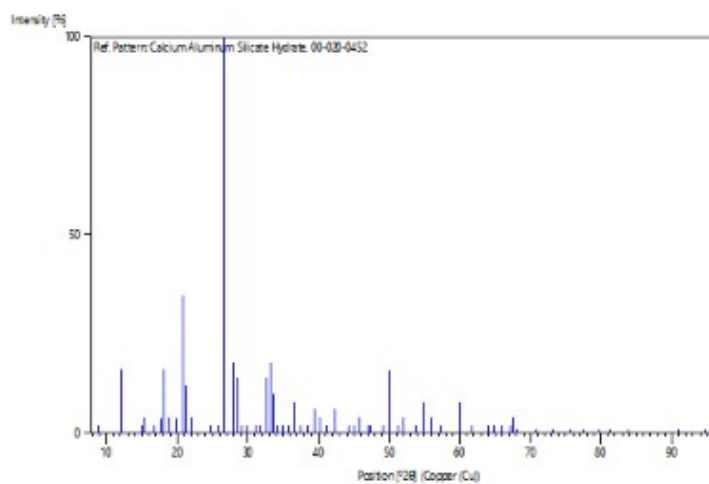
Structure

No.	Name	Element	X	Y	Z	Biso	sof	Wyck.
1	SI1	Si	0,41500	0,11300	0,18200	0,5000	1,0000	4e
2	SI2	Si	0,90800	0,87000	0,16000	0,5000	1,0000	4e
3	AL1	Al	0,09700	0,11300	0,17000	0,5000	1,0000	4e
4	AL2	Al	0,59000	0,86700	0,14900	0,5000	1,0000	4e
5	CA1	Ca	0,72000	0,07700	0,35400	0,5000	1,0000	4e
6	O1	O	0,07800	0,15400	0,99900	0,5000	1,0000	4e
7	O2	O	0,26200	0,07500	0,21200	0,5000	1,0000	4e
8	O3	O	0,43800	0,14500	0,02600	0,5000	1,0000	4e
9	O4	O	0,24600	0,40700	0,30300	0,5000	1,0000	4e
10	O5	O	0,00000	0,98300	0,21500	0,5000	1,0000	4e
11	O6	O	0,04400	0,24200	0,26100	0,5000	1,0000	4e
12	O7	O	0,46300	0,22400	0,27600	0,5000	1,0000	4e
13	O8	O	0,51100	0,99500	0,22600	0,5000	1,0000	4e
14	O9	O	0,25700	0,10700	0,50500	0,5000	1,0000	4e
15	O10	O	0,59000	0,12700	0,53900	0,5000	1,0000	4e
16	O11	O	0,91100	0,11900	0,50100	0,5000	1,0000	4e
17	O12	O	0,77000	0,21000	0,17000	0,5000	0,5000	4e
18	O13	O	0,74000	0,18000	0,89500	0,5000	0,5000	4e

Stick Pattern

Date: 23.01.2019 Time: 10:05:31 File: HighScore Plus - 4-120°_24min_A_LithoFill_T

User: hradil



Date: 23.01.2019 Time: 10:22:47 File: HighScore Plus - 4-120°_24min_D_LithoExtern

User: hradii

Name and formula

Reference code: 01-085-1415
 Mineral name: Anorthite, sodian, syn
 Compound name: Sodium Calcium Aluminum Silicate
 Common name: sodium calcium tecto-alumosilicate, anorthite (Na-exchanged), syn
 Empirical formula: $\text{Al}_{1,55}\text{Ca}_{0,55}\text{Na}_{0,45}\text{O}_8\text{Si}_{2,45}$
 Chemical formula: $(\text{Na}_{0,45}\text{Ca}_{0,55})(\text{Al}_{1,55}\text{Si}_{2,45}\text{O}_8)$
 Mineral classification: Feldspar (Family), plagioclase (Supergroup)

Crystallographic parameters

Crystal system: Anorthic
 Space group: C-1
 Space group number: 2
 a (Å): 8,1700
 b (Å): 12,8600
 c (Å): 7,1100
 Alpha (°): 93,6000
 Beta (°): 116,3000
 Gamma (°): 89,8000
 Volume of cell (10^6 pm^3): 334,06
 Z: 4,00
 RIR: 0,58

Subfiles and quality

Subfiles: ICSD Pattern, Inorganic, Mineral, Mineral - Mineral, Mineral - Synthetic
 Quality: Blank (B)

Comments

ANX: ABC3X8
 ICSD collection code: 64800
 Creation Date: 01.09.1999
 Modification Date: 01.09.2011
 Cross-References: ICSD:64800, ICDD:01-085-1415, ICDD:04-011-6816 (related phase)
 ANX: ABC3X8
 Analysis: $\text{Al}_{1,55}\text{Ca}_{0,55}\text{Na}_{0,45}\text{O}_8\text{Si}_{2,45}$
 Formula from original source: $(\text{Na}_{0,45}\text{Ca}_{0,55})(\text{Al}_{1,55}\text{Si}_{2,45}\text{O}_8)$
 ICSD Collection Code: 64800
 Calculated Pattern Original Remarks: For refinement in C1 cf. 9287, R=0.097
 Mean T-O: 1.697, 1.644, 1.647, 1.658
 Minor Warning: Magnitude of e.s.d. on cell dimension is >1000 ppm
 Significant Warning: 12%<R factor (for single crystal)
 Wyckoff Sequence: i13(C1-)
 Unit Cell Data Source: Single Crystal.

References

Primary reference: Toman, K., Frueh, A.J., *Z. Kristallogr., Kristallgeom., Kristallphys., Kristallchem.*, **138**, 337, (1973)
 Structure: Toman, K., Frueh, A.J., *Z. Kristallogr., Kristallgeom., Kristallphys., Kristallchem.*, **138**, 337, (1973)

Peak list

No.	h	k	l	d [Å]	2 θ [°]	I [%]
1	0	2	0	6,43477	13,751	5,4
2	-1	1	0	6,43477	13,751	5,4
3	0	0	1	6,35913	13,915	0,5
4	1	1	0	6,28585	14,078	0,3
5	-1	-1	1	5,84186	15,154	2,6
6	-1	1	1	5,63495	15,714	0,6
7	0	-2	1	4,67882	18,952	5,5
8	0	2	1	4,36941	20,308	0,1
9	-2	0	1	4,04141	21,976	49,2
10	1	-1	1	3,88467	22,874	11,1
11	1	1	1	3,75893	23,650	19,7

Date: 23.01.2019 Time: 10:22:47 File: HighScore Plus - 4-120°_24min_D_LithoExtern

User: hradil

12	-1	3	0	3,73733	23,789	22,0
13	1	3	0	3,64983	24,368	24,3
14	2	0	0	3,64983	24,368	24,3
15	-1	-3	1	3,63428	24,474	8,7
16	-1	3	1	3,47623	25,605	9,6
17	-1	-1	2	3,47623	25,605	9,6
18	-2	-2	1	3,44025	25,877	4,5
19	-1	1	2	3,36539	26,463	14,5
20	-2	2	0	3,21739	27,704	41,0
21	0	4	0	3,20601	27,805	100,0
22	-2	0	2	3,20601	27,805	100,0
23	0	0	2	3,17956	28,041	58,8
24	2	2	0	3,14292	28,374	26,2
25	1	-3	1	3,01019	29,654	13,7
26	0	-4	1	2,94587	30,316	20,4
27	0	-2	2	2,92957	30,489	12,7
28	-2	-2	2	2,92093	30,581	6,1
29	1	3	1	2,84116	31,462	13,4
30	-1	-3	2	2,81927	31,713	7,1
31	-2	2	2	2,81927	31,713	7,1
32	0	4	1	2,78824	32,075	0,3
33	0	2	2	2,77441	32,239	0,2
34	2	0	1	2,69709	33,190	0,1
35	-1	3	2	2,64966	33,802	7,8
36	-2	-4	1	2,52892	35,468	21,0
37	-3	-1	2	2,52892	35,468	21,0
38	1	-1	2	2,51705	35,641	4,0
39	-2	4	1	2,49614	35,949	11,2
40	-3	1	2	2,49614	35,949	11,2
41	1	1	2	2,45665	36,547	0,3
42	-1	5	0	2,44386	36,745	2,8
43	2	2	1	2,44386	36,745	2,8
44	-1	-5	1	2,42022	37,117	2,5
45	-3	1	0	2,40960	37,287	2,7
46	1	5	0	2,40127	37,421	0,8
47	3	1	0	2,38566	37,675	2,2
48	2	4	0	2,38060	37,758	2,3
49	-1	5	1	2,34610	38,335	2,2
50	-2	-4	2	2,32080	38,770	1,0
51	-1	-1	3	2,32080	38,770	1,0
52	-3	-3	1	2,29234	39,271	5,1
53	-3	3	1	2,29234	39,271	5,1
54	-1	1	3	2,26716	39,725	1,9
55	1	-3	2	2,24403	40,152	0,7
56	-2	4	2	2,21919	40,621	4,5
57	1	-5	1	2,21919	40,621	4,5
58	0	4	2	2,18470	41,291	1,0
59	-3	3	2	2,17209	41,542	0,2
60	-2	2	3	2,15743	41,838	1,3
61	-1	-5	2	2,14492	42,093	1,6
62	-3	3	0	2,14492	42,093	1,6
63	0	6	0	2,13831	42,230	6,3
64	2	-4	1	2,11600	42,696	8,1
65	-1	-3	3	2,10542	42,922	5,3
66	1	5	1	2,10542	42,922	5,3
67	3	3	0	2,09305	43,188	1,7
68	-3	1	3	2,09305	43,188	1,7
69	0	-6	1	2,06997	43,694	0,5
70	0	-2	3	2,05493	44,031	0,1
71	-4	0	2	2,02070	44,817	2,3
72	-1	5	2	2,02070	44,817	2,3
73	-4	0	1	2,01227	45,015	1,7
74	2	0	2	2,00089	45,285	0,5
75	3	-1	1	1,99188	45,501	1,7
76	-1	3	3	1,99188	45,501	1,7
77	0	6	1	1,98622	45,638	1,9
78	0	2	3	1,97292	45,963	0,6
79	3	1	1	1,96384	46,188	0,8
80	-3	-3	3	1,94729	46,604	1,5
81	-2	-4	3	1,94233	46,730	1,8
82	2	-2	2	1,94233	46,730	1,8
83	-4	-2	2	1,93479	46,923	2,3
84	-4	2	2	1,91999	47,306	5,9
85	-2	-6	1	1,90061	47,819	0,6
86	-3	3	3	1,87947	48,391	4,3
87	2	2	2	1,87947	48,391	4,3
88	-2	6	0	1,86867	48,688	3,4
89	-3	5	1	1,86867	48,688	3,4
90	-4	0	3	1,84962	49,223	6,5

Date: 23.01.2019 Time: 10:22:47 File: HighScore Plus - 4-120°_24min_D_LithoExtern

User: hradi

91	3	-3	1	1,84351	49,397	1,1
92	-2	4	3	1,83966	49,507	0,8
93	1	-1	3	1,83040	49,775	8,3
94	4	0	0	1,83040	49,775	8,3
95	0	-4	3	1,82492	49,934	4,4
96	2	6	0	1,82492	49,934	4,4
97	-2	-6	2	1,81714	50,163	3,0
98	1	1	3	1,79583	50,800	5,6
99	-3	5	2	1,78948	50,993	2,2
100	-1	7	0	1,78948	50,993	2,2
101	-1	-7	1	1,78363	51,173	1,4
102	3	3	1	1,78363	51,173	1,4
103	-2	0	4	1,77389	51,474	14,1
104	-4	2	0	1,77389	51,474	14,1
105	-4	2	3	1,76221	51,841	0,4
106	1	5	2	1,74765	52,305	2,0
107	4	2	0	1,74765	52,305	2,0
108	2	-4	2	1,74355	52,437	5,2
109	-2	6	2	1,74355	52,437	5,2
110	-2	-2	4	1,73811	52,614	1,6
111	1	-3	3	1,72448	53,062	0,9
112	-3	-1	4	1,72448	53,062	0,9
113	-1	-1	4	1,72012	53,207	4,5
114	-4	-4	2	1,72012	53,207	4,5
115	2	-6	1	1,71706	53,310	1,5
116	0	4	3	1,71534	53,367	1,5
117	-4	4	1	1,71097	53,515	1,7
118	1	-7	1	1,70412	53,747	0,7
119	-4	4	2	1,69946	53,906	2,9
120	-4	-4	1	1,69946	53,906	2,9
121	-1	1	4	1,68966	54,244	0,3
122	-2	2	4	1,68269	54,488	2,1
123	-3	-5	3	1,67991	54,585	1,7
124	-1	5	3	1,67193	54,868	0,7
125	-1	-7	2	1,67193	54,868	0,7
126	2	4	2	1,65519	55,470	1,9
127	1	3	3	1,64425	55,871	0,2
128	-3	-3	4	1,63383	56,259	1,4
129	-1	-3	4	1,63383	56,259	1,4
130	-4	-4	3	1,62505	56,591	0,7
131	-2	-6	3	1,62505	56,591	0,7
132	3	-1	2	1,61762	56,874	0,1
133	3	-5	1	1,61243	57,074	1,0
134	-3	5	3	1,60702	57,284	2,1
135	-4	4	0	1,60702	57,284	2,1
136	0	8	0	1,60373	57,412	1,7
137	-4	0	4	1,60373	57,412	1,7
138	-2	-4	4	1,59550	57,736	0,1
139	3	1	2	1,59550	57,736	0,1
140	0	0	4	1,58978	57,964	0,3
141	-1	7	2	1,58978	57,964	0,3
142	-5	1	1	1,57986	58,363	1,4
143	0	-8	1	1,57986	58,363	1,4
144	-5	-1	1	1,57507	58,557	0,5
145	4	4	0	1,57194	58,685	1,6
146	-4	-2	4	1,57194	58,685	1,6
147	-5	-1	3	1,56832	58,834	1,7
148	0	-2	4	1,56832	58,834	1,7
149	-5	1	3	1,55880	59,229	1,2
150	2	0	3	1,55880	59,229	1,2
151	4	-2	1	1,55087	59,562	0,2
152	3	5	1	1,54535	59,797	1,7
153	3	-3	2	1,54195	59,942	0,9
154	1	-5	3	1,53896	60,070	1,6
155	-4	2	4	1,53896	60,070	1,6
156	2	-2	3	1,53668	60,169	1,1
157	-2	6	3	1,53445	60,265	0,6
158	0	8	1	1,53235	60,356	1,0
159	1	-7	2	1,53235	60,356	1,0
160	-5	-3	2	1,52857	60,521	0,6
161	4	2	1	1,52372	60,734	0,3
162	-5	3	2	1,52372	60,734	0,3
163	0	2	4	1,51906	60,940	0,7
164	-3	-7	1	1,51906	60,940	0,7
165	-2	4	4	1,51245	61,235	1,3
166	-3	-7	2	1,50955	61,365	0,5
167	2	-6	2	1,50510	61,567	1,2
168	-5	3	1	1,49755	61,911	2,0
169	-2	-8	1	1,49755	61,911	2,0

Date: 23.01.2019 Time: 10:22:47 File: HighScore Plus - 4-120°_24min_D_LithoExtern

User: hradil

170	3	3	2	1,48856	62,327	3,6
171	-5	-3	3	1,48856	62,327	3,6
172	-5	-3	1	1,48386	62,546	4,4
173	-2	8	0	1,48386	62,546	4,4
174	-4	-6	2	1,47859	62,794	0,5
175	-1	-5	4	1,47546	62,943	0,7
176	-3	7	2	1,47151	63,131	2,8
177	-4	6	1	1,47151	63,131	2,8
178	-5	3	3	1,46793	63,303	1,3
179	0	-4	4	1,46479	63,455	0,4
180	-4	6	2	1,45895	63,738	3,4
181	-4	-6	1	1,45895	63,738	3,4
182	0	6	3	1,45647	63,860	3,0
183	2	8	0	1,45449	63,957	3,0
184	5	1	0	1,45043	64,157	0,3
185	1	5	3	1,44680	64,338	0,9
186	3	7	0	1,44680	64,338	0,9
187	4	-4	1	1,44234	64,561	0,5
188	1	7	2	1,44234	64,561	0,5
189	2	-4	3	1,43737	64,811	2,1
190	-5	-1	4	1,43737	64,811	2,1
191	-5	1	4	1,42757	65,311	1,3
192	2	6	2	1,42058	65,673	2,6
193	-4	-6	3	1,42058	65,673	2,6
194	-4	6	0	1,40871	66,297	2,6
195	1	1	4	1,40871	66,297	2,6
196	-1	9	0	1,40646	66,417	0,6
197	-1	-9	1	1,40646	66,417	0,6
198	4	4	1	1,39671	66,941	2,0
199	-3	1	5	1,39671	66,941	2,0

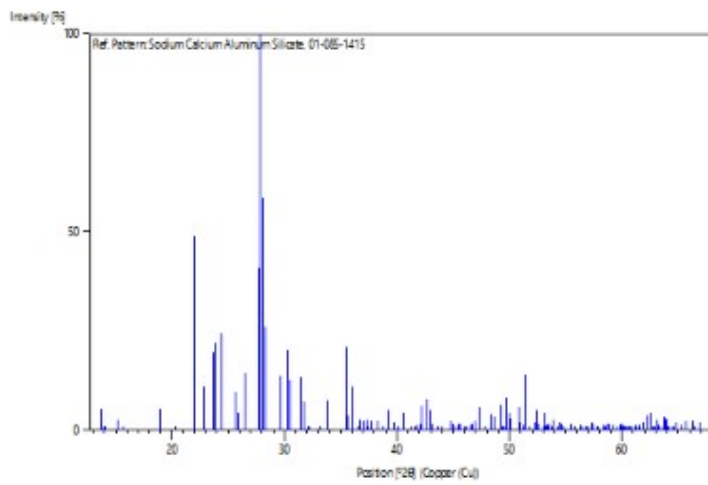
Structure

No.	Name	Element	X	Y	Z	Biso	sof	Wyck.
1	NA1	Na	0,26940	0,01450	0,12190	5,5200	0,4500	4*
2	CA1	Ca	0,26940	0,01450	0,12190	5,5200	0,5500	4*
3	AL1	Al	0,00590	0,16490	0,21540	0,9800	0,6500	4*
4	SI1	Si	0,00590	0,16490	0,21540	0,9800	0,3500	4*
5	AL2	Al	0,00430	0,81910	0,23270	0,6900	0,3000	4*
6	SI2	Si	0,00430	0,81910	0,23270	0,6900	0,7000	4*
7	AL3	Al	0,68590	0,10960	0,31860	0,7300	0,3000	4*
8	SI3	Si	0,68590	0,10960	0,31860	0,7300	0,7000	4*
9	AL4	Al	0,68140	0,88020	0,35640	0,6800	0,3000	4*
10	SI4	Si	0,68140	0,88020	0,35640	0,6800	0,7000	4*
11	O1	O	0,00720	0,12800	0,97830	1,8300	1,0000	4*
12	O2	O	0,58350	0,99590	0,27560	0,6900	1,0000	4*
13	O3	O	0,81300	0,10520	0,18570	1,2900	1,0000	4*
14	O4	O	0,81940	0,85540	0,24520	2,3700	1,0000	4*
15	O5	O	0,01630	0,29480	0,27950	2,3700	1,0000	4*
16	O6	O	0,01350	0,69020	0,21590	1,7300	1,0000	4*
17	O7	O	0,19600	0,10730	0,38400	1,4200	1,0000	4*
18	O8	O	0,19280	0,86700	0,43190	1,7000	1,0000	4*

Stick Pattern

Date: 23.01.2019 Time: 10:22:47 File: HighScore Plus - 4-120°_24min_D_LithoExtern

User: hradil



D. Composition of Clinoptilolite in Different Publications

	1		2		3		4		5	
	wt%	moles								
SiO₂	66.40	1.1050	65.30	1.0867	65.21	1.0852	64.70	1.0763	63.69	1.0599
Al₂O₃	11.64	0.1141	11.47	0.1125	12.61	0.1236	12.43	0.1219	12.47	0.1223
Fe₂O₃	0.47	0.0029	1.36	0.0085	0.40	0.0025	0.44	0.0028	0.62	0.0039
MgO	0.86	0.0213	1.22	0.0303	1.09	0.0270	0.34	0.0084	1.42	0.0352
CaO	2.55	0.0455	1.80	0.0321	1.84	0.0328	1.26	0.0223	2.25	0.0401
Na₂O	1.85	0.0298	1.76	0.0284	1.76	0.0284	4.32	0.0697	2.46	0.0397
K₂O	1.93	0.0205	2.49	0.0264	3.79	0.0402	2.28	0.0242	1.80	0.0191

Table D.1: Chemical composition of clinoptilolites. Adapted from (Sand and Mumpton, 1978, p. 166)

	(1)
SiO₂	66.00
TiO₂	0.04
Al₂O₃	11.67
Fe₂O₃	0.16
FeO	0.13
MnO	0.08
MgO	0.47
CaO	1.78
SrO	0.42
Na₂O	1.54
K₂O	3.08
H₂O(+)	8.96
H₂O(-)	5.64
P₂O₅	0.03
Totals	100.00
Mean ref.	1.478
index	± 0.002

Table D.2: Chemical composition of a K-rich clinoptilolite in rhyolitic vitric tuff of the Hakobuchi Group of Late Cretaceous; Chikubetsu coal mine abandoned, Haboro Town, Rumoi, Hokkaido. The SrO values is corrected. Adapted from (Sand and Mumpton, 1978, p. 182)

	1	2	3	4	5	6
SiO₂	66.27	66.64	66.71	69.78	66.77	67.98
Al₂O₃	11.87	11.78	11.67	11.96	11.62	12.08
K₂O	6.16	6.06	4.70	5.44	2.56	6.42
Na₂O	2.01	2.29	0.75	1.24	0.44	1.25
CaO	0.45	0.53	2.50	1.14	3.40	0.63
MgO	0.28	0.30	0.35	0.59	0.96	0.62
FeO (a)		0.21				
H₂O (b)	12.96	12.19	13.32	9.85	14.25	11.02
Totals	100	100	100	100	100	100

Number of cations on the basis of 72 oxygens

Si	29.77	29.73	29.84	30.00	29.82	29.73
Al	6.28	6.19	6.15	6.06	6.12	6.23
K	3.53	3.45	2.68	2.98	1.45	3.58
Na	1.75	1.98	0.65	1.03	0.37	1.06
Ca	0.22	0.25	1.20	0.52	1.63	0.29
Mg	0.18	0.20	0.23	0.38	0.64	0.40
Si/Al	4.74	4.79	4.85	4.95	4.87	4.77
Na/K	0.49	0.57	0.02	0.34	0.02	0.30
E_b (c)	3.12	-2.37	-0.65	3.94	-3.80	3.00

Table D.3: Chemical composition of deep-sea clinoptilolites. Adapted from (Sand and Mump-ton, 1978, p. 205).

(a) Total iron given as FeO. Inclusion impurity; not included in cell content calculations.

(b) By difference.

(c) $E_b = \frac{Al - \sum_{cat}}{Al}$ where $\sum_{cat} = 2(Mg + Ca) + (Na + K)$

(1) DSDP 105-14-cc; lower Cretaceous, black, carbonaceous clay sampled at 349 m; 34° 54'N, 69° 10'W.

(2) DSDP 105-17-cc; lower Cretaceous. black. carbonaceous clay sampled at 405 m; same location as (1).

(3) DSDP 105-21-cc; lower Cretaceous clay sampled at 457 m; same location as (1).

(4) DSDP 9A-1-6; middle Eocene siliceous clay sampled at 682 m; 32° 46'N, 59° 12'W.

(5) DSDP 163-27-1; upper Cretaceous nannochalk sampled at 271 m; 11° 15'N, 150° 17'W.

(6) DSDP 59.2-5-1; Eocene brown clay in association with phillipsite. sampled at 127 m; 11° 47'N, 147° 35'E.

	105-5-2	105-12-2	105-12-2	105-13-cc	105-14-cc	105-14-cc
SiO₂	60.13	61.69	64.25	70.40	64.61	66.27
Al₂O₃	12.07	11.41	11.49	12.04	11.62	11.87
K₂O	4.50	4.57	6.26	5.30	5.92	6.16
Na₂O	1.76	0.54	0.76	1.69	1.60	2.01
CaO	0.89	1.85	0.95	1.09	0.45	0.45
MgO	0.83	0.71	0.41	0.27	0.26	0.28
FeO (t)	0.71	0.80	0.20			
H₂O (tt)	19.11	18.43	15.68	9.21	15.54	12.96
Totals	100	100	100	100	100	100

Number of cations on the basis of 72 oxygens (anhydrous cell)

Si	29.07	29.47	29.77	30.05	29.82	29.77
Al	6.87	6.43	6.28	6.05	6.33	6.28
K	2.77	2.78	3.70	2.89	3.49	3.53
Na	1.65	0.50	0.68	1.40	1.43	1.75
Ca	0.46	0.94	0.47	0.50	0.22	0.22
Mg	0.59	0.50	0.28	0.17	0.18	0.18
Si/Al	4.23	4.59	4.74	4.96	4.71	4.74
Si+Al	35.94	35.90	36.05	36.10	36.15	36.05
Σ_{cat}	6.53	6.18	5.90	5.63	5.73	6.08
E_b (§)	4.93	3.78	5.83	6.84	9.39	3.12

Table D.4: Chemical composition of clinoptilolites. Each analysis represents a separate crystal from the stated horizon. Adapted from (Sand and Mumpton, 1978, p. 229-230).

(t) Inclusion impurities - not included in cell contents. Total iron given as FeO.

(tt) By difference.

(§) $E_b = \frac{Al - \Sigma_{cat}}{Al} \cdot 100$ where $sum_{cat} = 2(Mg + Ca) + (Na + K)$

	105-15-6	105-15-6	105-16-cc	105-17-cc	105-17-cc	105-19-3
SiO₂	69.18	69.20	69.65	66.06	66.64	68.79
Al₂O₃	12.03	12.58	11.82	11.57	11.78	11.64
K₂O	7.97	8.10	6.95	5.07	6.06	5.25
Na₂O	1.01	1.25	1.43	1.38	2.29	2.12
CaO	0.57	0.52	0.60	1.27	0.53	0.83
MgO	0.28	0.21		0.41	0.30	0.22
FeO (t)					0.21	
H₂O (tt)	8.96	8.14	9.55	14.24	12.19	11.17
Totals	100	100	100	100	100	100

Number of cations on the basis of 72 oxygens

	(anhydrous cell)					
Si	29.87	29.67	30.09	28.89	29.73	30.06
Al	6.13	6.37	6.02	6.17	6.19	5.99
K	4.39	4.43	3.83	2.92	3.45	2.93
Na	0.84	1.04	1.19	1.21	1.98	1.79
Ca	0.26	0.24	0.28	0.62	0.25	0.38
Mg	0.18	0.13		0.28	0.20	0.14
Si/Al	4.88	4.66	5.00	4.84	4.79	5.02
Si+Al	36.00	36.04	36.11	36.06	35.92	36.05
Σ_{cat}	6.12	6.21	5.58	5.93	6.34	5.78
E_b (§)	0.08	2.36	7.19	3.90	-2.37	3.55

Table D.5: Continuation of D.4.

Chemical composition of clinoptilolites. Each analysis represents a separate crystal from the stated horizon. Adapted from (Sand and Mumpton, 1978, p. 229-230).

(t) Inclusion impurities - not included in cell contents. Total iron given as FeO.

(tt) By difference.

(§) $E_b = \frac{Al - \Sigma_{cat}}{Al} \cdot 100$ where $\Sigma_{cat} = 2(Mg + Ca) + (Na + K)$

	105-19-3	105-19-3	105-21-cc	105-21-cc	163-17-5	163-19-5
SiO₂	70.13	68.99	69.20	66.71	66.82	68.51
Al₂O₃	12.59	11.85	12.52	11.67	11.92	11.84
K₂O	4.80	5.33	3.43	4.70	5.93	2.69
Na₂O	2.91	2.35	0.70	0.75	0.72	0.40
CaO	1.09	0.59	3.12	2.50	0.89	3.36
MgO	0.21		0.42	0.35	0.63	0.66
FeO (t)					0.22	
H₂O (tt)	8.27	10.89	10.61	13.32	12.87	12.54
Totals	100	100	100	100	100	100

Number of cations on the basis of 72 oxygens

Si	29.73	30.06	29.77	29.84	29.83	29.98
Al	6.29	6.09	6.35	6.15	6.27	6.10
K	2.59	2.96	1.88	2.68	3.38	1.47
Na	2.39	1.98	0.58	0.65	0.62	0.31
Ca	0.50	0.27	1.43	1.20	0.43	1.58
Mg	0.13		0.27	0.23	0.42	0.42
Si/Al	4.72	4.94	4.62	4.85	4.75	4.91
Si+Al	36.02	36.15	36.12	35.99	36.10	36.08
Σ_{cat}	6.24	5.49	5.88	6.19	5.70	5.78
E_b (§)	0.73	9.71	7.39	-0.65	9.18	5.20

Table D.6: Continuation of D.5.

Chemical composition of clinoptilolites. Each analysis represents a separate crystal from the stated horizon. Adapted from (Sand and Mumpton, 1978, p. 229-230).

(t) Inclusion impurities - not included in cell contents. Total iron given as FeO.

(tt) By difference.

(§) $E_b = \frac{Al - \Sigma_{cat}}{Al} \cdot 100$ where $\Sigma_{cat} = 2(Mg + Ca) + (Na + K)$

	163-27-1	59.2-5-1 (2-62 μ)	59.2-5-1 (2-62 μ)	59.2-5-1 (2-62 μ)	59.2-3-2	59.2-4-1	SCAN 16P 500 cm (2-6 μ)
SiO₂	66.77	65.84	66.60	67.98	68.98	68.19	65.55
Al₂O₃	11.62	12.18	11.61	12.08	11.24	12.73	11.76
K₂O	2.56	6.94	6.35	6.42	2.79	3.47	4.67
Na₂O	0.44	0.90	1.11	1.25	2.61	0.96	1.23
CaO	3.40	0.45	0.43	0.63	2.12	2.81	1.79
MgO	0.96	0.90	0.57	0.62		0.45	0.49
FeO (t)		0.54	0.42				
H₂O (tt)	14.25	12.25	12.91	11.02	12.26	11.10	14.51
Totals	100	100	100	100	100	100	100

Number of cations on the basis of 72 oxygens

Si	29.82	29.52	29.87	29.73	30.21	29.58	29.74
Al	6.12	6.44	6.14	6.23	5.80	6.51	6.28
K	1.45	3.97	3.63	3.58	1.55	1.92	2.70
Na	0.37	0.78	0.96	1.06	2.22	0.81	1.08
Ca	1.63	0.22	0.21	0.29	0.99	1.30	0.87
Mg	0.64	0.50	0.38	0.40		0.29	0.33
Si/Al	4.87	4.59	4.87	4.77	5.20	4.54	4.73
Si+Al	35.94	35.96	36.01	35.96	36.01	36.09	36.02
Σ_{cat}	6.35	6.18	5.78	6.04	5.76	5.93	6.19
E_b (§)	-3.80	3.90	5.80	3.00	0.60	8.90	1.50

Table D.7: Continuation of D.6.

Chemical composition of clinoptilolites. Each analysis represents a separate crystal from the stated horizon. Adapted from (Sand and Mumpton, 1978, p. 229-230).

(t) Inclusion impurities - not included in cell contents. Total iron given as FeO.

(tt) By difference.

(§) $E_b = \frac{Al - \Sigma_{cat}}{Al} \cdot 100$ where $\Sigma_{cat} = 2(Mg + Ca) + (Na + K)$

	(A)	(B)	(C)	(D)	(E)	(F)
SiO₂	72.40	71.58	71.83	71.11	72.75	67.80
Al₂O₃	13.17	13.71	14.27	14.22	15.03	16.12
Fe₂O₃	0.20	0.19	0.13	0.56	0.07	0.03
MgO	0.64	0.63	0.0	0.34	0.70	0.92
CaO	0.24	0.51	0.55	0.26	1.06	1.01
Na₂O	2.92	2.19	2.76	3.37	2.76	3.06
K₂O	4.93	3.16	5.88	5.09	5.83	5.76
Total*	94.50	91.97	95.42	94.95	98.20	94.70

Cell contents. based on 72 oxygens

Si	29.71	29.35	29.38	29.21	28.99	28.18
Al	6.37	6.62	6.88	6.88	7.05	7.89
Fe	0.06	0.06	0.04	0.17	0.02	0.01
Mg	0.39	0.38	0	0.21	0.41	0.57
Ca	0.11	0.22	0.24	0.11	0.45	0.45
Na	2.32	2.19	2.19	2.69	2.13	2.46
K	2.58	3.16	3.07	2.67	2.96	3.06
Si/Al	4.66	4.43	4.27	4.25	4.11	3.57

Table D.8: Chemical composition of deep-sea clinoptilolites. Adapted from (Sand and Mump-ton, 1978, p. 238).

(A) East Indian Ocean, 4696 m water depth, 89 m below sea bed, zeolite clay, Cretaceous.

(B) West Pacific Ocean, 5696 m water depth, 103 m below sea bed, radiolarian-bearing altered volcanic ash, Cretaceous.

(C) Indian Ocean, 1655 m water depth, 335.6 m below sea bed, glauconitic carbonate sand, Paleocene.

(D) North Atlantic Ocean, 5361 m water depth, 71.5 m below sea bed, silty clay, Cretaceous.

(E) Indian Ocean, 1655 m water depth, 335.4 m below sea bed, glauconitic carbonate sand, Paleocene.

(F) Indian Ocean, 1655 m water depth, 390.4 m below sea bed, lignite, Paleocene.

* The remainder is H₂O; Sr and Ba looked for, but not found. Fe₂O₃ is total iron.

	(1)
SiO₂	61.77
Al₂O₃	13.26
Fe₂O₃	0.59
MgO	0.51
CaO	0.89
SrO	0.03
BaO	0.10
Na₂O	4.19
K₂O	4.04
TiO₂	0.41
H₂O(+)	14.78
H₂O(-)	
Total	100.57

Unit-cell contents on basis of 72 oxygens

Si	28.50
Al	7.21
Fe⁺³	0.20
Mg	0.35
Ca	0.44
Sr	0.01
Ba	0.02
Na	3.75
K	2.38

Table D.9: Chemical composition of clinoptilolite from Tom Bowling Formation, 5 km south-west of North Cape. Adapted from (Sand and Mumpton, 1978, p. 311)

	Clinop. (t)		Unit-cell	
	(wt. %)		content (O=72)	
SiO₂	65.2	(29)	Si	29.27
Al₂O₃	13.2	(18)	Al	6.98
CaO	0.1	(18)	Ca	0.05
Na₂O	1.1	(11)	Na	0.95
K₂O	8.6	(11)	K	4.92
H₂O(+)				
H₂O(-)	11.8		H₂O	17.67
Total	100.0		Si:Al	4.19

Table D.10: Chemical composition of synthetic clinoptilolite. Adapted from (Sand and Mump-ton, 1978, p. 338)

	Hector Calif.	Baroid Mine. Hector. Calif.	Opal Mountain. Calif.	Barstow. Calif.	Shoshone. Calif.	Jersey Valley. Nevada	Eastgate. Nevada
Si/Al	5.15	5.20	4.40	3.90	3.90	4.05	4.10
K/Al	0.14	0.10	0.23	0.08	0.45	0.38	0.29
Na/Al	0.79	0.94	0.21	0.62	0.52	0.05	0.35
Ca/Al	0.09	0.19	0.35	0.29	0.04	0.35	0.10
Mg/Al	0.06	0.10			0.14	0.27	0.08
	1.08	1.33	0.79	0.99	1.15	1.05	0.82

NH₄ - exchanged samples

Si/Al	5.15	5.60	4.45	4.35	4.05	4.35	4.10
K/Al	0.04	0.04	0.07	0.08	0.07	0.07	0.05
Na/Al	0.03	0.03	0.06	0.02	0.01	0	0.01
Ca/Al	0.02	0.02	0.02	0.01	0	0.01	0.10
Mg/Al	0.05	0.05	0.05				0.08
NH₄/Al	0.86	0.86	0.80	0.89	0.92	0.92	0.76

Table D.11: Chemical composition of natural clinoptilolite from specific ores. Adapted from (Sand and Mumpton, 1978, p. 412)

	Ol₁	K-Ol₁	Ol₃	K-Ol₃
SiO₂	66.18		67.30	
Al₂O₃	11.69	11.15	12.17	11.86
Fe₂O₃	0.90	0.84	1.02	1.09
CaO	3.90	2.34	2.22	1.43
MgO	0.19	0.30	0.69	0.24
Na₂O	1.05	0.30	1.86	0.40
K₂O	3.21	6.20	4.16	7.83
H₂O(+)	12.85		10.65	
H₂O(-)				
sum	99.97		100.07	

Table D.12: Chemical composition of native and K-exchanged clinoptilolite in wt.%. Adapted from (Sand and Mumpton, 1978, p. 433).

Ol₁ = clinoptilolite, first Oligocene horizon.

Ol₃ = clinoptilolite, third Oligocene horizon.

K-Ol₁ and K-Ol₃ = potassium ion-exchanged forms.

	1	2	3	4	5	6	7	8
SiO₂	69.07	64.70	65.47	62.36	65.90	69.30	64.65	64.82
Al₂O₃	10.88	12.43	11.48	13.14	11.72	11.41	11.65	11.50
Fe₂O₃	0.08	0.44	0.61	1.63	0.71	0.38	0.76	1.19
FeO			1.25		0.12			
MgO	0.18	0.34	1.46	0.92	0.88	0.45	1.17	1.02
CaO	0.39	1.26	2.04	2.72	3.35	2.70	4.17	3.40
Na₂O	4.23	4.32	3.50	3.99	3.10	1.59	0.33	0.58
K₂O	2.52	2.28	2.60	1.20	1.25	2.86	2.33	1.87
H₂O	12.38	13.56	11.58	13.65	10.38	11.49	14.49	14.93

Table D.13: Chemical composition of clinoptilolite in wt.%. Adapted from (Tsitsishvili et al., 1992, p. 77).

1: Patagonia; 2: California, USA; 3: Transcarpathias, USSR; 4: Georgia, USA; 5: Azerbaidzhan, USSR; 6: Rhodopes, Bulgaria; 7: Rhodopes, Bulgaria; 8: Las Villas, Cuba

	1	2	3	4	5
SiO₂	68.82	71.75	66.44	66.18	66.47
Al₂O₃	11.51	12.58	11.69	11.69	13.47
CaO	2.68	2.88	2.07	3.9	3.25
K₂O	2.22	2.54	5.53	3.21	2.6
Na₂O	0.26	0.55	0.24	1.05	2.09
Fe₂O₃	0.74	1.31		0.9	1.05
MgO	0.63	0.93	0.69	0.19	0.65
MnO	0.001	0.03			0.02
TiO₂	0.1	0.16			0.15
H₂O	4.13	6.73		12.8	10
Si/Al	5.12	5.7	5.68	5.64	4.93

Table D.14: Chemical composition of clinoptilolite in wt.%. Adapted from [Rajec et al. \(1998\)](#). Zeolite content: 1 - Nizny Hrabovec, 60%; 2 - Majerovce, 52-65 %; 3 - Sklenne Teplice, 50 %; 4 - Beli Plast, 75 %; 5 - Metaxades, 58 %.

	(1)
SiO₂	66.84
Al₂O₃	13.09
TiO₂	0.15
Fe₂O₃	1.32
CaO	2.09
MgO	0.26
MnO	0.11
Na₂O	1.57
K₂O	3.66
SO₃	0.05
Σ H₂O	10.36
(Na+K)/(Ca+Mg)	2.92
Si/Al	4.33

Table D.15: Chemical composition of clinoptilolite in wt.%. Adapted from [Bogdanovich et al. \(2008\)](#)

E. Calculations for the Capacity Determination Experiments

*	...	activated
A_{old}	...	activity of the parent solution strontium at 14.12.2018
A_{new}	...	activity of the parent solution strontium at 07.01.2019
m_{CsNO_3}	...	mass of caesium nitrate
M_{CsNO_3}	...	molar mass of caesium nitrate
$m_{Sr(NO_3)_2}$...	mass of strontium nitrate
$M_{Sr(NO_3)_2}$...	molar mass of strontium nitrate
V_{PSC}	...	volume of parent solution caesium
V_{PSS}	...	volume of parent solution strontium

Table E.1: Explanation of the variable names for the calculations in Appendix E.

Calculations for Stock Solution 1 Strontium

Aim: $0.055 \frac{\text{mol Sr}}{\text{l solution}}$

total volume of 50 ml

just use the active parent solution strontium to get the wished concentration

$$\frac{m_{\text{Sr}(\text{NO}_3)_2^*} \text{ in g}}{V_{\text{PSS}} \text{ in l}} \cdot \frac{1}{M_{\text{Sr}(\text{NO}_3)_2} \text{ in } \frac{\text{g}}{\text{mol}}} = \frac{7.09508^* \text{ g}}{0.02 \text{ l}} \cdot \frac{1 \text{ mol}}{211.63 \text{ g}} = 1.68 \frac{\text{mol Sr}}{\text{l solution}} \quad (\text{E.0.1})$$

$$0.055 \frac{\text{mol Sr}}{\text{l solution}} \cdot 50 \text{ ml} = 1.68 \frac{\text{mol Sr}}{\text{l solution}} \cdot x \quad (\text{E.0.2})$$

$$x = 1.64 \text{ ml parent solution strontium} \quad (\text{E.0.3})$$

The parent solution strontium has a concentration of $1.68 \frac{\text{mol Sr}}{\text{l solution}}$. To prepare the 50 ml stock solution 1 strontium SL_1_Sr with a concentration of $0.055 \frac{\text{mol Sr}}{\text{l solution}}$ it is necessary to use 1.64 ml of the parent solution strontium.

Calculations for Stock Solution 2 Strontium

Aim: $0.55 \frac{\text{mol Sr}}{\text{l solution}}$

total volume of 50 ml

use the active parent solution strontium and inactive $\text{Sr}(\text{NO}_3)_2$ to get the wished concentration

$$m_{\text{Sr}(\text{NO}_3)_2} = 0.55 \frac{\text{mol Sr}}{\text{l solution}} \cdot 50 \text{ ml} \cdot 211.63 \frac{\text{g}}{\text{mol}} = 5.82 \text{ g} \quad (\text{E.0.4})$$

$$A_{\text{current}} : A_{\text{old}} = V_{\text{PSC added old}} : x \quad (\text{E.0.5})$$

$$x = \frac{4.73 \cdot 10^4}{3.63 \cdot 10^4} \cdot 1.6 \text{ ml} = 2.1 \text{ ml parent solution strontium} \quad (\text{E.0.6})$$

$$m_{\text{Sr}(\text{NO}_3)_2^*} = 1.68 \frac{\text{mol Sr}}{\text{l solution}} \cdot 2.1 \text{ ml} \cdot 211.63 \frac{\text{g}}{\text{mol}} = 0.75 \text{ g} \quad (\text{E.0.7})$$

$$m_{\text{Sr}(\text{NO}_3)_2} - m_{\text{Sr}(\text{NO}_3)_2^*} = 5.07 \text{ g Sr}(\text{NO}_3)_2 \quad (\text{E.0.8})$$

The parent solution strontium has a concentration of $1.68 \frac{\text{mol Sr}}{\text{l solution}}$. To prepare the 50 ml stock solution 2 strontium SL_2_Sr with a concentration of $0.55 \frac{\text{mol Sr}}{\text{l solution}}$ it is necessary to use 2.1 ml of the parent solution strontium and dissolve additional inactive 5.07 g of strontium nitrate.

Calculations for Stock Solution 1 Caesium

Aim: $0.11 \frac{\text{mol Cs}}{\text{l solution}}$

total volume of 50 ml

use the active parent solution caesium and inactive CsNO_3 to get the wished concentration

activity of 3.3 kBq

$$\frac{m_{\text{CsNO}_3^*} \text{ in g}}{V_{\text{PSC}} \text{ in l}} \cdot \frac{1}{M_{\text{CsNO}_3} \text{ in } \frac{\text{g}}{\text{mol}}} = \frac{0.01043^* \text{ g}}{0.01 \text{ l}} \cdot \frac{1 \text{ mol}}{194.91 \text{ g}} = 0.00535 \frac{\text{mol Cs}}{\text{l solution}} \quad (\text{E.0.9})$$

$$0.01043 \text{ g} : 10^5 \text{ Bq} = x : 3.3 \text{ kBq} \quad (\text{E.0.10})$$

$$x = 3.4419 \cdot 10^{-4} \text{ g} \quad (\text{E.0.11})$$

$$V_{\text{PSC}} : m_{\text{CsNO}_3^*} = y : x \quad (\text{E.0.12})$$

$$y = 3.3 \cdot 10^{-4} \text{ l} = 330 \mu\text{l parent solution caesium} \quad (\text{E.0.13})$$

$$m_{\text{CsNO}_3} = 0.11 \frac{\text{mol Cs}}{\text{l solution}} \cdot 50 \text{ ml} \cdot 194.91 \frac{\text{g}}{\text{mol}} = 1.072005 \text{ g} \quad (\text{E.0.14})$$

The parent solution caesium has a concentration of $5.35 \frac{\text{m mol Cs}}{\text{l solution}}$. To prepare the 50 ml stock solution 1 caesium with a concentration of $0.11 \frac{\text{mol Cs}}{\text{l solution}}$ it is necessary to dissolve additional 1.072005 g of caesium nitrate and add 330 μl of the parent solution caesium.

Calculations for Stock Solution 2 Caesium

Aim: $1.11 \frac{\text{mol Cs}}{\text{l solution}}$

total volume of 50 ml

use the active parent solution caesium and inactive CsNO_3 to get the wished concentration

$$m_{\text{CsNO}_3} = 1.11 \frac{\text{mol Cs}}{\text{l solution}} \cdot 50 \text{ ml} \cdot 194.91 \frac{\text{g}}{\text{mol}} = 10.817505 \text{ g} \quad (\text{E.0.15})$$

The parent solution caesium has a concentration of $5.35 \frac{\text{m mol Cs}}{\text{l solution}}$. To prepare the 50 ml stock solution 2 caesium with a concentration of $1.11 \frac{\text{mol Cs}}{\text{l solution}}$ it is necessary to dissolve additional 10.817505 g of caesium nitrate and add 330 μl of the parent solution caesium.

F. Experimental Procedure for Capacity Determination

Preparation of Parent Solution Strontium

1. Add two times 5 ml of triply distilled water to a vial.
2. Work under the fume hood with the vial.
3. Open the micro tube with tweezers.
4. Fill the radioactive $\text{Sr}(\text{NO}_3)_2^*$ ($m = 7.09508$ g) into the vial.
5. Close the vial and shake it.
6. Add again 5 ml of triply distilled water to the vial because not everything of the $\text{Sr}(\text{NO}_3)_2^*$ is dissolved.
7. Close the vial and shake it.
8. Empty the mixture into a 20 ml volumetric flask out of glass.
9. Give 2 ml of triply distilled water in the empty vial.
10. Empty the vial again into the flask.
11. Fill the flask up to the 20 ml mark with triply distilled water.
12. Empty the flask in a new vial.
13. Close the vial.

→ **Parent Solution Strontium PS_Sr**

Preparation of Parent Solution Caesium

1. Work under the fume hood.
2. Open the micro tube with tweezers.
3. Fill the radioactive CsNO_3^* ($m = 0.01043$ g) into a vial.
4. Add two times 5 ml of triply distilled water to the vial.
5. Close the vial and swivel it sideways.

→ **Parent Solution Caesium PS_Cs**

Preparation of Stock Solution 1 Strontium

1. Work under the fume hood.
2. Add 1.6 ml of Parent Solution Strontium to a 50 ml volumetric flask out of glass.
3. Fill the flask up to the 50 ml mark with triply distilled water.
4. Empty the flask in a new vial.
5. Close the vial.

→ **Stock Solution 1 Strontium SL_1_Sr**

Preparation of Stock Solution 2 Strontium

1. Weigh 5.09452 g of inactive $\text{Sr}(\text{NO}_3)_2$ in a vial.
2. Add five times 5 ml of triply distilled water to the vial (equal to 24.78 g).
3. Close the vial and swivel it sideways under warm tap water.
4. Add four times 5 ml of triply distilled water to the vial (in total equal to 44.69 g).
5. Close the vial and swivel it sideways under warm tap water. Everything of $\text{Sr}(\text{NO}_3)_2$ is dissolved.
6. Add 2.8 ml of triply distilled water to the vial (in total equal to 47.47 g). In total it was added an amount of 47.8 ml or 47.47 g of triply distilled water to the vial.
7. Work under the fume hood.
8. Add 2.2 ml of Parent Solution Strontium to the vial.
9. Close the vial.

→ **Stock Solution 2 Strontium SL_2_Sr**

Preparation of Stock Solution 1 Caesium

1. Weigh 1.07780 g of inactive CsNO₃ in a vial.
2. Add 50.04 g triply distilled water.
3. Work under the fume hood.
4. Add 40 µl of Parent Solution Caesium to the vial.
5. Add 360 µl of Parent Solution Caesium to the vial.
6. Close the vial.

→ **Stock Solution 1 Caesium SL_1_Cs**

Preparation of Stock Solution 2 Caesium

1. Weigh 10.85546 g of inactive CsNO₃ in a vial.
2. Add three times 5 ml of triply distilled water to the vial (equal to 14.99 g).
3. Close the vial and swivel it sideways under warm tap water.
4. Add two times 5 ml of triply distilled water to the vial (in total equal to 24.89 g).
5. Close the vial and swivel it sideways under warm tap water.
6. Add three times 5 ml of triply distilled water to the vial (in total equal to 39.85 g).
7. Be patient.
8. Close the vial and swivel it sideways under warm tap water. Everything of CsNO₃ is dissolved.
9. Add 5 ml of triply distilled water to the vial (in total equal to 44.86 g).
10. Add 3 ml of triply distilled water to the vial (in total equal to 47.86 g). In total it was added an amount of 48 ml or 47.86 g of triply distilled water to the vial.
11. Work under the fume hood.
12. Add five times 400 µl of Parent Solution Caesium to the vial.
13. Close the vial.

→ **Stock Solution 2 Caesium SL_2_Cs**

Procedure of the Capacity Experiment

Do the following procedure eight times - for each zeolite type twice. For each zeolite type the experiment is done with the strontium and the caesium stock solution.

1. Weigh 500 mg of the zeolite in a centrifuge tube.
2. Add 1 ml of the radioactive stock solution to the centrifuge tube.
3. Vortex the centrifuge tube for 20 s. Watch out not to spill something of the mixture.
4. Add 4 ml of the radioactive stock solution to the centrifuge tube.
5. Swivel the centrifuge tube sideways until all air bubbles are gone.
6. Add 5 ml of the radioactive stock solution to the centrifuge tube.
7. Put a stubble on the centrifuge tube.
 - (a) Strontium experiment: A cannula is pierced through the stubble.
 - (b) Caesium experiment: Just a normal stubble is used.
 - (c) Experiment with stock solution 2: Instead of the stubble the centrifuge tube was sealed with parafilm.
8. Let the mixture in the centrifuge tube rest over night under a fume hood.
 - (a) Strontium experiment: Put the centrifuge tube into an oil bath with the temperature of 53°C.
 - (b) Caesium experiment: Put the centrifuge tube into a beaker glass and let it rest by room temperature.
9. Take the centrifuge tube out of the fume hood.
 - (a) Strontium experiment: Clean the centrifuge tube first.
 - (b) Caesium experiment: Just put the centrifuge tube out.
10. Put the centrifuge tube into the centrifuge. Keep in mind to load the centrifuge evenly.
11. Run the centrifuge for 10 minutes with a rotor of 4500 rpm.
12. Take the centrifuge tube out and put it right away in a stand. As the stand a titration flask was used.
13. Use a disposable pipette to collect the clear liquid into a vial.
14. Add 1 ml of triply distilled water to the centrifuge tube.
15. Vortex the centrifuge tube for 20 s. Watch out not to spill something of the mixture.

16. Add 4 ml of triply distilled water to the centrifuge tube.
17. Swivel the centrifuge tube sideways until all air bubbles are gone.
18. Add 5 ml of triply distilled water to the centrifuge tube.
19. Repeat steps 10 to 18.
20. Repeat steps 10 to 13.
21. Fill the vial up with four times 5 ml of triply distilled water to get a total amount of 50 ml.
22. Add 5 ml of triply distilled water to the zeolite in the centrifuge tube.
23. Use the same disposable pipette to put the mixture into another vial.
24. Add 5 ml of triply distilled water to the centrifuge tube.
25. Use the same disposable pipette to put the mixture into the same vial.
26. Repeat steps 24 to 25 twice.
27. Add two times 5 ml of triply distilled water to the centrifuge tube. Use it to flush the disposable pipette while putting the liquid into the vial.
28. Use 5 ml of triply distilled water to rinse the outside of the disposable pipette directly into the vial.
29. Add 5 ml of triply distilled water to the centrifuge tube. Pour it directly into the vial.
30. Add two times 5 ml of triply distilled water to the vial to get a total amount of 50 ml.

→ **First vial with the liquid sample**

Strontium experiment: [zeolitetype]_SL_[number of stock solution]_Sr_L

Caesium experiment: [zeolitetype]_SL_[number of stock solution]_Cs_L

→ **Second vial with zeolite particles**

Strontium experiment: [zeolitetype]_SL_[number of stock solution]_Sr_Z

Caesium experiment: [zeolitetype]_SL_[number of stock solution]_Cs_Z

Procedure of the Capacity Experiment for A_SL_1_Sr

All the steps were the same until the centrifuge tube shattered while taking it out of the centrifuge for the last time in step 20. Some of the zeolite particles got lost during the cleaning of the centrifuge but most of them were rescued thanks to the stand. The titration flask caught most of the leaking zeolite particles and triply distilled water. So the following procedure is a bit different.

21. Fill the vial up with six times 5 ml of triply distilled water to get a total amount of 50 ml.
 22. Put 5 ml of triply distilled water into the centrifuge tube to rinse it directly into a new vial.
 23. Use two times 5 ml of triply distilled water to rinse the outside of the centrifuge tube directly into the vial.
 24. Add 5 ml of triply distilled water to the titration flask.
 25. Use the same disposable pipette as for the steps before step 21 to put the mixture into the vial.
 26. Repeat step 25.
 27. Use 5 ml of triply distilled water to rinse the outside of the disposable pipette directly into the vial.
 28. Add two times 5 ml of triply distilled water to the titration flask. Pour it directly into the vial. The vial has now a total amount of 50 ml.
- **First vial with the liquid sample (A_SL_1_Sr_L)**
- **Second vial with zeolite particles (A_SL_1_Sr_Z)**

G. Spectra of the Capacity Experiments

Sr Uptake Experiments

	Energy (keV)	Intensity (%)	Dose (MeV/Bq-s)
XR 1	1.69	2.59 % 15	4.38E-5 25
XR $k\alpha$ 2	13.336	17.3 % 11	0.00231 15
XR $k\alpha$ 1	13.395	33.4 % 22	0.0045 3
XR $k\beta$ 3	14.952	2.44 % 16	3.65E-4 24
XR $k\beta$ 1	14.961	4.7 % 3	7.1E-4 5
XR $k\beta$ 2	15.185	0.75 % 5	1.13E-4 8
	129.80 5	2.4E-4 % 24	3E-7 3
	151.18 3	0.0012 % 9	1.7E-6 13
	233 ?	1.9E-5 % 19	4E-8 4
	354.06 5	4.8E-4 % 19	1.7E-6 7
	362.82	0.00137 % 24	5.0E-6 9
	514.0048 22	96 %	0.492
	716.87 5	3.1E-4 % 3	2.20E-6 23
	868.06 5	0.0120 % 7	1.04E-4 6
	951.0 5	1.4E-5 % 14	1.4E-7 14

Table G.1: γ - Lines for $^{85}_{38}\text{Sr}$ and their intensities. ([National Nuclear Data Center \(c\)](#))

Sample	Zeolite	Stock Solution	Measurement time in s
SL_1_Sr_300s		1	300
A_SL_1_Sr_L_600s	A	1	600
B_SL_1_Sr_L_600s	B	1	600
C_SL_1_Sr_L_600s	C	1	600
D_SL_1_Sr_L_600s	D	1	600
SL_2_Sr		2	300
A_SL_2_Sr_L_600s	A	2	600
B_SL_2_Sr_L_600s	B	2	600
C_SL_2_Sr_L_600s	C	2	600
D_SL_1_Sr_L_600s	D	2	600

Table G.2: Explanation of the sample names for the strontium capacity measurements.

	Peak No.	Energy [keV]	Net Peak Area [cts]	Bkgnd [cts]	FWHM [keV]	Counts/sec	Error [%]	
F	1	6.22	22233	48611	1.793	7.41E+01	0.93	
M	2	72.57	4216	69725	1.261	1.41E+01	13.48	
m	3	74.74	7718	82497	1.265	2.57E+01	11.37	
m	4	84.39	3850	82913	1.282	1.28E+01	12	
F	5	123.27	8772	99137	1.355	2.92E+01	10.88	
F	6	215.41	5391	149511	1.434	1.80E+01	7.36	
F	7	232.23	7912	130917	3.726	2.64E+01	3.86	
F	8	267.59	8461	56321	1.43	2.82E+01	2.26	
F	9	372.52	2598	40017	1.286	8.66E+00	19.36	
F	10	387.7	2285772	38194	1.553	7.62E+03	0.09	
F	11	485.62	342	4348	1.329	1.14E+00	47.3	
F	12	495.42	6166	3861	1.612	2.06E+01	1.48	
F	13	513.09	225415	5348	1.646	7.51E+02	0.31	Sr85
F	14	563.01	314	1845	1.714	1.05E+00	51.27	
F	15	583.86	187	1704	1.341	6.23E-01	18.82	
F	16	619.06	420	1339	1.139	1.40E+00	8.61	
F	17	775.53	6334	2336	2.039	2.11E+01	4.38	
F	18	900.97	1128	1095	2.14	3.76E+00	16.2	
F	19	1131.72	78	946	1.166	2.61E-01	33.46	
F	20	1367.86	22495	561	2.38	7.50E+01	1.08	
F	21	1731.16	1424	366	3.074	4.75E+00	2.83	
F	22	2242.89	1880	675	3.995	6.27E+00	2.56	
F	23	2601.27	69	244	1.602	2.30E-01	22.07	
F	24	2754.28	11789	264	3.551	3.93E+01	0.92	
F	25	2772.24	22	47	1.194	7.23E-02	33.36	
F	26	3141.44	21	44	0.7	6.94E-02	3.97	

Table G.3: γ - Spectrum data for SL_1_Sr_300s. Errors quoted at 1.00 sigma.

	Peak No.	Energy [keV]	Net Peak Area [cts]	Bkgnd [cts]	FWHM [keV]	Counts/sec	Error [%]	
F	1	75.29	248	2048	0.637	4.1382E-01	4.73	
F	2	123.70	958	2546	1.220	1.5973E+00	13.55	
F	3	215.78	682	2210	1.355	1.1371E+00	6.58	
F	4	372.70	306	1170	1.208	5.0943E-01	10.13	
F	5	485.73	56	358	0.647	9.2582E-02	68.97	
F	6	495.74	766	644	1.431	1.2759E+00	11.87	
F	7	513.40	64476	414	1.549	1.0746E+02	0.58	Sr85
F	8	619.53	48	5	1.147	8.0034E-02	34.84	

Table G.4: γ - Spectrum data for A_SL_1_Sr_L_600s. Errors quoted at 1.00 sigma.

	Peak No.	Energy [keV]	Net Peak Area [cts]	Bkgnd [cts]	FWHM [keV]	Counts/sec	Error [%]	
F	1	84.65	115	1595	0.736	1.9090E-01	27.98	
F	2	123.66	806	2619	1.284	1.3431E+00	15.06	
F	3	215.67	527	2703	1.273	8.7864E-01	8.28	
F	4	372.72	228	995	1.050	3.8051E-01	43.24	
F	5	495.80	618	618	1.526	1.0297E+00	16.20	
F	6	513.41	64433	444	1.542	1.0739E+02	0.59	Sr85
F	7	619.30	45	9	1.582	7.4323E-02	16.07	
F	8	1367.91	45	1	1.854	7.5170E-02	15.39	

Table G.5: γ - Spectrum data for B_SL_1_Sr_L_600s. Errors quoted at 1.00 sigma.

	Peak No.	Energy [keV]	Net Peak Area [cts]	Bkgnd [cts]	FWHM [keV]	Counts/sec	Error [%]	
F	1	123.67	942	2470	1.207	1.5696E+00	16.43	
F	2	215.65	548	2987	1.065	9.1378E-01	27.33	
F	3	372.82	270	1316	1.153	4.4952E-01	35.94	
F	4	495.69	727	615	1.674	1.2113E+00	4.41	
F	5	513.41	65286	400	1.545	1.0881E+02	0.59	Sr85
F	6	619.57	39	3	1.522	6.5748E-02	16.49	

Table G.6: γ - Spectrum data for C_SL_1_Sr_L_600s. Errors quoted at 1.00 sigma.

	Peak No.	Energy [keV]	Net Peak Area [cts]	Bkgnd [cts]	FWHM [keV]	Counts/sec	Error [%]	
F	1	75.15	112	1911	0.844	1.8635E-01	31.18	
F	2	84.71	108	1475	0.683	1.7923E-01	31.88	
F	3	123.63	1479	3113	1.212	2.4657E+00	12.52	
F	4	215.65	956	3638	1.257	1.5934E+00	5.27	
F	5	249.15	146	2575	1.062	2.4344E-01	26.44	
F	6	268.19	203	2248	1.358	3.3773E-01	19.89	
F	7	372.80	407	1517	1.094	6.7792E-01	8.27	
F	8	495.74	1042	847	1.538	1.7373E+00	3.69	
F	9	513.40	76679	508	1.556	1.2780E+02	0.53	Sr85
F	10	584.52	19	12	1.082	3.1814E-02	27.62	
F	11	619.82	56	5	1.151	9.2686E-02	36.36	

Table G.7: γ - Spectrum data for D_SL_1_Sr_L_600s. Errors quoted at 1.00 sigma.

	Peak No.	Energy [keV]	Net Peak Area [cts]	Bkgnd [cts]	FWHM [keV]	Counts/sec	Error [%]	
F	1	75.03	505	5297	0.876	1.68E+00	12.55	
F	2	123.48	2437	9644	1.159	8.12E+00	12.84	
F	3	215.6	1850	11121	1.259	6.17E+00	16.44	
F	4	372.74	910	4406	1.2	3.03E+00	23.03	
F	5	495.59	1948	2226	1.45	6.49E+00	2.87	
F	6	513.3	235005	1786	1.565	7.83E+02	0.28	Sr85
F	7	619.45	136	25	1.467	4.52E-01	21.98	
F	8	880.46	61	10	1.414	2.03E-01	35.92	

Table G.8: γ - Spectrum data for SL_2_Sr_300s. Errors quoted at 1.00 sigma.

	Peak No.	Energy [keV]	Net Peak Area [cts]	Bkgnd [cts]	FWHM [keV]	Counts/sec	Error [%]	
F	1	123.57	776	3019	1.109	1.2931E+00	6.13	
F	2	215.78	550	3610	1.215	9.1727E-01	8.83	
F	3	495.77	631	603	1.545	1.0522E+00	165.07	
F	4	513.38	87599	588	1.556	1.4600E+02	0.49	Sr85

Table G.9: γ - Spectrum data for A_SL_2_Sr_L_600s. Errors quoted at 1.00 sigma.

	Peak No.	Energy [keV]	Net Peak Area [cts]	Bkgnd [cts]	FWHM [keV]	Counts/sec	Error [%]	
F	1	123.65	789	3417	1.323	1.3151E+00	21.71	
F	2	215.68	431	3513	1.258	7.1792E-01	10.92	
F	3	495.65	506	662	1.543	8.4384E-01	6.16	
F	4	513.39	86418	569	1.554	1.4403E+02	0.50	Sr85

Table G.10: γ - Spectrum data for B_SL_2_Sr_L_600s. Errors quoted at 1.00 sigma.

	Peak No.	Energy [keV]	Net Peak Area [cts]	Bkgnd [cts]	FWHM [keV]	Counts/sec	Error [%]	
F	1	123.66	706	3377	1.163	1.1762E+00	25.65	
F	2	215.77	472	3850	0.925	7.8711E-01	9.86	
F	3	495.66	590	849	1.596	9.8413E-01	5.47	
F	4	513.38	90830	564	1.553	1.5138E+02	0.49	Sr85

Table G.11: γ - Spectrum data for C_SL_2_Sr_L_600s. Errors quoted at 1.00 sigma.

	Peak No.	Energy [keV]	Net Peak Area [cts]	Bkgnd [cts]	FWHM [keV]	Counts/sec	Error [%]	
F	1	123.66	892	3298	1.153	1.4872E+00	18.95	
F	2	215.84	494	3344	1.137	8.2290E-01	10.02	
F	3	495.76	608	1032	1.505	1.0141E+00	5.47	
F	4	513.38	91591	579	1.560	1.5265E+02	0.47	Sr85

Table G.12: γ - Spectrum data for D_SL_2_Sr_L_600s. Errors quoted at 1.00 sigma.

Cs Uptake Experiments

	Energy (keV)	Intensity (%)	Dose (MeV/Bq-s)
XR 1	4.47	0.105 % 5	4.70E-6 21
XR $k\alpha$ 2	31.817	0.238 % 6	7.58E-5 18
XR $k\alpha$ 1	32.194	0.434 % 10	1.40E-4 3
XR $k\beta$ 3	36.304	0.0416 % 9	1.51E-5 3
XR $k\beta$ 1	36.378	0.0803 % 18	2.92E-5 6
XR $k\beta$ 2	37.255	0.0254 % 6	9.46E-6 21
	232.6 ?	5E-4 % 5	1.3E-6 13
	242.738 8	0.027 % 3	6.6E-5 7
	326.589 13	0.0162 % 10	5.3E-5 3
	475.365 2	1.477 % 7	0.00702 3
	563.246 5	8.338 % 14	0.04696 8
	569.331 3	15.373 % 17	0.08752 10
	604.721 2	97.62 % 11	0.5903 7
	795.864 4	85.46 % 6	0.6801 5
	801.953 4	8.688 % 16	0.06967 13
	1038.610 7	0.990 % 3	0.01028 3
	1167.968 5	1.790 % 5	0.02091 6
	1365.185 7	3.017 % 8	0.04119 11

Table G.13: γ - Lines for $^{134}_{55}\text{Cs}$ and their intensities. ([National Nuclear Data Center](#) (a))

Sample	Zeolite	Stock Solution	Measured time in s
SL_1_Cs		1	300
A_SL_1_Cs_L_3600s	A	1	3600
B_SL_1_Cs_L_3600s	B	1	3600
C_SL_1_Cs_L_3600s	C	1	3600
D_SL_1_Cs_L_3600s	D	1	3600
SL_2_Cs		2	300
A_SL_2_Cs_L_600s	A	2	600
B_SL_2_Cs_L_600s	B	2	600
C_SL_2_Cs_L_600s	C	2	600
D_SL_2_Cs_L_600s	D	2	600

Table G.14: Explanation of the sample names for the caesium capacity measurements.

Only the used peaks are "marked" in the tables.

	Peak No.	Energy [keV]	Net Peak Area [cts]	Bkgnd [cts]	FWHM [keV]	Counts/sec	Error [%]	
F	1	127.28	16028	3913	1.207	5.34E+01	1.78	
F	2	474.68	804	2105	1.458	2.68E+00	8.6	
M	3	562.59	3822	2003	1.583	1.27E+01	2.78	
m	4	568.67	6725	1929	1.587	2.24E+01	2.46	
F	5	604.04	44861	2029	1.636	1.50E+02	0.78	Cs134
M	6	795.06	31541	353	1.819	1.05E+02	0.86	Cs134
m	7	801.15	2954	289	1.822	9.85E+00	1.98	
F	8	1037.73	299	168	1.896	9.98E-01	6.76	
M	9	1167.14	615	139	2.078	2.05E+00	9.08	
m	10	1173.45	197	145	2.081	6.55E-01	10.99	
F	11	1364.54	863	35	2.42	2.88E+00	3.41	
M	12	1399.92	789	17	2.299	2.63E+00	3.58	
m	13	1406.18	56	1	2.302	1.87E-01	13.58	

Table G.15: γ - Spectrum data for SL_1_Cs_300s. Errors quoted at 1.00 sigma.

	Peak No.	Energy [keV]	Net Peak Area [cts]	Bkgnd [cts]	FWHM [keV]	Counts/sec	Error [%]	
F	1	75.09	326	3405	0.866	9.0582E-02	447.44	
F	2	474.84	1177	3191	1.372	3.2681E-01	4.65	
M	3	562.61	6247	3011	1.617	1.7352E+00	2.44	
m	4	568.65	11181	3115	1.621	3.1059E+00	2.21	
F	5	604.04	72494	3514	1.632	2.0137E+01	0.59	Cs134
M	6	795.05	51426	622	1.811	1.4285E+01	0.68	Cs134
m	7	801.14	4950	467	1.814	1.3751E+00	1.53	
F	8	1037.73	543	323	1.908	1.5094E-01	5.00	
M	9	1167.21	961	276	1.809	2.6704E-01	7.98	
m	10	1173.27	284	282	1.812	7.8883E-02	9.42	
F	11	1364.54	1551	52	2.317	4.3074E-01	4.59	
F	12	1399.84	1212	73	2.133	3.3674E-01	2.94	

Table G.16: γ - Spectrum data for A_SL_1_Cs_L_3600s. Errors quoted at 1.00 sigma.

	Peak No.	Energy [keV]	Net Peak Area [cts]	Bkgnd [cts]	FWHM [keV]	Counts/sec	Error [%]	
F	1	474.80	1116	1999	1.495	3.0991E-01	4.76	
M	2	562.60	5543	2891	1.625	1.5397E+00	2.53	
m	3	568.67	9851	2998	1.629	2.7365E+00	2.29	
F	4	604.05	64315	3006	1.634	1.7865E+01	0.68	Cs134
M	5	795.05	45012	555	1.797	1.2503E+01	0.73	Cs134
m	6	801.14	4401	446	1.800	1.2225E+00	1.63	
F	7	1037.75	471	239	2.075	1.3084E-01	5.41	
M	8	1167.23	878	251	1.887	2.4387E-01	8.73	
m	9	1173.22	213	290	1.890	5.9169E-02	11.03	
F	10	1364.50	1350	65	2.204	3.7488E-01	5.04	
F	11	1399.87	1064	68	2.028	2.9556E-01	6.47	

Table G.17: γ - Spectrum data for B_SL_1_Cs_L_3600s. Errors quoted at 1.00 sigma.

	Peak No.	Energy [keV]	Net Peak Area [cts]	Bkgnd [cts]	FWHM [keV]	Counts/sec	Error [%]	
F	1	474.75	1041	2767	1.310	2.8928E-01	4.99	
M	2	562.60	5626	2891	1.598	1.5627E+00	2.64	
m	3	568.67	10008	2931	1.602	2.7801E+00	2.39	
F	4	604.03	65910	3231	1.626	1.8308E+01	0.63	Cs134
M	5	795.04	46987	662	1.797	1.3052E+01	0.73	Cs134
m	6	801.13	4530	471	1.800	1.2584E+00	1.60	
F	7	1037.61	490	277	2.004	1.3613E-01	5.25	
M	8	1167.15	828	251	2.059	2.3009E-01	3.83	
m	9	1173.17	245	266	2.062	6.8048E-02	8.10	
F	10	1364.52	1398	45	2.298	3.8827E-01	5.20	
F	11	1399.78	1233	76	2.178	3.4241E-01	3.63	

Table G.18: γ - Spectrum data for C_SL_1_Cs_L_3600s. Errors quoted at 1.00 sigma.

	Peak No.	Energy [keV]	Net Peak Area [cts]	Bkgnd [cts]	FWHM [keV]	Counts/sec	Error [%]
F	1	75.17	300	3257	0.831	8.3247E-02	17.50
F	2	474.76	1482	3242	1.550	4.1153E-01	4.09
M	3	562.62	7312	3787	1.594	2.0312E+00	2.28
m	4	568.69	13631	3784	1.598	3.7863E+00	2.04
F	5	604.05	87544	4169	1.633	2.4318E+01	0.59
M	6	795.07	62413	844	1.803	1.7337E+01	0.64
m	7	801.16	5883	601	1.807	1.6342E+00	1.41
F	8	1037.73	652	394	2.049	1.8102E-01	13.34
M	9	1167.24	1209	287	2.054	3.3593E-01	7.43
m	10	1173.17	329	342	2.056	9.1478E-02	8.84
F	11	1364.60	1853	61	2.307	5.1475E-01	4.37
M	12	1399.86	1697	27	2.191	4.7135E-01	3.99
m	13	1406.01	128	24	2.194	3.5615E-02	9.60

Table G.19: γ - Spectrum data for D_SL_1_Cs_L_3600s. Errors quoted at 1.00 sigma.

	Peak No.	Energy [keV]	Net Peak Area [cts]	Bkgnd [cts]	FWHM [keV]	Counts/sec	Error [%]	
F	1	75.11	793	10165	1.094	2.64E+00	10.83	
F	2	474.64	3629	11602	1.556	1.21E+01	10.89	
M	3	562.48	18530	10303	1.621	6.18E+01	1.41	
m	4	568.56	33509	9782	1.625	1.12E+02	1.27	
F	5	603.93	219196	10830	1.651	7.31E+02	0.33	Cs134
M	6	794.94	156620	2222	1.828	5.22E+02	0.39	Cs134
m	7	801.03	14900	1760	1.831	4.97E+01	0.89	
F	8	1037.69	1590	900	2.013	5.30E+00	8.31	
M	9	1167.11	3016	782	2.085	1.01E+01	4.37	
m	10	1173.12	877	740	2.087	2.92E+00	5.57	
F	11	1364.5	4770	189	2.314	1.59E+01	2.7	
M	12	1399.83	4057	134	2.21	1.35E+01	3.09	
m	13	1405.96	311	57	2.213	1.04E+00	6.22	
F	14	1969.51	173	3	2.558	5.78E-01	7.66	

Table G.20: γ - Spectrum data for SL_2_Cs_300s. Errors quoted at 1.00 sigma.

	Peak No.	Energy [keV]	Net Peak Area [cts]	Bkgnd [cts]	FWHM [keV]	Counts/sec	Error [%]	
F	1	474.75	1463	3601	1.403	2.4379E+00	14.11	
M	2	562.54	7071	3728	1.612	1.1785E+01	1.34	
m	3	568.61	13204	3712	1.616	2.2007E+01	0.93	
F	4	603.99	83664	4009	1.640	1.3944E+02	0.61	
M	5	795.01	59633	700	1.811	9.9388E+01	0.62	Cs134
m	6	801.09	5680	524	1.815	9.4674E+00	1.42	Cs134
F	7	1037.78	557	301	1.970	9.2910E-01	5.02	
M	8	1167.18	1198	238	1.926	1.9974E+00	7.71	
m	9	1173.19	338	340	1.928	5.6278E-01	8.87	
F	10	1364.54	1822	66	2.143	3.0368E+00	4.24	
M	11	1399.91	1552	40	2.168	2.5871E+00	4.50	
m	12	1405.75	98	38	2.171	1.6336E-01	11.69	

Table G.21: γ - Spectrum data for A_SL_2_Cs_L_600s. Errors quoted at 1.00 sigma.

	Peak No.	Energy [keV]	Net Peak Area [cts]	Bkgnd [cts]	FWHM [keV]	Counts/sec	Error [%]	
F	1	75.22	331	4263	0.880	5.5246E-01	15.43	
F	2	474.71	1448	3864	1.492	2.4131E+00	14.08	
M	3	562.55	6998	3479	1.605	1.1664E+01	2.29	
m	4	568.62	12816	3564	1.609	2.1361E+01	2.06	
F	5	603.99	83128	3937	1.640	1.3855E+02	0.61	Cs134
M	6	795.01	58952	733	1.809	9.8253E+01	0.63	Cs134
m	7	801.08	5596	567	1.812	9.3267E+00	1.44	
F	8	1037.74	581	398	1.871	9.6884E-01	4.97	
M	9	1167.10	1228	210	2.343	2.0474E+00	7.77	
m	10	1173.26	373	226	2.345	6.2165E-01	9.16	
F	11	1364.51	1730	63	2.239	2.8835E+00	2.42	
M	12	1399.81	1600	32	2.244	2.6667E+00	2.51	
m	13	1406.10	113	12	2.247	1.8850E-01	9.65	

Table G.22: γ - Spectrum data for B_SL_2_Cs_L_600s. Errors quoted at 1.00 sigma.

	Peak No.	Energy [keV]	Net Peak Area [cts]	Bkgnd [cts]	FWHM [keV]	Counts/sec	Error [%]	
F	1	75.09	279	4628	0.735	4.6562E-01	17.09	
F	2	474.73	1442	3267	1.555	2.4036E+00	4.11	
M	3	562.55	6924	3911	1.613	1.1540E+01	2.45	
m	4	568.62	12702	3616	1.617	2.1170E+01	2.23	
F	5	604.00	83251	3922	1.644	1.3875E+02	0.56	Cs134
M	6	795.02	58711	829	1.809	9.7852E+01	0.66	Cs134
m	7	801.10	5742	515	1.812	9.5708E+00	1.42	
F	8	1037.84	655	326	1.939	1.0916E+00	12.05	
M	9	1167.15	1159	302	2.158	1.9322E+00	7.53	
m	10	1173.21	321	291	2.160	5.3457E-01	9.46	
F	11	1364.48	1771	73	2.299	2.9521E+00	4.47	
F	12	1399.77	1444	146	2.074	2.4068E+00	5.20	

Table G.23: γ - Spectrum data for C_SL_2_Cs_L_600s. Errors quoted at 1.00 sigma.

	Peak No.	Energy [keV]	Net Peak Area [cts]	Bkgnd [cts]	FWHM [keV]	Counts/sec	Error [%]	
F	1	75.01	276	3936	0.795	4.6034E-01	18.16	
F	2	474.73	1543	4286	1.571	2.5717E+00	13.10	
M	3	562.54	7412	3819	1.607	1.2354E+01	2.21	
m	4	568.62	13004	3758	1.611	2.1673E+01	2.01	
F	5	603.99	84825	4094	1.642	1.4137E+02	0.56	Cs134
M	6	795.00	60281	739	1.813	1.0047E+02	0.62	Cs134
m	7	801.10	5634	559	1.816	9.3897E+00	1.43	
F	8	1037.70	643	371	2.026	1.0711E+00	14.28	
M	9	1167.18	1161	319	2.152	1.9350E+00	3.19	
m	10	1173.15	337	266	2.154	5.6157E-01	6.55	
F	11	1364.53	1881	52	2.251	3.1355E+00	4.10	
M	12	1399.85	1548	50	2.214	2.5802E+00	2.57	
m	13	1406.13	82	18	2.217	1.3627E-01	12.16	

Table G.24: γ - Spectrum data for D_SL_2_Cs_L_600s. Errors quoted at 1.00 sigma.

H. Coal Fly Ash (CFA) Standard Data Sheet



National Institute of Standards & Technology

Certificate of Analysis

Standard Reference Material 1633b

Constituent Elements in Coal Fly Ash

This Standard Reference Material (SRM) is intended for use in the evaluation of analytical methods for the determination of constituent elements in coal fly ash or materials with a similar matrix. SRM 1633b is a bituminous coal fly ash that was sieved through a nominal sieve opening of 90 μm (170 mesh) and then blended to assure homogeneity. A unit of SRM 1633b consists of 75 g of powdered material.

The certified values for the constituent elements are given in Table 1. The values, except for Hg, are based on measurements using one definitive method or two or more independent and reliable analytical techniques. Noncertified values for a number of elements are given in Table 2 as additional information on the composition of the material. The noncertified values should not be used for calibration or quality control. Analytical methods used for the certification of this SRM are given in Table 3 along with analysts and cooperating laboratories. All values are based on measurements using a dry sample weight of at least 250 mg.

NOTICE AND WARNING TO USERS

Expiration of Certification: This certification is valid for 5 years from the date of shipment from NIST. Should any of the certified values change before the expiration of the certification, the purchaser will be notified by NIST.

Stability: This material is considered to be stable; however, its stability has not been rigorously assessed. NIST will monitor this material and will report any substantive changes in certification to the purchaser.

Use: A minimum dry sample weight (see Instructions for Drying) of 250 mg should be used for analytical determinations to be related to the certified values on this Certificate of Analysis.

To obtain the certified values, sample preparation procedures should be designed to affect complete dissolution. If volatile elements (e.g., Hg, As, Se) are to be determined, precautions should be taken in the dissolution of SRM 1633b to avoid volatilization losses.

Statistical consultation was provided by S.B. Schiller of the NIST Statistical Engineering Division.

The overall direction and coordination of the analyses were under the chairmanship of R.R. Greenberg of the NIST Inorganic Analytical Research Division.

The technical and support aspects involved in the preparation, certification, and issuance of this SRM were coordinated through the Standard Reference Materials Program by J.S. Kane.

Gaithersburg, MD 20899
June 22, 1993

Thomas E. Gills, Acting Chief
Standard Reference Materials Program

(over)

Instructions for Drying: When non-volatile elements are being determined, this material should be dried to constant weight before using. Recommended procedures for drying are: 1) Vacuum drying for 24 h at ambient temperature using a cold trap at or below -50 °C and a pressure not greater than 0.2 mm Hg (30 Pa); 2) drying for 2 h in an oven of 105 °C. Samples of the dried material weighing at least 250 mg should be used for analysis. When not in use, the material should be kept in a tightly sealed bottle. Volatile elements should be determined on an as-received basis, and corrected to dry weight. Correction should be based on a separate determination of moisture, using one of the above drying procedures.

Source and Preparation of the Material: The fly ash was supplied by a coal fired power plant and is the product of Pennsylvania and West Virginia coals. It was selected as a typical bituminous coal fly ash and is not intended as a fly ash from a specific coal or combustion process. The material was air dried, sieved, and blended for 24 h, before being placed in a series of bulk containers. X-ray fluorescence and inductively coupled plasma atomic emission analyses were performed on ten grab samples taken from the bulk for a preliminary homogeneity assessment before proceeding with bottling the material in 75 g units.

Analysis: The homogeneity of the bottled material was assessed by X-ray fluorescence spectrometry and instrumental neutron activation analysis, using selected elements as indicators. In some cases, statistically significant differences between samples were seen, and the variance due to material inhomogeneity is included in the overall uncertainties of the certified values. The estimated relative standard deviation for material inhomogeneity is less than 1% for those elements for which homogeneity was assessed, except Th, for which material inhomogeneity was estimated to be 2%.

Certified Values and Uncertainties: The certified values are weighted means of results of two or more independent analytical methods, or the means of results from a single definitive method, except for mercury. Mercury certification is based on cold vapor atomic absorption spectrometry measurements performed at NIST. The weights for the weighted means were computed according to the iterative procedure of Paule and Mandel (NBS Journal of Research 87, 1982, pp. 377-385). The stated uncertainty includes allowances for measurement imprecision, material variability, and differences among analytical methods. Each uncertainty is the sum of the half-width of a 95% prediction interval, and includes an allowance for the systematic error among the methods used. In the absence of systematic error, a 95% prediction interval predicts where the true concentrations of 95% of the samples of this SRM lie.

Table 1. Certified Values

Element	wt %	Element	mg/kg
Aluminum	15.05 ± 0.27	Arsenic	136.2 ± 2.6
Calcium	1.51 ± 0.06	Barium	709 ± 27
Iron	7.78 ± 0.23	Cadmium	0.784 ± 0.006
Magnesium	0.482 ± 0.008	Chromium	198.2 ± 4.7
Potassium	1.95 ± 0.03	Copper	112.8 ± 2.6
Silicon	23.02 ± 0.08	Lead	68.2 ± 1.1
Sodium	0.201 ± 0.003	Manganese	131.8 ± 1.7
Sulfur	0.2075 ± 0.0011	Mercury	0.141 ± 0.019
Titanium	0.791 ± 0.014	Nickel	120.6 ± 1.8
		Selenium	10.26 ± 0.17
		Strontium	1041 ± 14
		Thorium	25.7 ± 1.3
		Uranium	8.79 ± 0.36
		Vanadium	295.7 ± 3.6

Table 2. Noncertified Values

Element	mg/kg	Element	mg/kg
Antimony	6	Phosphorus	2300
Bromine	2.9	Rubidium	140
Cerium	190	Scandium	41
Cobalt	50	Samarium	20
Cesium	11	Tantalum	1.8
Dysprosium	17	Terbium	2.6
Europium	4.1	Thallium	5.9
Gadolinium	13	Thulium	2.1
Hafnium	6.8	Tungsten	5.6
Holmium	3.5	Ytterbium	7.6
Lanthanum	94	Zinc	210
Lutetium	1.2		
Neodymium	85		

Table 3. Analytical Methods Used for Certification Analyses of SRM 1633b

Element	Certification Methods
Al	INAA, XRF
As	FIA-HAAS, INAA
Ba	ICP-MS, INAA
Ca	ICP, INAA, XRF
Cd	ETAAS, IDTIMS
Cr	FAAS, INAA
Cu	FAAS, ICP-MS
Fe	INAA, XRF
Hg	CVAAS
K	FAES, INAA, XRF
Mg	ICP, IDTIMS
Mn	FAAS, INAA
Na	FAES, INAA
Ni	ETAAS, ICP
Pb	ETAAS, ICP-MS
Rb	FAES, INAA
S	IDTIMS
Sb	ETAAS, INAA
Se	FIA-HAAS, INAA
Si	GRAV, XRF
Sr	FAES, INAA, IDTIMS
Th	ICP-MS, INAA
Ti	INAA, XRF
U	ICP-MS, INAA
V	ICP, INAA

ID-TIMS - Isotope dilution thermal ionization mass spectrometry, mixed acid digestion.

ICP-MS - Inductively coupled plasma mass spectrometry; mixed acid digestion.

INAA - Instrumental neutron activation analysis.

XRF - Wavelength dispersive X-ray fluorescence on fused borate discs.

ICP-AES - Inductively coupled plasma atomic emission spectrometry; mixed acid digestion.

ETAAS - Electrothermal atomic absorption spectrometry; mixed acid digestion.

CVAAS - Cold vapor atomic absorption spectrometry.

FIA-HAAS - Flow injection analyses - Hydride generation atomic absorption spectrometry.

FAAS - Flame atomic absorption spectrometry; mixed acid digestion except for Au, leached with HBr-Br₂.

GRAV - Gravimetry; sodium carbonate fusion.

Most information values were determined by INAA only; P was determined by ICP-AES and XRF, Tl was determined by ICP-MS, and Zn was determined by FAAS and ICP-AES.

Participating NIST Analysts

Rocio Arvizu
Ellyn S. Beary
Diane S. Braverman
Michael S. Epstein
John D. Fassett
Karen M. Garrity
Robert R. Greenberg
W. Robert Kelly
Elizabeth A. Mackey
John R. Moody
Karen E. Murphy
Paul J. Paulsen
Theresa A. Rush
Rajananda Saraswati
Johanna M. Smeller
Thomas W. Vetter
Robert D. Vocke
Robert L. Watters, Jr.

Participating Laboratories

JoAnne Delles, Howard Kanare
Construction Technology Laboratories, Inc.
Skokie, IL 60077

Paul Briggs, David Siems
U. S. Geological Survey
Branch of Geochemistry
Lakewood, CO 80225

I. Uncertainty of the Pipette 5000

Protokollblatt Pipettenkalibrierung					
Hersteller:	Socorex		Pipettentyp:	0.5-5ml	
Seriennummer:	SOMP5000		Nennvolumen V_0:	5000	
kalibriert am:	23.04.2018		letzte Kalibrierung:		
kalibriert von:	Michaela Foster				
Geforderte Qualitätsmerkmale lt. EN ISO 8655:					
Messreihe	Prüfvolumen V_S [μ L]	Unrichtigkeit e_s [% RE]	Impräzision CV [% RSD]	Anzahl d. Messungen	geforderter Teilungswert d der Waage [mg]
1	5000	- 1.1	0.3	10	
2	2500	- 0.6	0.4	10	
3	500	6.1	0.6	10	
Messung:					
verwendete Waage:	Sart. Res.		Teilungswert d [mg]		
verwendetes Messgefäß:	Rollrandglas				
Messflüssigkeit:	Destilliertes Wasser				
entgast (ja/nein):	nein				
Pipettiermodus:	benetzt, jeweils neue Pipettenspitze pro Messreihe				
Z	1.0025				
Temperatur ($^{\circ}$C):	23.0				
Luftdruck (kPa):	101.4				
Messreihe 1					
					Prüfvolumen $V_S =$ Nennvolumen V_0 [μ L] 5000
Messung				gewogene Masse [mg]	berechnetes Volumen [μ L]
1				4934.57	4946.91
2				4908.71	4920.98
3				4914.48	4926.77
4				4920.42	4932.72
5				4930.85	4943.18
6				4933.38	4945.71
7				4932.45	4944.78
8				4943.87	4956.23
9				4957.91	4970.30
10				4940.76	4953.11
Mittelwert \bar{x} [μL]					4944.07
Standardabweichung s_r [μL]					14.496
Unrichtigkeit e_s [% RE]					- 1.12
Impräzision CV [% RSD]					0.29

Messreihe 2				Prüfvolumen $V_s =$ (ca. 50 % V_0) [μL] 2500
<i>Messung</i>		gewogene Masse [mg]		berechnetes Volumen [μL]
1		2450.07		2456.20
2		2480.69		2486.89
3		2483.59		2489.80
4		2485.81		2492.02
5		2478.73		2484.93
6		2482.72		2488.93
7		2478.75		2484.95
8		2484.08		2490.29
9		2482.98		2489.19
10		2482.06		2488.27
Mittelwert \bar{x} [μL]				2485.15
Standardabweichung s_r [μL]				10.419
Unrichtigkeit e_s [% RE]				- 0.59
Impräzision CV [% RSD]				0.42
Messreihe 3				Prüfvolumen $V_s =$ (untere Grenze des Nutzvolumens o. ca. 10 % V_0) [μL] 500
<i>Messung</i>		gewogene Masse [mg]		berechnetes Volumen [μL]
1		533.67		535.00
2		531.10		532.43
3		532.53		533.86
4		532.89		534.22
5		531.16		532.49
6		526.63		527.95
7		527.08		528.40
8		527.61		528.93
9		524.89		526.20
10		526.12		527.44
Mittelwert \bar{x} [μL]				530.69
Standardabweichung s_r [μL]				3.232
Unrichtigkeit e_s [% RE]				+ 6.14
Impräzision CV [% RSD]				0.61

Auswertung:	<i>Ist</i>	<i>Soll</i>	Sollwert eingehalten?
Messreihe 1			
<i>Unrichtigkeit e_s [% RE]</i>	- 1.12	- 1.1	ja
<i>Impräzision CV [% RSD]</i>	0.29	0.3	ja
Messreihe 2			
<i>Unrichtigkeit e_s [% RE]</i>	- 0.59	- 0.6	ja
<i>Impräzision CV [% RSD]</i>	0.42	0.4	ja
Messreihe 3			
<i>Unrichtigkeit e_s [% RE]</i>	+ 6.14	6.1	ja
<i>Impräzision CV [% RSD]</i>	0.61	0.6	ja
Gesamtbewertung:			
Unterschrift:			

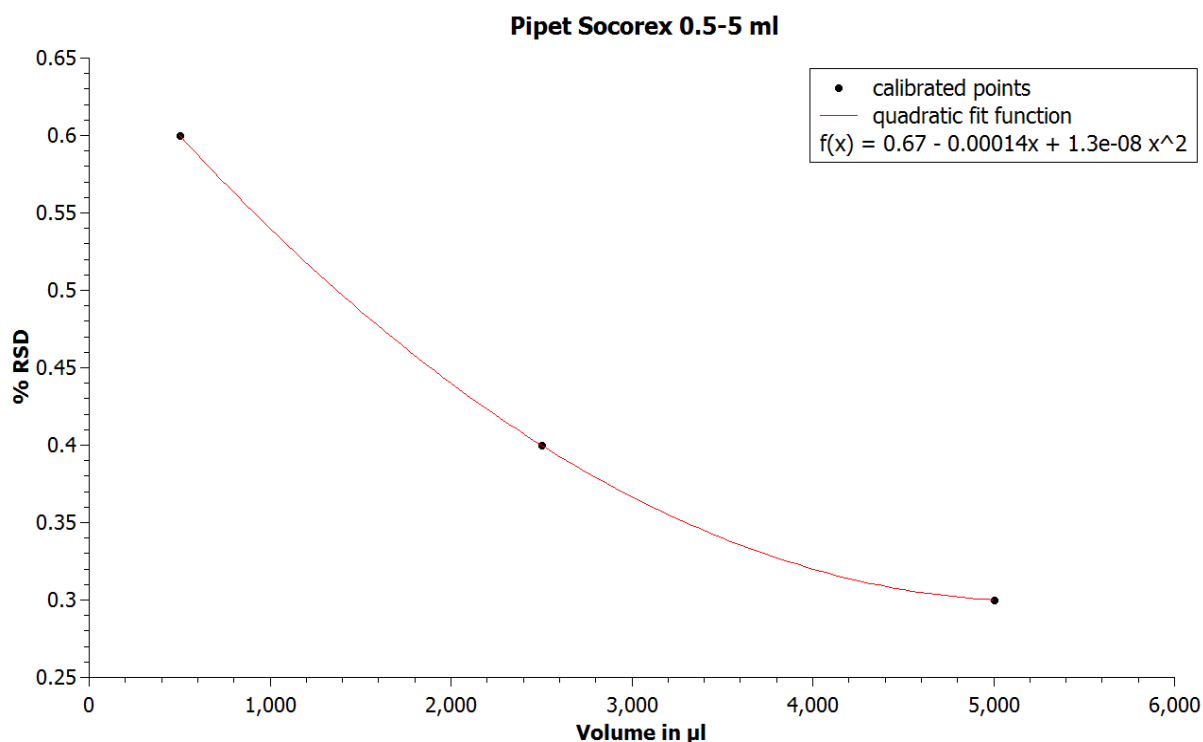


Figure I.1: Extrapolation of the three provided data points of the deviation of the pipetting volume of Pipette Socorex 5000 with the program QTI Plot.

Volume in μl	Deviation in % RSD
5000	0.3
2500	0.4
500	0.6

Table I.1: Deviation of the Pipette Socorex 5000 for the volumes 5000 μl , 2500 μl and 500 μl . Look up the labour protocol at Appendix I.

Volume in ml	Deviation in % RSD	Uncertainty in l
5.00	0.3	1.500E-05
4.00	0.3200	1.280E-05
2.80	0.3792	1.062E-05
2.20	0.4232	9.310E-06
1.00	0.5400	5.400E-06
1.60	0.4768	7.629E-06

Table I.2: Deviation and uncertainty of the Pipette Socorex 5000 for the used volumes during the experiment.

Protokollblatt Pipettenkalibrierung					
Hersteller:	Brand	Pipettentyp:	Transferpipette Fix 100µl		
Seriennummer:	BRTR100	Nennvolumen V_0:	100		
kalibriert am:	22.3.2018	letzte Kalibrierung:			
kalibriert von:	Michaela Foster				
Geforderte Qualitätsmerkmale lt. EN ISO 8655:					
Messreihe	Prüfvolumen V_S [µL]	Unrichtigkeit e_s [% RE]	Impräzision CV [% RSD]	Anzahl d. Messungen	geforderter Teilungswert d der Waage [mg]
1	100	- 0.9	0.7	12	
2 ohne Extremwerte	100	- 0.8	0.5	10	
Messung:					
verwendete Waage:	Sart. Res.				Teilungswert d [mg]
verwendetes Messgefäß:	Rollrandglas				
Messflüssigkeit:	Destilliertes Wasser				
entgast (ja/nein):	nein				
Pipettiermodus:	benetzt, jeweils neue Pipettenspitze pro Messreihe				
Z	1.0034				
Temperatur (°C):	22.5				
Luftdruck (kPa):	101.4				
Messreihe 1					Prüfvolumen $V_S =$ Nennvolumen V_0 [µL] 100
Messung				gewogene Masse [mg]	berechnetes Volumen [µL]
1				97.69	98.02
2				99.11	99.45
3				99.27	99.61
4				99.69	100.03
5				99.26	99.60
6				98.19	98.52
7				99.52	99.86
8				98.66	99.00
9				98.42	98.75
10				98.54	98.88
11				97.88	98.21
12				98.40	98.73
Mittelwert \bar{x} [µL]					99.05
Standardabweichung s_r [µL]					0.649
Unrichtigkeit e_s [% RE]					- 0.95
Impräzision CV [% RSD]					0.66

Protokollblatt Pipettenkalibrierung					
Hersteller:	Brand	Pipettentyp:	Transferpipette Fix 20µl		
Seriennummer:	BRTR20	Nennvolumen V_0:	20		
kalibriert am:	22.3.2018	letzte Kalibrierung:			
kalibriert von:	Michaela Foster				
Geforderte Qualitätsmerkmale lt. EN ISO 8655:					
Messreihe	Prüfvolumen V_S [µL]	Unrichtigkeit e_s [% RE]	Impräzision CV [% RSD]	Anzahl d. Messungen	geforderter Teilungswert d der Waage [mg]
1	20	0.3	0.7	12	
2 ohne Extremwerte	20	0.6	0.4	10	
Messung:					
verwendete Waage:		Sart. Res.		Teilungswert d [mg]	
verwendetes Messgefäß:		Rollrandglas			
Messflüssigkeit:		Destilliertes Wasser			
entgast (ja/nein):		nein			
Pipettiermodus:		benetzt, jeweils neue Pipettenspitze pro Messreihe			
Z		1.0033			
Temperatur (°C):		21.8			
Luftdruck (kPa):		102.6			
Messreihe 1					Prüfvolumen $V_S =$ Nennvolumen V_0 [µL] 20
Messung			gewogene Masse [mg]		berechnetes Volumen [µL]
1			20.11		20.18
2			20.05		20.12
3			20.11		20.18
4			19.90		19.97
5			20.13		20.20
6			19.94		20.01
7			20.06		20.13
8			20.07		20.14
9			19.69		19.75
10			20.09		20.16
11			20.13		20.20
12			19.76		19.83
Mittelwert \bar{x} [µL]					20.07
Standardabweichung s_r [µL]					0.150
Unrichtigkeit e_s [% RE]					+ 0.35
Impräzision CV [% RSD]					0.74

Bibliography

- L. Ádám, G. Kakasy, and P. I. Fekete. Removal of radioactive pollutants from water using mineral substances of natural domestic origin. *Publications of the hungarian mining research institute*, 14:209–212, 1971.
- Z. B. Alfassi, editor. *Determination of Trace Elements*. VCH Verlagsgesellschaft, Weinheim, 1994.
- L. L. Ames JR. Mass action relationships of some zeolites in the region of high competing cation concentrations. *The American Mineralogist*, 48:868–882, July-August 1963.
- S. M. Auerbach, K. A. Carrado, and P. K. Dutta, editors. *Handbook of Zeolite Science and Technology*. Marcel Dekker, Inc., New York, Basel, first edition, 2003.
- C. Baerlocher and L. McCusker. Database of Zeolite Structures. <http://www.iza-structure.org/databases/>. Accessed: 11.03.2019.
- C. Baerlocher, L. McCusker, and D. Olson. *Atlas of Zeolite Framework Types*. Elsevier, Netherlands, 6th edition, 2007.
- N. G. Bogdanovich, E. A. Grushicheva, T. O. Mishevets, S. N. Skomorokhova, E. M. Trifanova, V. P. Emel'yanov, G. N. Petrukhina, and O. V. Starkov. Recovery of ^{137}Cs and ^{90}Sr from wastewater by sorption on finely dispersed minerals under static conditions. *Radiochemistry*, 50, No. 4:395–401, 2008.
- M. E. Brown, editor. *Handbook of Thermal Analysis and Calorimetry: Principles and Practice*, volume 1 of *Handbook of Thermal Analysis and Calorimetry* (P. K. Gallagher, Series Editor). Elsevier, Amsterdam [u.a.], 1998.
- D. M. Byler, W. V. Gerasimowicz, V. M. Stockette, and D. D. Eberl. Infrared spectroscopic examination of the interaction of urea with the naturally occurring zeolite clinoptilolite. *Microchemical Journal*, 44, Issue 2:130–139, 1991.
- R. A. Clifton. Natural and Synthetic Zeolites. *Bureau of Mines Information Circular*, 9140, 1987.
- R. E. Dinnebier and S. J. L. Billinge, editors. *Powder Diffraction: Theory and Practice*. The Royal Society of Chemistry, 2008.

- K. Dorfner, editor. *Ion Exchangers*. Walter de Gruyter, Berlin, Germany, second edition, 1973.
- A. Dyer, A. Chimedtsogzol, L. Campbell, and C. Williams. Uptake of caesium and strontium radioisotopes by natural zeolites from mongolia. *Microporous and Mesoporous Materials*, 95:172–175, 2006.
- K. Elghniji, E. Elaloui, and Y. Moussaoui. Coating of anatase titania on clinoptilolite by metal organic chemical vapor deposition method: Enhanced mesoporosity and photocatalytic activity. *Chemical Papers*, 72, Issue 5:1159–1168, May 2018.
- V. M. Fedorova, S. A. Kobets, L. N. Puzyrnaya, G. N. Pshinko, and A. A. Kosorukov. Clinoptilolite/ Fe_3O_4 : a magnetic sorbent for removing ^{90}Sr from aqueous media. *Radiochemistry*, 59, No. 5:495–499, 2017.
- G. R. Frysinger. Caesium-sodium ion exchange on clinoptilolite. *Nature*, 194, No. 4826:351–353, 1962.
- Generalic, Eni. "Strontium." EniG. Periodic Table of the Elements. <https://www.periodni.com/sr.html>, Jan. 2019. KTF-Split, Accessed: 26.04.2019.
- G. R. Gilmore. *Practical Gamma-ray Spectrometry*. John Wiley & Sons, Ltd, 2nd edition, 2008.
- Q. He and D. E. Walling. Interpreting particle size effects in the adsorption of ^{137}Cs and unsupported ^{210}Pb by mineral soils and sediments. *I. Environ. Radioactivity*, 30, No. 2:117–137, 1996.
- IZA. Gismondine. <http://www.iza-online.org/natural/Datasheets/Gismondine/gismondine.htm>, a. Accessed: 12.03.2019.
- IZA. Terranovaite. <http://www.iza-online.org/natural/Datasheets/Terranovaite/Terranovaite.html>, b. Accessed: 12.03.2019.
- R. Klockenkämper and A. v. Bohlen. *Total-Reflection X-Ray Fluorescence Analysis and Related Methods*. Chemical Analysis (*M. F. Vitha, Series Editor*). Wiley, Hoboken, New Jersey, 2nd edition, 2015.
- J.-V. Kratz and K. H. Lieser. *Nuclear and Radiochemistry - Fundamentals and Applications*. Wiley-VCH Verlag GmbH & Co. KGaA, Germany, third, revised edition, 2013.
- N. Lihareva, L. Dimowa, O. Petrov, and Y. Tzvetanova. Evaluation of bulgarian clinoptilolite as ion-exchanger for Cs^+ removal from water solutions. *Journal of Radioanalytical and Nuclear Chemistry*, 316:37–47, 2018.
- L. Malvern Panalytical. Phase identification. <https://www.malvernpanalytical.com/en/products/measurement-type/phase-identification/index.html>, 2019. Accessed: 13.03.2019.

- P. Misaelides. Application of natural zeolites in environmental remediation: A short review. *Microporous and Mesoporous Materials*, 144:15–18, 2011.
- F. A. Mumpton. Clinoptilolite redefined. *The American Mineralogist*, 45:351–369, March-April 1960.
- K. Murakami, T. Wajima, T. Kato, K. Sugawara, and T. Sugawara. Thermodynamic and kinetic studies on cs^+ - and sr^{2+} -exchange in natural zeolite from akita, japan. *Toxicological & Environmental Chemistry*, 91, No. 6:1023–1034, 2009.
- Y. e. Murakami and 7th International Zeolite Conference Tokio. *New developments in zeolite science and technology*. Studies in surface science and catalysis ; 28. Elsevier, Amsterdam [u.a.], 1986.
- National Nuclear Data Center. NuDat 2.7 - 134Cs Decay Radiation. <https://www.nndc.bnl.gov/nudat2/decaysearchdirect.jsp?nuc=134CS&unc=nds>, a. Accessed: 14.02.2019.
- National Nuclear Data Center. NuDat 2.7 - 133Cs Thermal neutron capture cross sections. <https://www.nndc.bnl.gov/nudat2/reCenter.jsp?z=55&n=78>, b. Accessed: 27.04.2019.
- National Nuclear Data Center. NuDat 2.7 - 85Sr Decay Radiation. <https://www.nndc.bnl.gov/nudat2/decaysearchdirect.jsp?nuc=85SR&unc=nds>, c. Accessed: 14.02.2019.
- National Nuclear Data Center. NuDat 2.7 - 84Sr Thermal neutron capture cross sections. <https://www.nndc.bnl.gov/nudat2/reCenter.jsp?z=38&n=46>, d. Accessed: 26.04.2019.
- National Nuclear Data Center. NuDat 2.7 - 88Sr Thermal neutron capture cross sections. <https://www.nndc.bnl.gov/nudat2/reCenter.jsp?z=38&n=50>, e. Accessed: 26.04.2019.
- National Nuclear Data Center. NuDat 2.7. <http://www.nndc.bnl.gov/nudat2/>, f. Accessed: 18.11.2018.
- H. Nishita, R. M. Haug, and M. Hamilton. Influence of minerals on sr^{90} and cs^{137} uptake by bean plants. *Soil Science*, 105, No. 4:237–243, 1967.
- R. H. Perry, D. W. Green, and J. O. Maloney, editors. *Perry's Chemical Engineers' Handbook*. The McGraw-Hill Companies, Inc., United States of America, 7th edition, 1999.
- A. Peter, L. Mihaly Cozmuta, A. Mihaly Cozmuta, N. Camelia, L. Barbu-Tudoran, A. Vulpoi, and L. Baia. Photocatalytic efficiency of zeolite-based tio_2 composites for reduction of cu (ii): Kinetic models. *International Journal of Applied Ceramic Technology*, 11:568–581, 2014.

- P. Rajec, F. Macfigek, M. Féder, P. Misaelides, and E. Šamajovfá. Sorption of caesium and strontium on clinoptilolite- and mordenite-containing sedimentary rocks. *Journal of Radioanalytical and Nuclear Chemistry*, 229, Nos 1-2:49–55, 1998.
- M. Sadeghi, S. Yekta, H. Ghaedi, and E. Babanezhad. Effective removal of radioactive ^{90}Sr by CuO nps/ag-clinoptilolite zeolite composite adsorbent from water sample: isotherm, kinetic and thermodynamic reactions study. *Int J Ind Chem*, 7:315–331, 2016.
- L. B. Sand and F. A. Mumpton, editors. *Natural Zeolites - Occurrence, Properties, Use*. Pergamon Press, Oxford, 1st edition, 1978.
- J. Siddall. Evolution of NIR Spectroscopy: Past, Present and Future. R&D. <https://www.rdmag.com/article/2014/11/evolution-nir-spectroscopy-past-present-and-future>, November 2014. Accessed: 09.03.2019.
- R. Snellings, G. Mertens, and J. Elsen. The pozzolanic reaction between clinoptilolite and portlandite: A time and spatially resolved IR study. *European Journal of Mineralogy*, 22: 767–777, 12 2010.
- H. Sperrer. Adsorption von im Wasser gelöstem Strontium durch Zeolithe. project work, TU Wien, Vienna, Austria, 2013.
- J. H. Sterba, H. Sperrer, F. Wallenko, and J. M. Welch. Adsorption characteristics of a clinoptilolite-rich zeolite compound for Sr and Cs. *Journal of Radioanalytical and Nuclear Chemistry*, 318, Issue 1:267–270, 2018.
- T. Tamura and E. G. Struxness. Reactions affecting strontium removal from radioactive wastes. *Health Physics*, 9:697–704, 1963.
- G. Tsitsishvili, T. Andronikashvili, G. Kirov, and L. Filizova. *Natural Zeolites*. Ellis Horwood Limited, Chichester, West S, England, 1992.
- J. Čejka, H. van Bekkum, A. Corma, and F. Schüth, editors. *Introduction to Zeolite Science and Practice*, volume Studies in Surface Science and Catalysis 168. Elsevier, Hungary, 3rd revised edition, 2007.
- J. Čejka, A. Corma, and S. Zones, editors. *Zeolites and Catalysis - Synthesis, Reactions and Applications*, volume 1. Wiley-VCH Verlag GmbH & Co. KGaA, Weinheim, 2010.
- F. Wallenko. Adsorption of cesium on clinoptilolite. project work, TU Wien, Vienna, Austria, 2013.

List of Figures

2.1	Ion exchange isotherms for three different cases plotted as the mole fraction in solution against the mole fraction in the zeolite, always for the same cation. Green: Zeolite prefers the entering cation, cation of solution replaces a cation of the zeolite; Red: Opposite of green line, zeolite is non selective for entering cation, cation of solution stays in solution; Blue: Selectivity for the entering cation varies during exchange; Grey: straight isotherm. Adapted from Dorfner (1973)	5
2.2	Chemical compositions of heulandites (H, blue) and clinoptilolites (C, green). Adapted from Tsitsishvili et al. (1992)	6
2.3	A and B are the 10- and 8-membered channels which are parallel to [001] and C are the 8-tetrahedral channels which are along [100]. Reproduced from Tsitsishvili et al. (1992)	6
2.4	Coordinate environment for Ca and Na (M1 and M2), K (M3) and Mg (M4) ions. Reproduced from Tsitsishvili et al. (1992)	7
2.5	Output of a STA measurement for sample A.	10
2.6	Diffractiongram of sample A using one major phase.	11
2.7	Flow chart of a general experimental set up for capacity determination.	18
3.1	IR spectra for the four zeolite samples.	20
3.2	STA curves for zeolite A. Red: VG_A; Blue: VG_A_voll; Green: VG_A_wait_voll.	23
3.3	STA curves for all measurements.	23
3.4	Position of the sample for the activation process.	24
3.5	Distribution of the main elements Si, Al, Ca, Mg, K and Na in the four zeolites.	27
3.6	Occurrence in percent of Al, Si, Ca, K and Na in the zeolites.	30
3.7	Occurrence in percent of Mg, Ti, Mn and V in the zeolites.	31
3.8	Occurrence in percent of all detected components in the zeolites.	32
3.9	Occurrence in percent of all detected components except Si in the zeolites.	32
3.10	TXRF spectrum of sample A on carrier one (shortcut: A01). Element specific concentration proportional constants in Appendix Tab. B.1.	34
3.11	TXRF spectrum of the CFA on carrier one (shortcut: CFA01). Element specific concentration proportional constants in Appendix Tab. B.2.	35
3.12	Diffractiongram of sample A using the major phase 1.	41

3.13	Diffractogram of sample A using phase 1 to 3.	42
3.14	Diffractogram of sample B using phase 1 to 3.	42
3.15	Diffractogram of sample C using phase 1 to 3.	43
3.16	Diffractogram of sample D using phase 1 to 4.	43
4.1	General saturation curve for the uptake of an ion into the zeolite.	45
4.2	Flow chart of the experimental set up of the capacity determination. Two dif- ferent stock solutions (Number = 1, 2) for each radiotracer (Ion = Sr, Cs) were prepared. The second stock solution had a ten-fold higher concentration than the first stock solution.	47
4.3	Procedure of main steps for the capacity experiments.	52
4.4	Uptake of Sr for the two different stock solutions.	59
4.5	Uptake of Cs for the two different stock solutions.	66
I.1	Extrapolation of the three provided data points of the deviation of the pipetting volume of Pipette Socorex 5000 with the program QTI Plot.	155

List of Tables

2.1	Structure sensitivity and insensitive lattice vibrations of zeolites. Adapted from Auerbach et al. (2003)	8
2.2	Typical frequency ranges for clinoptilolite. Adapted from Tsitsishvili et al. (1992)	8
2.3	Parameters and their units for PXRD.	11
2.4	Parameters and their units for NAA.	13
2.5	Energy and intensity of the detected γ -peaks in the zeolite and Coal Fly Ash (CFA) samples. The information about the energy and intensity of the elements was extracted from the NuDat 2 Database from the National Nuclear Data Center (f)	14
2.6	Parameters for TXRF.	17
2.7	Chemical properties of the stable strontium isotopes in $\text{Sr}(\text{NO}_3)_2$. The atomic mass of the element M (Generalic, Eni., 2019), the relative abundance of the nuclide H (Generalic, Eni., 2019), the cross section $\sigma_{\text{Sr}84 \rightarrow \text{Sr}85}$ (National Nuclear Data Center, d) and the cross section $\sigma_{\text{Sr}88 \rightarrow \text{Sr}89}$ (National Nuclear Data Center, e) are listed.	17
3.1	Explanation of the STA data names.	22
3.2	The mass of the measured samples and the mass loss in %.	22
3.3	Element composition of the four zeolites.	28
3.4	Element composition of the four zeolites converted to the oxide form.	29
3.5	Range of the chemical composition of clinoptilolite in wt.% after Appendix D.	29
3.6	Difference in per cent between the ratio of the TXRF data to the ratio of the NAA data.	35
3.7	Corrected ratios of the elements Al, Si, K, Ca, Ti and Fe for sample A.	36
3.8	Ratios of the elements Al, Si, K, Ca and Ti for sample A calculated with NAA data.	36
3.9	Corrected ratios of the elements Al, Si, K, Ca, Ti and Fe for sample B.	37
3.10	Ratios of the elements Al, Si, K, Ca and Ti for sample B calculated with NAA data.	37
3.11	Corrected ratios of the elements Al, Si, K, Ca, Ti and Fe for sample C.	37
3.12	Ratios of the elements Al, Si, K, Ca and Ti for sample C calculated with NAA data.	37

3.13	Corrected ratios of the elements Al, Si, K, Ca, Ti and Fe for sample D.	38
3.14	Ratios of the elements Al, Si, K, Ca and Ti for sample D calculated with NAA data.	38
3.15	Calculation of the device-specific sensitivity factors for the elements.	38
3.16	Results of the quantitative content of the elements determined with TXRF and NAA are compared.	39
3.17	Explanation of phase numbers.	41
4.1	Used terminology for the capacity experiment.	48
4.2	Variables for capacity experiment analysis.	54
4.3	Description of the variable names for the strontium capacity experiment.	56
4.4	Necessary values for the calculation of the concentrations for the strontium capacity experiment for SL_1_Sr.	57
4.5	Equations for the calculation of the concentrations for the strontium capacity experiment for SL_1_Sr.	57
4.6	Calculated concentrations of the SL_1_Sr.	58
4.7	Additional values for the calculation of the concentrations for the strontium capacity experiment for SL_2_Sr.	58
4.8	Equations for the calculation of the concentrations for the strontium capacity experiment for SL_2_Sr.	58
4.9	Calculated values for the strontium capacity experiment for SL_2_Sr.	59
4.10	Uptake of Sr for stock solution 1 and stock solution 2.	59
4.11	Description of the variable names for the caesium capacity experiment.	62
4.12	Values for the calculation of the concentrations for the caesium capacity experiment for SL_1_Cs.	63
4.13	Equations for the calculation of the concentrations for the caesium capacity experiment for SL_1_Cs.	63
4.14	Calculated values for the caesium capacity experiment for SL_1_Cs.	64
4.15	Additional values for the calculation of the concentrations for the caesium capacity experiment for SL_2_Cs.	64
4.16	Equations for the calculation of the concentrations for the caesium capacity experiment for SL_2_Cs.	64
4.17	Calculated values for the caesium capacity experiment for SL_2_Cs.	65
4.18	Uptake of Cs for stock solution 1 and stock solution 2.	65
4.19	variable names for the analysis of the absorbed Sr or Cs particles.	69
4.20	Mass of the zeolite powder used for the capacity experiments.	69
4.21	Number of particles calculated with the NAA results for the elements Al, Si, Ca, Mg, K, Na, Ti, Mn and V.	70
4.22	Absorbed Sr or Cs particles for stock solution 1 and stock solution 2.	70

A.1	Parameters for the calculation of the specific activity to choose the right irradiation time for the NAA.	76
A.2	Calculation of the specific activity for different irradiation times for the NAA.	76
A.3	Mass and irradiation time of the samples for the qualitative NAA measurements.	76
A.4	Mass and irradiation time of the samples and the standard Coal Fly Ash (CFA) for the quantitative NAA measurements.	77
A.5	Acquisition and measured time of the samples and the standard Coal Fly Ash (CFA) for the quantitative NAA measurements.	77
A.6	NAA spectrum data for A. Errors quoted at 1.00 sigma.	79
A.7	NAA spectrum data for CFA_A. Errors quoted at 1.00 sigma.	80
A.8	NAA spectrum data for B. Errors quoted at 1.00 sigma.	81
A.9	NAA spectrum data for CFA_B. Errors quoted at 1.00 sigma.	82
A.10	NAA spectrum data for C. Errors quoted at 1.00 sigma.	83
A.11	NAA spectrum data for CFA_C. Errors quoted at 1.00 sigma.	84
A.12	NAA spectrum data for D. Errors quoted at 1.00 sigma.	85
A.13	NAA spectrum data for CFA_D. Errors quoted at 1.00 sigma.	86
B.1	Element specific concentration proportional constants (corrected intensities for fundamental parameters) and their mean values for CFA with TXRF. The values are given by Atomika 8030C and the element silicon was set to the internal standard. This means, that the proportional constant for silicon was set to 1000.	89
B.2	Element specific concentration proportional constants (corrected intensities for fundamental parameters) and their mean values for A with TXRF. The values are given by Atomika 8030C and the element silicon was set to the internal standard. This means, that the proportional constant for silicon was set to 1000.	89
B.3	Element specific concentration proportional constants (corrected intensities for fundamental parameters) and their mean values for B with TXRF. The values are given by Atomika 8030C and the element silicon was set to the internal standard. This means, that the proportional constant for silicon was set to 1000.	90
B.4	Element specific concentration proportional constants (corrected intensities for fundamental parameters) and their mean values for C with TXRF. The values are given by Atomika 8030C and the element silicon was set to the internal standard. This means, that the proportional constant for silicon was set to 1000.	90
B.5	Element specific concentration proportional constants (corrected intensities for fundamental parameters) and their mean values for D with TXRF. The values are given by Atomika 8030C and the element silicon was set to the internal standard. This means, that the proportional constant for silicon was set to 1000.	90
D.1	Chemical composition of clinoptilolites. Adapted from (Sand and Mumpton, 1978 , p. 166)	110

- D.2 Chemical composition of a K-rich clinoptilolite in rhyolitic vitric tuff of the Hakobuchi Group of Late Cretaceous; Chikubetsu coal mine abandoned, Haboro Town, Rumoi, Hokkaido. The SrO values is corrected. Adapted from (Sand and Mumpton, 1978, p. 182) 110
- D.3 Chemical composition of deep-sea clinoptilolites. Adapted from (Sand and Mumpton, 1978, p. 205). (a) Total iron given as FeO. Inclusion impurity; not included in cell content calculations. (b) By difference. (c) $E_b = \frac{Al - \sum_{cat}}{Al}$ where $\sum_{cat} = 2(Mg + Ca) + (Na + K)$ (1) DSDP 105-14-cc; lower Cretaceous, black, carbonaceous clay sampled at 349 m; 34° 54'N, 69° 10'W. (2) DSDP 105-17-cc; lower Cretaceous. black. carbonaceous clay sampled at 405 m; same location as (1). (3) DSDP 105-21-cc; lower Cretaceous clay sampled at 457 m; same location as (1). (4) DSDP 9A-1-6; middle Eocene siliceous clay sampled at 682 m; 32° 46'N, 59° 12'W. (5) DSDP 163-27-1; upper Cretaceous nanochalk sampled at 271 m; 11° 15'N, 150° 17'W. (6) DSDP 59.2-5-1; Eocene brown clay in association with phillipsite. sampled at 127 m; 11° 47'N, 147° 35'E. 111
- D.4 Chemical composition of clinoptilolites. Each analysis represents a separate crystal from the stated horizon. Adapted from (Sand and Mumpton, 1978, p. 229-230). (t) Inclusion impurities - not included in cell contents. Total iron given as FeO. (tt) By difference. (§) $E_b = \frac{Al - \sum_{cat}}{Al} \cdot 100$ where $sum_{cat} = 2(Mg + Ca) + (Na + K)$ 112
- D.5 Continuation of D.4. Chemical composition of clinoptilolites. Each analysis represents a separate crystal from the stated horizon. Adapted from (Sand and Mumpton, 1978, p. 229-230). (t) Inclusion impurities - not included in cell contents. Total iron given as FeO. (tt) By difference. (§) $E_b = \frac{Al - \sum_{cat}}{Al} \cdot 100$ where $\sum_{cat} = 2(Mg + Ca) + (Na + K)$ 113
- D.6 Continuation of D.5. Chemical composition of clinoptilolites. Each analysis represents a separate crystal from the stated horizon. Adapted from (Sand and Mumpton, 1978, p. 229-230). (t) Inclusion impurities - not included in cell contents. Total iron given as FeO. (tt) By difference. (§) $E_b = \frac{Al - \sum_{cat}}{Al} \cdot 100$ where $\sum_{cat} = 2(Mg + Ca) + (Na + K)$ 114
- D.7 Continuation of D.6. Chemical composition of clinoptilolites. Each analysis represents a separate crystal from the stated horizon. Adapted from (Sand and Mumpton, 1978, p. 229-230). (t) Inclusion impurities - not included in cell contents. Total iron given as FeO. (tt) By difference. (§) $E_b = \frac{Al - \sum_{cat}}{Al} \cdot 100$ where $\sum_{cat} = 2(Mg + Ca) + (Na + K)$ 115

D.8	Chemical composition of deep-sea clinoptilolites. Adapted from (Sand and Mumpton, 1978, p. 238). (A) East Indian Ocean, 4696 m water depth, 89 m below sea bed, zeolite clay, Cretaceous. (B) West Pacific Ocean, 5696 m water depth, 103 m below sea bed, radiolarian-bearing altered volcanic ash, Cretaceous. (C) Indian Ocean, 1655 m water depth, 335.6 m below sea bed, glauconitic carbonate sand, Paleocene. (D) North Atlantic Ocean, 5361 m water depth, 71.5 m below sea bed, silty clay, Cretaceous. (E) Indian Ocean, 1655 m water depth, 335.4 m below sea bed, glauconitic carbonate sand, Paleocene. (F) Indian Ocean, 1655 m water depth, 390.4 m below sea bed, lignite, Paleocene. * The remainder is H ₂ O; Sr and Ba looked for, but not found. Fe ₂ O ₃ is total iron.	116
D.9	Chemical composition of clinoptilolite from Tom Bowling Formation, 5 km southwest of North Cape. Adapted from (Sand and Mumpton, 1978, p. 311) . .	117
D.10	Chemical composition of synthetic clinoptilolite. Adapted from (Sand and Mumpton, 1978, p. 338)	118
D.11	Chemical composition of natural clinoptilolite from specific ores. Adapted from (Sand and Mumpton, 1978, p. 412)	118
D.12	Chemical composition of native and K-exchanged clinoptilolite in wt.%. Adapted from (Sand and Mumpton, 1978, p. 433). Ol ₁ = clinoptilolite, first Oligocene horizon. Ol ₃ = clinoptilolite, third Oligocene horizon. K-Ol ₁ and K-Ol ₃ = potassium ion-exchanged forms.	119
D.13	Chemical composition of clinoptilolite in wt.%. Adapted from (Tsitsishvili et al., 1992, p. 77). 1: Patagonia; 2: California, USA; 3: Transcarpathias, USSR; 4: Georgia, USA; 5: Azerbaidzhan, USSR; 6: Rhodopes, Bulgaria; 7: Rhodopes, Bulgaria; 8: Las Villas, Cuba	119
D.14	Chemical composition of clinoptilolite in wt.%. Adapted from Rajec et al. (1998). Zeolite content: 1 - Nizny Hrabovec, 60%; 2 - Majerovce, 52-65 %; 3 - Sklenne Teplice, 50 %; 4 - Beli Plast, 75 %; 5 - Metaxades, 58 %	120
D.15	Chemical composition of clinoptilolite in wt.%. Adapted from Bogdanovich et al. (2008)	120
E.1	Explanation of the variable names for the calculations in Appendix E.	122
G.1	γ - Lines for ⁸⁵ ₃₈ Sr and their intensities. (National Nuclear Data Center (c)) . . .	134
G.2	Explanation of the sample names for the strontium capacity measurements. . .	134
G.3	γ - Spectrum data for SL_1_Sr_300s. Errors quoted at 1.00 sigma.	135
G.4	γ - Spectrum data for A_SL_1_Sr_L_600s. Errors quoted at 1.00 sigma.	135
G.5	γ - Spectrum data for B_SL_1_Sr_L_600s. Errors quoted at 1.00 sigma.	136
G.6	γ - Spectrum data for C_SL_1_Sr_L_600s. Errors quoted at 1.00 sigma.	136
G.7	γ - Spectrum data for D_SL_1_Sr_L_600s. Errors quoted at 1.00 sigma.	136
G.8	γ - Spectrum data for SL_2_Sr_300s. Errors quoted at 1.00 sigma.	136

G.9	γ - Spectrum data for A_SL_2_Sr_L_600s. Errors quoted at 1.00 sigma.	137
G.10	γ - Spectrum data for B_SL_2_Sr_L_600s. Errors quoted at 1.00 sigma.	137
G.11	γ - Spectrum data for C_SL_2_Sr_L_600s. Errors quoted at 1.00 sigma.	137
G.12	γ - Spectrum data for D_SL_2_Sr_L_600s. Errors quoted at 1.00 sigma.	137
G.13	γ - Lines for $^{134}_{55}\text{Cs}$ and their intensities. (National Nuclear Data Center (a)) . . .	138
G.14	Explanation of the sample names for the caesium capacity measurements.	138
G.15	γ - Spectrum data for SL_1_Cs_300s. Errors quoted at 1.00 sigma.	139
G.16	γ - Spectrum data for A_SL_1_Cs_L_3600s. Errors quoted at 1.00 sigma.	139
G.17	γ - Spectrum data for B_SL_1_Cs_L_3600s. Errors quoted at 1.00 sigma.	139
G.18	γ - Spectrum data for C_SL_1_Cs_L_3600s. Errors quoted at 1.00 sigma.	140
G.19	γ - Spectrum data for D_SL_1_Cs_L_3600s. Errors quoted at 1.00 sigma.	140
G.20	γ - Spectrum data for SL_2_Cs_300s. Errors quoted at 1.00 sigma.	141
G.21	γ - Spectrum data for A_SL_2_Cs_L_600s. Errors quoted at 1.00 sigma.	141
G.22	γ - Spectrum data for B_SL_2_Cs_L_600s. Errors quoted at 1.00 sigma.	142
G.23	γ - Spectrum data for C_SL_2_Cs_L_600s. Errors quoted at 1.00 sigma.	142
G.24	γ - Spectrum data for D_SL_2_Cs_L_600s. Errors quoted at 1.00 sigma.	143
I.1	Deviation of the Pipette Socorex 5000 for the volumes 5000 μl , 2500 μl and 500 μl . Look up the labour protocol at Appendix I.	155
I.2	Deviation and uncertainty of the Pipette Socorex 5000 for the used volumes during the experiment.	155